

Tesis Doctoral

**ESTIMACIÓN MULTIFUENTE DE LA
EVAPOTRANSPIRACIÓN EN MEDIOS
SEMIÁRIDOS MEDIANTE TELEDETECCIÓN:
Evaluación de métodos directos y residuales**

Laura Morillas González



Universidad de Almería

TESIS DOCTORAL

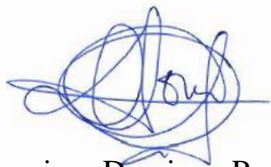
Estimación multifuente de la evapotranspiración en
medios semiáridos mediante teledetección:

Evaluación de modelos directos y residuales

Memoria presentada por **Laura Morillas González** para optar al Grado de Doctor en
Ciencias Biológicas por la Universidad de Almería

Esta Tesis ha sido dirigida por Francisco Domingo Poveda, Investigador Científico del CSIC de la Estación Experimental de Zonas Áridas, Luis Villagarcía Saiz, Profesor Titular del Departamento de Sistemas Físicos, Químicos y Naturales de la Universidad Pablo Olavide y Monica García García investigadora del Instituto de Geografía y Geología de la Universidad de Copenhague (Dinamarca).

Vº Bº Director Tesis



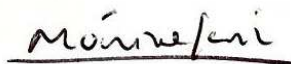
Francisco Domingo Poveda

Vº Bº Director Tesis



Luis Villagarcía Saiz

Vº Bº Director Tesis



Monica García García



Enero 2013



Este trabajo ha sido posible gracias a la concesión de una beca predoctoral adscrita al proyecto de Excelencia “Balance hídrico en zonas degradadas semiáridas” AQUASEM (P06-RNM-01732) financiado por la Consejería de Innovación, Ciencia y Empresa de la Junta de Andalucía y fondos European Regional Development Fund (ERDF) y European Social Fund (ESF) de la Unión Europea. El trabajo se ha financiado también parcialmente por los proyectos GEOCARBO (RNM-3721), GLOCHARID y RNM-6685 financiados por la Junta de Andalucía, CARBORAD (CGL2011-27493) y CARBORED-II (CGL2010-22193-C04-02) financiados por el Ministerio de Ciencia e Innovación también incluyendo fondos ERDF y ESF de la Unión Europea, el proyecto GHG-Europe (grant agreement n° 244122) del FP7/2007-2013 de la Unión Europea y la beca 09-070382 del Consejo Danés para Independent Research and Technology and Production Sciences (FTP). Los datos MODIS se obtuvieron a través de la plataforma online de la NASA Land Processes Distributed Active Archive Center (LP DAAC), USGS/Earth Resources Observation and Science Center (http://lpdaac.usgs.gov/get_data). Así mismo el programa europeo EUMESAT proporcionó los datos MSG-SEVIRI.



UNION EUROPEA
FONDO EUROPEO DE
DESARROLLO REGIONAL
"Una manera de hacer Europa"



*A mis padres,
por educarme en el esfuerzo, la honradez y la libertad*

*A mis abuelos, Pepita, Ismael y Cati,
por ser mi ejemplo de vida*

*A David,
por ser la luz que me dio esperanza
en todas estas últimas tormentas*

“It's always darkest before the dawn,
just keep following the heartlines on your hand”

Florence and the machine

AGRADECIMIENTOS

Uno sueña tantas veces con este momento, el de escribir los agradecimientos, que ahora que me encuentro haciéndolo... apenas puedo creerlo. Una Tesis doctoral es mucho más que un reto intelectual, es un reto personal en el más amplio sentido. Todos comenzamos este camino ingenuos, ilusionados y sobre todo, desconocedores de los muchos obstáculos que nos encontraremos y aprenderemos a superar. Esta es una carrera de fondo, con muchas etapas, de la que una de las cosas más maravillosas que te llevas es el haber encontrado a mucha gente en el camino que, de mil formas distintas, ha hecho posible que tú llegues al final. Gracias a ellos me veo hoy escribiendo los agradecimientos. Así que, allá voy, igual de ilusionada que empecé este camino, a despedirme de él agradeciendo a muchos su enorme contribución.

A mis directores de Tesis, Paco, Luis y Mónica, me gustaría agradecerles, sobre todo, el haberme enseñado, con su trabajo, a aceptar las críticas, una dura lección sin la cual uno sería incapaz de descubrir todo su potencial. A Paco Domingo gracias por haberme dado la oportunidad de asomarme a este complejo campo de la ciencia y por tu apoyo y buen hacer en momentos decisivos. A Luis Villagarcía agradecerle el haberme enseñado el complejo mundo de la Micro-meteorología y de la Ecología con el cariño y cercanía de un profesor vocacional y a Mónica García, por enseñarme que “en ciencia, cuanto más digas con menos palabras, mejor” y que las escalas espacio-temporales son un quebradero de cabeza traspasable en el mundo del Remote Sensing. A ella me gustaría agradecerle además, el haberme apoyado incluso cuando se encontró en situaciones laborales complejas que harían flaquear a cualquiera.

El “chumbo”, como siempre lo hemos llamado, me ha dado tantos buenos amigos que me es difícil pensar que alguno se me olvidará en esta lista ya que han sido muchos años “de cosecha” y muy mala es mi memoria. De mi primera fase en el chumbo quiero agradecerles sin duda, a Ana López, Laura Martínez, Bea Vidal, Lupe Corcobado, Pepa, Miguel Calero e Iván Prieto por haber sido mis amigos y compañeros de aventuras. Con vosotros, que ibais más adelantados, comencé a asomarme a este mundillo de la investigación y sobre todo a disfrutar de unos años divertidos en los que hicimos cosas de lo más variopintas: excursiones camperas, karaokes, fiestas de disfraces, talleres de velas, excursiones en Kayak, cenas internacionales y un largo etcétera que no tendría hojas para enumerar. Muchas gracias chicos por quererme como soy y por enseñarme a ver la vida de una forma tan amplia. Mención especial se llevan Anita y Laura en esos años. La primera por su infinita capacidad de escucha y empatía, que tanto me ayudó en muchos momentos difíciles, y por su dulzura y fortaleza de la que aún intento aprender; la segunda por ser “mi novia”, mi confidente y compañera inseparable de aventuras con su siempre contagiosa vitalidad. De esa misma etapa guardo también un entrañable recuerdo de Sonia Chamizo, que comenzó sus Tesis a la vez que yo y con la que compartí despacho e incertidumbres los dos primeros años. Cuanto nos reímos en

tus campañas de simulación de lluvia o en el SIAGA y qué de veces nos hemos visto en el campo a horas y en condiciones inverosímiles. ¡Gracias guapa por ser un ejemplo en muchos sentidos y por ayudarme siempre que ha estado en tu mano! Mónica Ladrón se unió después a nuestro despacho y con ella también he compartido muchas horas de campo que sin duda no olvidaré nunca, con nuestra sombrilla, nevera y latas de ensalada Calvo para sobrellevar el largo día estival en Balsa Blanca midiendo fotosíntesis.

Hablando de trabajo de campo, sería imposible pasar por alto la labor de Alfredo y Julen, el primero por su inventiva, paciencia y profesionalidad en el diseño de las más imposibles instalaciones de campo. ¡Eres un genio Alfredo! contigo lo imposible se convertía en fácil. A Julen por su entrega y nobleza, por su humor en aquellas largas horas de campo, por estar siempre dispuesto a todo con una sonrisa y un montón de bromas. Era un alivio tenerte con nosotros. También gracias a Penélope Serrano y Enrique Pérez, siempre dispuestos desde Granada a asesorarme y ayudarme con la programación de loggers e instrumentos de los que no sabía ni el nombre al principio.

Este centro está lleno de muchos profesionales, muchos. Durante estos años siempre me he alegrado de decir que todo el personal de nuestro centro es trabajador al máximo y ha sido un placer trabajar con vosotros. Olga Delgado es un claro ejemplo de ello. Como me ayudaste Olga en todas mis estancias... siempre tan ordenada y eficaz en tu cruzada con la Junta de Andalucía, llevándonos por el buen camino como si fuéramos tus pollitos y tú mamá gallina. Todavía recuerdo cómo lloraba contándote que no me podría ir a Australia la segunda vez porque me pedían mil papeles para el visado y como tú, paciente e infinitamente maternal, me ayudaste a buscar traductores, a contratar seguros médicos y todo lo que fue necesario. De verdad mil gracias. Muchos sois de los que me llevo un gran ejemplo de trabajo y profesionalidad: Sebas Vidal, Juan Leiva, Manolo Arrufat, Andrés Castro, Javi Toledo, Enrique Cortés, Ramón Ordiales, Alberto Ruiz.... A todos, muchas gracias por hacer posible que trabajar en este centro haya sido un placer.

Y los años pasaron y nos mudamos al nuevo chumbo y algunos comenzasteis a iros, a Valencia, a Francia, a Italia, a Nueva Zelanda.... pero llegaron refuerzos, y qué refuerzos! Nuria Pistón, Sara Hortal, Christian Schoeb, Yudi Lozano, Meire Telles, Carmen Estruch, Ángela Martínez.... comencé a compartir despacho con Olga Uclés..... y otra vez comenzaron las excursiones, las salidas al Demodé, las fiestas de navidad, las películas en el cineclub.....aunque yo comenzaba a salir menos y a encerrarme más a escribir. Pero era estupendo, llegar al chumbo y saludaros por la mañana, los cafés con bizcocho en la segunda planta, el poder llamar a vuestra puerta en busca de consuelo por mis múltiples agobios que iban "in crescendo". Olguita, has sido la compañera de despacho perfecta, creo que nos hemos ayudado mucho mutuamente con nuestras divagaciones ecológicas y nuestros agobios compartidos. He podido contar siempre contigo para cualquier ayuda de campo que he necesitado, y tenerte enfrente ha sido

crucial en ocasiones, sobre todo cuando quería saltar por la ventana el día de mi depósito de Tesis y tú acudiste en mi ayuda eficaz y resolutive como siempre. Muchas gracias por tu paciencia y por tu compañía, ya sabes, estamos juntas en “el incomprensible mundo de los procesos micro-meteorológicos”. ¡Y que decir de Miriam Amate! cuantas risas en los pasillos, cuanto cariño cuando me encendía la estufa de mi despacho para que al llegar estuviera calentito. A ti, a Luisa y a Marcela, gracias por cuidarnos y hacer de este nuestro segundo hogar.

En esta última etapa los despachos 304, 303 y 302 han sido mi particular triángulo de las Bermudas, iba y venía, a veces como loca, de uno a otro en busca de asesoría y apoyo casi cada día. Cristina Armas (303), gracias, gracias, gracias, por haberme ayudado tanto y de tan diversas maneras en estos últimos 5 meses. Sin tu punto de vista y tu aplomo hubiera sido mucho más difícil. El chumbo pierde un diamante con tu marcha y los chilenos aún no saben lo que se llevan. Eres una profesional como la copa de un pino, una “crack”, absolutamente siempre dispuesta a ayudar a los muchos que tocamos a tu puerta a lo largo del día. Gracias. A Nuria, Carme y Yudi (302)... ¿qué puedo decir? si no he irrumpido en vuestro despacho unas 4 veces al día presa del pánico o en busca de desconexión, es que Dios existe y es mi vecino, ja,ja,ja,ja. Gracias chicas, de verdad, por vuestra paciencia, por vuestra frescura, por vuestra alegría, por vuestra ilusión, por quererme, por echarme a Scooby Doo cantando por la puerta y hacerme reír tanto. Como todas las grandes victorias se hacen esperar y yo no soy una mujer paciente, en los últimos momentos tuve que buscar refuerzos extra para mis ataques de ansiedad y allí estuvieron, Oriol, Miguel Gironés, Meire y Lupe, gracias infinitas, por escucharme, por aconsejarme, por aclararme el camino cuando yo ya no lo veía. Sin todos vosotros hubiera sido imposible.

Además quiero agradecer específicamente a aquellos que me ayudaron a materializar este manuscrito de Tesis, a Alberto Ruiz por hacer milagros con las Figuras y enseñarme como se edita una Tesis siempre dispuesto. A Josep Berenguel, Chico y Sara Hortal por el diseño de esta portada de Tesis hecha con tanto amor, a Gustavo por ayudarme con la paginación, a Yudi, Carmen y Nuria por ayudarme con la bibliografía y el repaso final, a Olga Uclés por socorrerme en la impresión y depósito final. En definitiva GRACIAS a todos mis compañeros del chumbo de esta última fase, por cogerse de mi mano y andar a mi lado este tortuoso camino de final de Tesis. Gracias por vuestros mails, vuestras llamadas y por estar ahí para mí incluso en mis momentos más bajos.

Esta Tesis, además de mucho trabajo y crecimiento personal, me permitió volar allende los mares y conocer gente estupenda que me enseñó lo que es la ciencia fuera de España. I want to thank Helen Cleugh, Philippe Choler and Ray Leuning from CSIRO Australia, for showing me the pleasure to work with the highest professional researchers. It was amazing to discuss with you my scientific doubts and learn from you about Hydrology, model programming and Ecology. Thank you Ray for letting me

learn from your wisdom. I also want to thank Peter Briggs and Kara Youngentob for being my friends in PyeLab and for showing me the natural secrets of Australia. También tuve el placer de pasar unos meses en el Geography and Geology Department de la University of Copenhagen. Thank you Hector Nieto, Simon Proud, Nathalie Van Vilet, Gorka and Rado Guzinski for making my life easy in Denmark, for those field trips and all those football table matches to refresh our boiling scientific minds.

Pero no todo ha sido trabajo durante estos años, y ha habido otros muchos que desde fuera de este loco mundillo científico me habéis ayudado a mantener la perspectiva adecuada, el contacto con la otra realidad. Mi madre y mi padre encabezan este grupo. Esta Tesis de algún modo hizo posible que me quedara en Almería estos seis años y que pudiéramos estar juntos después de muchos años fuera. A ellos tendría todo por agradecerles, pero en especial quiero darles las gracias por apoyarme incondicionalmente, por darme siempre ánimos para seguir en esto que a veces ellos vieron una locura, por intentar ponérmelo siempre fácil para que pudiera centrarme y avanzar. También mis amigos de toda la vida Olga y Nazaret Salmerón, Javi de Las Nieves, Irene Muñoz y Elena Consuegra han hecho mucho. Gracias a todos por escucharme en persona o por teléfono, por tener la paciencia de entender mis largas ausencias, por estar ahí para mí cuando necesitaba evadirme, por estar a mi lado en las duras y en las maduras. También a María Carreño y a Rosa Olivo gracias por esas muchas horas de risas y empatía.

Por último quiero dar las gracias a David Blanco, por haber hecho esto posible. Por haber estado a mi lado en mis horas más críticas, cuando pocos me hubieran aguantado, por animarme cuando yo lo veía todo perdido. Por no pedir nada para él y dármele todo a mí para que pudiera acabar este proyecto. Por quererme tanto y llenar mi vida de comprensión y apoyo ilimitado cuando más lo necesitaba. Por subirse a este loco tren de la ciencia conmigo para mudarnos a Estados Unidos.

Muchos son los que me dejo en el tintero, lo sé, pero sería eterno.... sin embargo creo que aún así, sabéis que lo habéis hecho posible. A los presentes y ausentes en estos agradecimientos, gracias por haberme ayudado a hacer realidad este sueño.

INDICE

INTRODUCCION	1
<i>Importancia de la evapotranspiración</i>	1
<i>La evapotranspiración en ecosistemas áridos y semiáridos.....</i>	2
<i>Sistemas de medida 'in-situ' de la evapotranspiración.....</i>	3
<i>La modelización regional de E en ecosistemas semiáridos.....</i>	4
<i>Objetivos y estructura de la Tesis.....</i>	9
REFERENCIAS	11
CAPITULO 1	15
USING RADIOMETRIC TEMPERATURE FOR SURFACE ENERGY FLUX ESTIMATION IN MEDITERRANEAN DRYLANDS FROM A TWO-SOURCE PERSPECTIVE	
ABSTRACT	16
INTRODUCTION.....	17
MODEL DESCRIPTION	20
MATERIAL AND METHODS.....	26
<i>Study site and field measurements</i>	26
<i>Satellite and airborne campaign data</i>	29
<i>Pre-processing of radiometric measurements</i>	30
<i>Model validation.....</i>	32
<i>Analysis of spatial heterogeneity.....</i>	33
RESULTS	35
<i>Analyses of spatial heterogeneity</i>	35
<i>Series vs. parallel original TSM version</i>	36
<i>Evaluating the iteration procedure included in the original TSM.....</i>	41
DISCUSSION	43
<i>Accuracy of the TSM for surface flux estimation under Mediterranean semiarid conditions</i>	43
<i>Practical aspects for use of the TSM in Mediterranean drylands</i>	45
CONCLUSIONS	48
REFERENCES.....	49
CAPITULO 2	55
ENVIRONMENTAL FACTORS AFFECTING THE ACCURACY OF SURFACE FLUXES FROM A TWO-SOURCE MODEL IN MEDITERRANEAN DRYLANDS: UPSCALING INSTANTANEOUS TO DAYTIME ESTIMATES	
ABSTRACT	56
INTRODUCTION.....	57
EXPERIMENTAL DATASET AND FIELD SITE MEASUREMENTS.....	59
METHODS	61
<i>Analyzing the diurnal behaviour of the TSM.....</i>	61
<i>Assessing model response to environmental factors.....</i>	62
<i>Extrapolation from instantaneous to daytime fluxes</i>	64
RESULTS	66
<i>Diurnal behaviour of the TSM.....</i>	66
<i>TSM response under different environmental conditions</i>	68
<i>Daytime fluxes extrapolation from instantaneous values</i>	72
DISCUSSION	75
<i>Diurnal behaviour of the TSM.....</i>	75
<i>TSM response under different environmental conditions</i>	75
<i>Daytime fluxes extrapolation from instantaneous values</i>	77
CONCLUSIONS	79
REFERENCES.....	80

CAPITULO 3	83
IMPROVING EVAPOTRANSPIRATION ESTIMATES IN MEDITERRANEAN DRYLANDS: THE ROLE OF SOIL EVAPORATION.....	83
ABSTRACT	84
INTRODUCTION.....	85
MODEL DESCRIPTION	87
<i>Penman-Monteith-Leuning model (PML) description.....</i>	87
<i>Methods for f estimation.....</i>	89
MATERIAL AND METHODS.....	91
<i>Validation field sites and measurements</i>	91
<i>Remotely sensed data</i>	93
<i>Model performance evaluation.....</i>	94
RESULTS	95
DISCUSSION	101
CONCLUSIONS	104
REFERENCES.....	105
CAPITULO 4	109
ACTUAL EVAPOTRANSPIRATION IN DRYLANDS DERIVED FROM IN-SITU AND SATELLITE DATA: ASSESSING BIOPHYSICAL CONSTRAINTS.....	109
ABSTRACT	110
INTRODUCCION	111
FIELD SITES AND DATA.....	114
<i>Sahelian Open Woody Savannah site</i>	115
<i>Mediterranean grassland site.....</i>	116
<i>Satellite Data.....</i>	118
METHODS	119
<i>PT-JPL-daily Model Description</i>	119
<i>Global sensitivity analyses (EFAST) approach.....</i>	123
<i>Evaluation of the PT-JPL-daily evapotranspiration model.....</i>	124
RESULTS AND DISCUSSION.....	126
<i>Global Sensitivity Analyses (EFAST) approach.....</i>	126
<i>Evaluation of the PT-JPL-daily evapotranspiration model with Eddy Covariance data.....</i>	127
<i>Comparison with other Evapotranspiration Models in Global Dryland Ecosystems.....</i>	137
CONCLUSIONS	141
REFERENCES.....	143
CONCLUSIONES GENERALES	151

INTRODUCCION

Dada la importancia cuantitativa y funcional de la evapotranspiración en zonas semiáridas, su estimación regional es crucial para la gestión hídrica de las mismas (Glenn et al. 2007) así como para la comprensión de la mayor parte de procesos biológicos asociados a la disponibilidad hídrica en estos ambientes, (Noy-Meir 1973). Sin embargo, el desarrollo de modelos para la estimación regional de la evapotranspiración basados en datos facilitados mediante teledetección, es aún escaso en zonas semiáridas. En esta Tesis profundizaremos en el conocimiento de las vías metodológicas óptimas para la cuantificación regional de la evapotranspiración en ecosistemas semiáridos mediante la evaluación y reformulación de aquellos modelos que presentan un mayor potencial en este tipo de ambientes.

Importancia de la evapotranspiración

La evapotranspiración (E), definida como la transferencia total de agua desde una superficie vegetada a la atmósfera, es fruto de dos procesos simultáneos: i) la evaporación o proceso físico de transferencia de agua de las superficies, incluyendo el agua de lluvia interceptada por la vegetación, a la atmósfera, y ii) la transpiración o proceso fisiológico vegetal por el que el agua absorbida por medio de las raíces se transfiere a la atmósfera a través de los estomas. La energía que acompaña la evapotranspiración se conoce como calor latente, λE (también escrito LE), donde λ es el calor latente de vaporización. En esta Tesis E , λE (o LE) se usarán para referir al mismo proceso, según éste sea considerado desde el punto de vista hídrico (E) o desde el punto de vista energético (λE o LE).

De este modo la evapotranspiración es el elemento común entre el balance hídrico y energético de la superficie terrestre, ambos resumidos en las ecuaciones 1 y 2 respectivamente:

$$P = E + R + Gr + \Delta S + L \quad (1)$$

$$Rn = LE + H + G \quad (2)$$

En la ecuación 1, P es la precipitación, R la escorrentía superficial, Gr la variación de la reserva hídrica subterránea, ΔS es la variación en la reserva de agua del suelo y L la entrada o

salida de escorrentía lateral (todas ellas en mm). En la ecuación 2, Rn es la radiación neta, G es el calor transmitido al suelo, H es el calor sensible (todas ellas en $W m^{-2}$).

La evapotranspiración es la componente mas importante del balance hídrico terrestre después de la precipitación (Leuning et al. 2008). En promedio, el 57% de la precipitación global es devuelta a la atmósfera por este medio (Glenn et al. 2007) y tres quintas partes de la radiación neta terrestre son usadas en forma de calor latente, con estimas provenientes de distintos modelos variando entre el 48 al 88% (Trenberth et al. 2009). Debido a su vinculación con el balance hídrico y energético, E repercute en el enfriamiento de la superficie terrestre y en la formación de nubes. La evapotranspiración es, por tanto, un factor clave en la interacción entre la superficie terrestre y la atmósfera (Domingo et al. 2004) pudiendo afectar al clima a escala local y regional (Kustas & Norman 1996). Por todo ello, E es uno de los componentes fundamentales a considerar en la modelización del cambio climático, balance hídrico, productividad primaria, inundaciones y sequías (Fisher et al. 2008).

La evapotranspiración en ecosistemas áridos y semiáridos

En zonas áridas y semiáridas, la importancia de E se amplifica ya que, en ellas, dicho proceso devuelve a la atmósfera entre el 90 y 100% de la precipitación anual (Glenn et al. 2007). Las zonas áridas y semiáridas existen en todos los continentes y cubren más del 45% de la superficie terrestre (Asner et al. 2003; Schlesinger et al. 1990). Estas regiones mantienen al 37% de la población humana, estando previsto, según la tendencia del cambio climático, un aumento de la aridez (Reynolds et al. 2007). Específicamente, las zonas semiáridas son las que ocupan mayor superficie siendo éstas muy sensibles a perturbaciones tales como cambio climático, fuego, sequía o cambios de uso del suelo (Safriel et al. 2003). Es por ello que el conocimiento del intercambio hídrico entre la superficie y la atmósfera es especialmente crucial en dichas áreas.

Las áreas semiáridas, son extremadamente dinámicas con una variabilidad interanual de las precipitaciones de $\pm 23-30\%$ de la media a largo plazo (Rasmusson 1987). En ellas el patrón temporal y espacial de E , estrechamente ligado la disponibilidad hídrica, presenta particularidades específicas. En zonas semiáridas la disponibilidad hídrica suele presentar una dinámica pulsátil debido al régimen irregular de las precipitaciones (Schwinning et al. 2004). El carácter generalmente disperso de la vegetación y la marcada heterogeneidad superficial de las áreas semiáridas (Puigdefabregas et al. 1999) determina las fluctuaciones temporales y

espaciales de la disponibilidad hídrica repercutiendo en el patrón espacio-temporal de E (Villagarcía et al. 2010). Además es importante considerar que en áreas semiáridas existe una fuerte conexión entre los ciclos de agua y carbono (Baldocchi 2008; Domingo et al. 2011) ya que la disponibilidad hídrica es el principal factor de control sobre la actividad biológica (Brogaard et al. 2005) lo que afecta al control que la vegetación ejerce sobre la componente transpirativa de E .

La correcta estimación de E en áreas semiáridas es vital para la gestión hídrica de las mismas, el estudio de la recarga de acuíferos, el estudio del efecto de los cambios de uso del suelo sobre el balance hídrico así como para determinar si en dichas áreas la vegetación es capaz de acceder a fuentes de agua alternativas a la precipitación (Villagarcía et al. 2010). El desarrollo de métodos para la estimación de E a escala de paisaje en dichas áreas es, por tanto, un área de investigación prioritaria. Especialmente si consideramos la dificultad y coste de las mediciones de dicho proceso en zonas semiáridas que ocupan áreas de gran extensión a menudo remotas (Domingo et al. 1999). La teledetección es la única fuente capaz de proporcionar datos espacialmente distribuidos del estado hídrico y energético de la superficie así como de sus propiedades biofísicas (Kustas & Norman 1996) y por lo tanto, la única vía factible hasta ahora para la estimación de E a escalas regionales con un razonable grado de exactitud (Kalma et al. 2008).

Sistemas de medida 'in-situ' de la evapotranspiración

En los últimos años, se han desarrollado múltiples métodos para la medición in-situ de E (ver revisiones en Glenn et al. 2007; Rana & Katerji 2000; Shuttleworth 2007; Verstraeten et al. 2008) lo que a su vez ha posibilitado el avance en la modelización regional dada la necesidad de medidas fiables para la validación y evaluación de los modelos basados en teledetección. Entre los sistemas de medida, los más ampliamente usados para la validación de modelos han sido los lisímetros de precisión, los métodos de medición de flujos micro-meteorológicos (método de la razón de Bowen y el método de correlación de remolinos o *Eddy Covariance (EC)*) y los métodos hidrológicos basados en el balance hídrico de superficie. Los métodos hidrológicos están principalmente enfocados a la estimación regional de E a escalas temporales largas (mensual, anual, interanual) y precisan de datos rigurosos de precipitación y escorrentía (Wang & Dickinson 2012). Los lisímetros de precisión ofrecen medidas continuas con un alto grado de exactitud (Howell et al. 1995) sin embargo están limitadas a varios metros cuadrados (Wang & Dickinson 2012) y su aplicación en áreas de vegetación natural es problemática debido a la

variabilidad y mayor profundidad de sus sistemas radiculares (Glenn et al. 2007). Por su parte los métodos de flujos micro meteorológicos, ofrecen medidas en continuo a escalas espaciales medias (alrededor de 1 km²) (Horst 1999; Kljun et al. 2004) comparables con la resolución ofrecida por los sistemas de teledetección (Glenn et al. 2007). Por ello, finalmente la técnica de correlación de remolinos se ha convertido en el estándar para la medida en superficie de los flujos de vapor de agua (Baldocchi 2003; Scott 2010) y el principal medio para la validación y evaluación de métodos de estimación regional de E (Glenn et al. 2007). Actualmente se ha creado una serie de redes de medición de E mediante EC alrededor del mundo como parte del programa FLUXNET (Baldocchi et al. 2001) que incluye instalaciones en Europa (CarboEurope), Norteamérica (Ameriflux y Fluxnet_Cánada), Brasil, Asia (AsiaFlux), Australia (OzFlux) y África. Hasta hace pocos años las mediciones de E mediante EC en áreas semiáridas eran escasas estando la mayor parte de las estaciones de medición ubicadas en áreas forestales o agrícolas. Sin embargo durante los últimos años el interés de la “comunidad FLUXNET” por las áreas semiáridas se ha intensificado (FluxLetter 2010) con la consiguiente ampliación de la red de mediciones en zonas semiáridas lo que posibilita el desarrollo de la modelización regional de E en dichas áreas (Domingo et al. 2011).

La modelización regional de E en ecosistemas semiáridos

Desde los años 80, coincidiendo con el comienzo de las aplicaciones de la teledetección, la visión científica general se ha volcado en el desarrollo de métodos para la cuantificación de E a escala de paisaje debido a la importancia de su variabilidad espacial (Kalma et al. 2008). Muchos de los modelos de estimación de E se han desarrollado, sin embargo, en regiones templadas del mundo siendo aún escaso su desarrollo en ecosistemas áridos y semiáridos. Esto se debe en parte, a que las particularidades propias de estos ecosistemas hacen especialmente difícil la modelización de E empleando datos remotos.

La magnitud de E en ecosistemas semiáridos es generalmente baja presentando aumentos puntuales tras los pulsos de lluvia (D’Odorico & Porporato 2006). Para modelizar el patrón pulsátil que presenta E en estas condiciones se requieren datos a una escala temporal diaria o superior que solo algunos sensores remotos ofrecen, como MODIS (*Moderate Resolution Imaging Spectrometer*) o SEVIRI (*Spinning Enhanced Visible Infrared Imager*), a costa de una resolución espacial inferior (1-3 km) (Domingo et al. 2011). En áreas semiáridas mediterráneas en las que la disponibilidad hídrica y energética presentan asincronía temporal (Serrano-Ortiz et al. 2007) E puede alcanzar magnitudes similares al error promedio que afecta a los modelos

basados en teledetección ($\sim 0.8 \text{ mm día}^{-1}$, Seguin et al. 1999) lo que dificulta su estimación (Domingo et al. 2011). Otra particularidad es que en estas áreas en las que la vegetación suele ser dispersa y agregada, el suelo y la vegetación responden a factores de control diferentes y presentan dinámicas distintas. Mientras la evaporación del suelo (E_s) ocurre principalmente durante e inmediatamente después de la precipitación empleando el agua de las capas superficiales del suelo, la transpiración por parte de la vegetación (E_c) sucede de un modo más progresivo empleando agua de capas más profundas y depende tanto del control biológico como de la radiación solar (Wang & Dickinson 2012).

Para la modelización de E en áreas heterogéneas con vegetación dispersa, como las semiáridas, suelen emplearse modelos multifuente que describen el intercambio de los flujos turbulentos, H y LE , entre la superficie y la atmósfera a través de un símil eléctrico controlado mediante un sistema de resistencias aerodinámicas y superficiales (Lhomme et al. 2012). En su versión más sencilla, éstos dividen la superficie en dos componentes (modelos de dos fuentes): suelo y vegetación. Los modelos de dos fuentes fueron propuestos para mejorar la modelización de E mediante teledetección en áreas de vegetación dispersa (Wang & Dickinson 2012) ya que permiten la consideración de los procesos diferenciales que afectan a ambos componentes. Así, los modelos de dos fuentes han resultado en mejores estimaciones de E en áreas semiáridas que los modelos mono-fuente, que asumen la superficie como un dosel vegetal continuo y homogéneo, (Anderson et al. 2007; Norman et al. 1995). Además, este tipo de modelos aportan una información más detallada de los flujos en superficie ya que permiten cuantificar la partición de E , entre suelo (E_s) y vegetación (E_c), que ha sido señalada como un factor de vital importancia para la comprensión de las dinámicas de la vegetación en sistemas áridos y semiáridos (Huxman et al. 2005). Por todo ello en esta Tesis nos centraremos en la evaluación de modelos que permitan esta perspectiva multifuente.

Son muchos los modelos desarrollados en los últimos años para la estimación regional de E utilizando datos de teledetección (ver revisiones en Courault et al. 2005; Glenn et al. 2007; Kalma et al. 2008; Kustas & Norman 1996; Li et al. 2009). A grandes rasgos y en el marco de esta Tesis podemos distinguir dos tipos de modelos para la estimación de E empleando datos de teledetección : i) Modelos residuales que obtienen LE como un residuo de la ecuación del balance energético (Ec. 2) mediante estimación de las restantes variables de la ecuación (Rn , G y H) y ii) Modelos directos que estiman LE de forma directa mediante la caracterización de las resistencias superficiales que rigen el flujo de vapor de agua entre la superficie y la atmósfera.

Los modelos residuales han sido hasta ahora los modelos mas populares para la estimación de E en áreas semiáridas (Garcia et al. 2007; Domingo et al. 2011). Estos modelos se basan en la estimación directa del calor sensible, H , mediante la denominada “*ecuación de resistencia global para la transferencia de calor*” (Brutsaert 1982) según la cual H depende del gradiente térmico entre la superficie y el aire, así como de la resistencia aerodinámica que dificulta la transferencia de calor desde la superficie a la atmósfera. Uno de los modelos residuales mas robustos para estimar E bajo una perspectiva multifuente y que mejores resultados ha demostrado en condiciones extremas (Kustas & Anderson 2009; Zhan et al. 1996) es el modelo de dos fuentes de Norman et al. (1995), conocido como *Two-source model* (TSM). La formulación del TSM ha sido evaluada con éxito en áreas de vegetación dispersa (Kustas y Norman, 1999) y áreas semiáridas (Timmermans et al. 2007) aunque principalmente bajo condiciones de irrigacion (Colaizzi et al. 2012; French et al. 2007; Gonzalez-Dugo et al. 2009). La aplicación del TSM precisa la temperatura superficial de las dos fuentes, suelo (T_s) y vegetación (T_c), mientras que la resolución espacial de los sensores remotos actuales es aún demasiado grosera para distinguir entre ambas, ofreciendo, en la mayoría de los casos, una temperatura superficial agregada de ambas (T_R). Para solventar esta limitación el TSM incluye un proceso iterativo (Norman et al. 1995), basado en la estimación de un valor inicial de T_c asumiendo que ésta transpira a su nivel potencial (Priestley & Taylor 1972). Dicho valor inicial de T_c se recalcula en caso de que el balance energético (Ec. 2) no se cumpla. Este proceso iterativo y las asunciones en las que se basa no han sido probados en áreas con fuertes limitaciones hídricas en las que la transpiración potencial raramente se alcanza. Aunque existen dos formulaciones posibles del TSM, con resistencias *en serie* o *en paralelo*, en función de si se asume o no interacción entre las temperaturas de vegetación y suelo, no está claro cual de las dos es más eficaz en condiciones semiáridas naturales. Un problema adicional que afecta a los modelos residuales, como el TSM, aplicados a partir de datos remotos, es que H y por tanto LE , puede ser calculado únicamente a escala instantánea ya que la formulación para el cálculo de H no permite su aplicación con datos de temperatura promediados a escala diaria o superior. Sin embargo para muchas aplicaciones datos de LE son requeridos a escalas diarias, diurnas o superiores para lo que se emplean métodos de extrapolación temporal que a su vez conllevan cierto error asociado (Glenn et al. 2007).

Los modelos directos, por su parte, estiman LE de forma directa mediante la ecuación de Penman Monteith (Monteith 1964) o alguna de sus simplificaciones como la ecuación de Priestley-Taylor (Priestley & Taylor 1972). La ecuación de Penman-Monteith (ecuación PM)

considera que el flujo de vapor de agua (LE) desde una superficie vegetada está determinado por la energía disponible y el déficit de presión de vapor y que dicho flujo está restringido fundamentalmente por la resistencia superficial que opone la superficie vegetada al paso de vapor de agua, aunque también por una resistencia aerodinámica. El parámetro clave para la aplicación de la ecuación PM es la resistencia superficial, especialmente en áreas semiáridas, en donde ésta es mucho mayor que la resistencia aerodinámica (Leuning et al. 2008; Were et al. 2007). Uno de los primeros modelos que aplicó de forma regional la ecuación de PM empleando datos de teledetección propuso una relación empírica de la resistencia superficial con el índice de área foliar ofrecido por el sensor MODIS (Cleugh et al. 2007). Este trabajo dio lugar a una línea de modelización regional de E que evolucionó hacia una perspectiva multifuente mediante la consideración de los factores que afectan, tanto al suelo como a la vegetación, para la estimación de la resistencia superficial del sistema (Leuning et al. 2008; Mu et al. 2007; Zhang et al. 2010). Leuning et al. (2008) propusieron un modelo de aplicación regional, conocido como *Penman-Monteith-Leuning model* (PML), en el que la componente transpirativa se modeliza en base a la radiación absorbida y el déficit de presión de vapor, mientras que la evaporación del suelo se considera una fracción constante de su tasa de evaporación en equilibrio. Dicho modelo precisa de datos meteorológicos de amplia disponibilidad y del índice de área foliar procedente de teledetección, así como dos parámetros que pueden obtenerse mediante optimización: la conductancia máxima de las hojas (g_{sx}) y la humedad del suelo (f) que controla la evaporación del suelo y que se considera constante. El modelo PML presentó buenos resultados en áreas de muy diferente clima y tipo de vegetación incluyendo áreas de vegetación dispersa tipo sabana. Aún así, la eficacia del modelo fue inferior en áreas más secas debido a la consideración del parámetro f constante (Leuning et al. 2008).

Fisher et al. (2008) propusieron una vía alternativa para la estimación directa de E empleando la ecuación de Priestley-Taylor (ecuación PT) (Priestley & Taylor 1972). Dicha ecuación permite la estimación regional de E en equilibrio, aquella que tiene lugar en condiciones ideales de disponibilidad hídrica y atmósfera saturada, reemplazando las resistencias superficiales y aerodinámicas por un factor constante conocido como constante de Priestley-Taylor (Zhang et al. 2009). El modelo propuesto por Fisher et al. (2008), al que nos referiremos como *Priestley-Taylor-Jet Propulsion Laboratory model* (modelo PT-JPL), emplea una serie de parámetros biofísicos limitadores que reducen la tasa de E en equilibrio hasta su tasa real en función de las condiciones de la superficie. El modelo distingue entre los factores que afectan al suelo y a la vegetación bajo una perspectiva multifuente y fue diseñado para estimar E a escala

mensual. El modelo PT-JPL presentó buenos resultados en 36 áreas de la red FLUXNET bajo diferentes condiciones climáticas y tipos de vegetación mostrando mejores resultados en áreas hídricamente limitadas que otros modelos previos (Fisher et al. 2008; 2009). La principal fortaleza del modelo PT-JPL es que presenta una gran potencialidad para aplicaciones globales dada su sencillez y por estar basado mayoritariamente en datos procedentes de sensores remotos (índices de vegetación, radiación neta, radiación PAR absorbida) (García et al. 2013). Sin embargo dos aspectos limitan aún su aplicabilidad: i) la resolución temporal de sus estimas (mensual), que resulta demasiado grosera para muchas aplicaciones y ii) su dependencia de ciertos datos que aún no ofrecen los sensores remotos, como son la humedad relativa y el déficit de presión de vapor, necesarios para determinar el parámetro biofísico que controla la evaporación del suelo.

Objetivos y estructura de la Tesis

A pesar del gran desarrollo que la modelización regional de E ha tenido durante los últimos años, pocos son los modelos diseñados y puestos a prueba en áreas semiáridas naturales con fuertes limitaciones hídricas en donde la modelización de la evapotranspiración es aún un reto. En esta Tesis abordaremos diversas cuestiones teóricas y prácticas en relación al desarrollo de modelos de estimación de la evapotranspiración bajo estas condiciones extremas. Gran parte del trabajo se realiza en áreas semiáridas mediterráneas del sureste español en donde en los últimos años se han instalado diversas estaciones meteorológicas que incluyen sistemas de medición de flujos micro meteorológicos mediante EC (Domingo et al. 2011). Haciendo uso de las mediciones in-situ facilitadas en dichas estaciones, evaluaremos tres modelos de estimación de la evapotranspiración de aplicabilidad regional, un modelo residual (*Two-source model*, TSM) y dos modelos directos (*Penman-Monteith-Leuning model*, PML y *Priestley-Taylor-Jet Propulsion Laboratory model*, PT-JPL). Estos modelos han demostrado gran potencial para su aplicación en áreas semiáridas de vegetación dispersa pero no han sido probados aún bajo condiciones tan extremas de estrés hídrico como las estudiadas en la presente Tesis. Así mismo, desarrollaremos diversas modificaciones de la formulación original de dichos modelos, para mejorar su eficacia en ecosistemas naturales semiáridos de vegetación dispersa.

Los objetivos específicos de esta Tesis abordados en los cuatro siguientes capítulos son:

1) Evaluar la eficacia de un modelo residual (TSM) a escala instantánea (estimaciones de H y LE cada 15 min) en condiciones semiáridas naturales mediterráneas y determinar como sus dos formulaciones posibles, con resistencias *en serie* o *en paralelo*, responden ante dichas condiciones (Capítulo 1).

2) Determinar los principales factores que afectan a la eficacia del un modelo residual (TSM) para ofrecer estimas instantáneas en condiciones semiáridas naturales mediterráneas y determinar la capacidad de este tipo de modelos para obtener valores diarios de H y LE mediante métodos de extrapolación temporal (Capítulo 2).

3) Evaluar la eficacia de un modelo directo (PML) para estimar valores diarios de LE en áreas naturales semiáridas mediante la reformulación del parámetro f como una variable temporal dependiente de los cambios en la humedad del suelo (Capítulo 3).

4) Evaluar y adaptar un modelo directo (PT-JPL) para estimar LE a escala diaria en vez de mensual y reformular el parámetro biofísico que controla la evaporación del suelo basado exclusivamente en datos remotos de temperatura superficial y albedo (Capítulo 4).

REFERENCIAS

- Anderson, M.C., Norman, J.M., Mecikalski, J.R., Otkin, J.A., & Kustas, W.P. (2007). A climatological study of evapotranspiration and moisture stress across the continental United States based on thermal remote sensing: 1. Model formulation. *Journal of Geophysical Research D: Atmospheres*, 112, D10117
- Asner, G.P., Borghi, C.E., & Ojeda, R.A. (2003). Desertification in Central Argentina: Changes in ecosystem carbon and nitrogen from imaging spectroscopy. *Ecological Applications*, 13, 629-648
- Baldocchi, D.D. (2003). Assessing the eddy covariance technique for evaluating carbon dioxide exchange rates of ecosystems: past, present and future. *Global Change Biology*, 9, 479-492
- Baldocchi, D.D. (2008). Turner review No. 15. 'Breathing' of the terrestrial biosphere: Lessons learned from a global network of carbon dioxide flux measurement systems. *Australian Journal of Botany*, 56(1), 1-26
- Baldocchi, D.D., Falge, E., Gu, L., Olson, R., Hollinger, D., Running, S., Anthoni, P., Bernhofer, C., Davis, K., Evans, R., Fuentes, J., Goldstein, A., Katul, G., Law, B., Lee, X., Malhi, Y., Meyers, T., Munger, W., Oechel, W., Paw, U.K.T., Pilegaard, K., Schmid, H.P., Valentini, R., Verma, S., Vesala, T., Wilson, K., & Wofsy, S. (2001). FLUXNET: A New Tool to Study the Temporal and Spatial Variability of Ecosystem-Scale Carbon Dioxide, Water Vapor, and Energy Flux Densities. *Bulletin of the American Meteorological Society*, 82, 2415-2434
- Brogaard, S., Runnström, M., & Seaquist, J.W. (2005). Primary production of Inner Mongolia, China, between 1982 and 1999 estimated by a satellite data-driven light use efficiency model. *Global and Planetary Change*, 45, 313-332
- Brutsaert, W. (1982). Evaporation into the atmosphere-Theory, history, and applications. Dordrecht, Holland: D. Reidel Publishing Company, pp.299.
- Cleugh, H.A., Leuning, R., Mu, Q., & Running, S.W. (2007). Regional evaporation estimates from flux tower and MODIS satellite data. *Remote Sensing of Environment*, 106, 285-304
- Colaizzi, P.D., Kustas, W.P., Anderson, M.C., Agam, N., Tolk, J.A., Evett, S.R., Howell, T.A., Gowda, P.H., & O'Shaughnessy, S.A. (2012). Two-source energy balance model estimates of evapotranspiration using component and composite surface temperatures. *Advances in Water Resources*, 50, 134-151
- Courault, D., Seguin, B., & Olioso, A. (2005). Review on estimation of evapotranspiration from remote sensing data: From empirical to numerical modeling approaches. *Irrigation and Drainage Systems*, 19, 223-249
- D'Odorico, P., & Porporato, A. (2006). Ecohydrology of arid and semiarid ecosystems: an Introduction. In: P. D'Odorico, A. Porporato A. (Ed) *Dryland Ecohydrology*, (pp. 4-10). The Netherlands: Springer
- Domingo, F., Serrano-Ortiz, P., Were, A., Villagarcía, L., García, M., Ramírez, D.A., Kowalski, A.S., Moro, M.J., Rey, A., & Oyonarte, C. (2011). Carbon and water exchange in semiarid ecosystems in SE Spain. *Journal of Arid Environments*, 75, 1271-1281
- Domingo, F., Villagarcía, L., Brenner, A.J., & Puigdefábregas, J. (1999). Evapotranspiration model for semi-arid shrub-lands tested against data from SE Spain. *Agricultural and Forest Meteorology*, 95, 67-84

- Domingo, F., Villagarcía, L., & Were, A. (2004). ¿Como se puede medir y estimar la evapotranspiración? Estado actual y evolución. *Ecosistemas*, 4, 1-15
- Fisher, J.B., Malhi, Y., Bonal, D., Da Rocha, H.R., De Araújo, A.C., Gamo, M., Goulden, M.L., Rano, T.H., Huete, A.R., Kondo, H., Kumagai, T., Loescher, H.W., Miller, S., Nobre, A.D., Nouvellon, Y., Oberbauer, S.F., Panuthai, S., Rouspard, O., Saleska, S., Tanaka, K., Tanaka, N., Tu, K.P., & Von Randow, C. (2009). The land-atmosphere water flux in the tropics. *Global Change Biology*, 15, 2694-2714
- Fisher, J.B., Tu, K.P., & Baldocchi, D.D. (2008). Global estimates of the land-atmosphere water flux based on monthly AVHRR and ISLSCP-II data, validated at 16 FLUXNET sites. *Remote Sensing of Environment*, 112, 901-919
- FluxLetter 2010. Vol. 2 N° 4 – January.
- French, A.N., Hunsaker, D.J., Clarke, T.R., Fitzgerald, G.J., Luckett, W.E., & Pinter Jr, P.J. (2007). Energy balance estimation of evapotranspiration for wheat grown under variable management practices in central Arizona. *Transactions of the ASABE*, 50, 2059-2071
- García, M., Villagarcía, L., Contreras, S., Domingo, F., & Puigdefábregas, J. (2007). Comparison of three operative models for estimating the surface water deficit using ASTER reflective and thermal data. *Sensors*, 7, 860-883
- García, M., Sandholt, I., Ceccato, P., Ridler, M., Mougin, E., Kergoat, L., Morillas, L., Timouk, F., Fensholt, R., & Domingo, F. (2013). Actual evapotranspiration in drylands derived from in-situ and satellite data: Assessing biophysical constraints. *Remote Sensing of Environment*, 131, 103-118
- Glenn, E.P., Huete, A.R., Nagler, P.L., Hirschboeck, K.K., & Brown, P. (2007). Integrating remote sensing and ground methods to estimate evapotranspiration. *Critical Reviews in Plant Sciences*, 26, 139-168
- Gonzalez-Dugo, M.P., Neale, C.M.U., Mateos, L., Kustas, W.P., Prueger, J.H., Anderson, M.C., & Li, F. (2009). A comparison of operational remote sensing-based models for estimating crop evapotranspiration. *Agricultural and Forest Meteorology*, 149, 1843-1853
- Horst, T.W. (1999). The footprint for estimation of atmosphere-surface exchange fluxes by profile techniques. *Boundary-Layer Meteorology*, 90, 171-188
- Howell, T.A., Schneider, A.D., Dusek, D.A., Marek, T.H., & Steiner, J.L. (1995). Calibration and scale performance of Bushland weighing lysimeters. *Transactions - American Society of Agricultural Engineers*, 38, 1019-1024
- Huxman, T.E., Wilcox, B.P., Breshears, D.D., Scott, R.L., Snyder, K.A., Small, E.E., Hultine, K., Pockman, W.T., & Jackson, R.B. (2005). Ecohydrological implications of woody plant encroachment. *Ecology*, 86, 308-319
- Kalma, J.D., McVicar, T.R., & McCabe, M.F. (2008). Estimating land surface evaporation: A review of methods using remotely sensed surface temperature data. *Surveys in Geophysics*, 29, 421-469
- Kljun, N., Calanca, P., Rotach, M.W., & Schmid, H.P. (2004). A simple parameterisation for flux footprint predictions. *Boundary-Layer Meteorology*, 112, 503-523
- Kustas, W., & Anderson, M. (2009). Advances in thermal infrared remote sensing for land surface modeling. *Agricultural and Forest Meteorology*, 149, 2071-2081
- Kustas, W.P., & Norman, J.M. (1996). Use of remote sensing for evapotranspiration monitoring over land surfaces. *Hydrological Sciences Journal*, 41, 495-516

- Leuning, R., Zhang, Y.Q., Rajaud, A., Cleugh, H., & Tu, K. (2008). A simple surface conductance model to estimate regional evaporation using MODIS leaf area index and the Penman-Monteith equation. *Water Resources Research*, *44*, W10419
- Lhomme, J.P., Montes, C., Jacob, F., & Prévot, L. (2012). Evaporation from heterogeneous and sparse canopies: On the formulations related to multi-source representations. *Boundary-Layer Meteorology*, *144*, 243-262
- Li, Z.L., Tang, R., Wan, Z., Bi, Y., Zhou, C., Tang, B., Yan, G., & Zhang, X. (2009). A review of current methodologies for regional evapotranspiration estimation from remotely sensed data. *Sensors*, *9*, 3801-3853
- Monteith, J.L. (1964). Evaporation and environment. In: *The state and movement of water in living organisms. Symposium of society of experimental biology*, Vol 19 (pp. 205-234). Swansea, UK: Cambridge University Press.
- Mu, Q., Heinsch, F.A., Zhao, M., & Running, S.W. (2007). Development of a global evapotranspiration algorithm based on MODIS and global meteorology data. *Remote Sensing of Environment*, *111*, 519-536
- Norman, J.M., Kustas, W.P., & Humes, K.S. (1995). Source approach for estimating soil and vegetation energy fluxes in observations of directional radiometric surface temperature. *Agricultural and Forest Meteorology*, *77*, 263-293
- Noy-Meir, I. (1973). Desert ecosystems: environment and producers. *Annual Reviews*, *4*, 25-51
- Priestley, C.H.B., & Taylor, R.J. (1972). On the assessment of surface heat flux and evaporation using large-scale parameters. *Monthly Weather Review*, *100*, 81-92
- Puigdefabregas, J., Sole, A., Gutierrez, L., Del Barrio, G., & Boer, M. (1999). Scales and processes of water and sediment redistribution in drylands: Results from the Rambla Honda field site in Southeast Spain. *Earth Science Reviews*, *48*, 39-70
- Rana, G., & Katerji, N. (2000). Measurement and estimation of actual evapotranspiration in the field under Mediterranean climate: A review. *European Journal of Agronomy*, *13*, 125-153
- Rasmusson, E.M. (1987). Global climate change and variability: effects on drought and desertification in Africa. *Drought and hunger in Africa*, 3-22
- Reynolds, J.F., Stafford Smith, D.M., Lambin, E.F., Turner II, B.L., Mortimore, M., Batterbury, S.P.J., Downing, T.E., Dowlatabadi, H., Fernández, R.J., Herrick, J.E., Huber-Sannwald, E., Jiang, H., Leemans, R., Lynam, T., Maestre, F.T., Ayarza, M., & Walker, B. (2007). Ecology: Global desertification: Building a science for dryland development. *Science*, *316*, 847-851
- Safriel, U., Adeel, Z., Niemeijer, D., Puigdefábregas, J., White, R., Lal, R., Winslow, M., Ziedler, J., Prince, S., Archer, E., & King, C. (2003). Dryland systems. In: R. Hassan, R. Scholes, and N. Ash (Ed) *Ecosystems and human well-being: Current state and trends*, Vol 1 (pp. 623-662). Washington D.C, USA: Island Press
- Scott, R.L. (2010). Using watershed water balance to evaluate the accuracy of eddy covariance evaporation measurements for three semiarid ecosystems. *Agricultural and Forest Meteorology*, *150*, 219-225
- Schlesinger, W.H., Reynolds, J.F., Cunningham, G.L., Huenneke, L.F., Jarrell, W.M., Virginia, R.A., & Whitford, W.G. (1990). Biological feedbacks in global desertification. *Science*, *247*, 1043-1048

- Schwinning, S., Sala, O.E., Loik, M.E., & Ehleringer, J.R. (2004). Thresholds, memory, and seasonality: Understanding pulse dynamics in arid/semi-arid ecosystems. *Oecologia*, *141*, 191-193
- Seguin, B., Becker, F., Phulpin, T., Gu, X.F., Guyot, G., Kerr, Y., King, C., Lagouarde, J.P., Ottlé, C., Stoll, M.P., Tabbagh, A., & Vidal, A. (1999). IRSUTE: A Minisatellite Project for Land Surface Heat Flux Estimation from Field to Regional Scale. *Remote Sensing of Environment*, *68*, 357-369
- Serrano-Ortiz, P., Kowalski, A.S., Domingo, F., Rey, A., Pegoraro, E., Villagarcía, L., & Alados-Arboledas, L. (2007). Variations in daytime net carbon and water exchange in a montane shrubland ecosystem in southeast Spain. *Photosynthetica*, *45*, 30-35
- Shuttleworth, W.J. (2007). Putting the 'vap' into evaporation. *Hydrology and Earth System Sciences*, *11*, 210-244
- Timmermans, W.J., Kustas, W.P., Anderson, M.C., & French, A.N. (2007). An intercomparison of the Surface Energy Balance Algorithm for Land (SEBAL) and the Two-Source Energy Balance (TSEB) modeling schemes. *Remote Sensing of Environment*, *108*, 369-384
- Trenberth, K.E., Fasullo, J.T., & Kiehl, J. (2009). Earth's global energy budget. *Bulletin of the American Meteorological Society*, *90*, 311-323
- Verstraeten, W.W., Veroustraete, F., & Feyen, J. (2008). Assessment of evapotranspiration and soil moisture content across different scales of observation. *Sensors*, *8*, 70-117
- Villagarcía, L., Were, A., García, M., & Domingo, F. (2010). Sensitivity of a clumped model of evapotranspiration to surface resistance parameterisations: Application in a semi-arid environment. *Agricultural and Forest Meteorology*, *150*, 1065-1078
- Wang, K., & Dickinson, R.E. (2012). A review of global terrestrial evapotranspiration: Observation, modeling, climatology, and climatic variability. *Reviews of Geophysics*, *50*, RG2005
- Were, A., Villagarcía, L., Domingo, F., Alados-Arboledas, L., & Puigdefábregas, J. (2007). Analysis of effective resistance calculation methods and their effect on modelling evapotranspiration in two different patches of vegetation in semi-arid SE Spain. *Hydrology and Earth System Sciences*, *11*, 1529-1542
- Zhan, X., Kustas, W.P., & Humes, K.S. (1996). An intercomparison study on models of sensible heat flux over partial canopy surfaces with remotely sensed surface temperature. *Remote Sensing of Environment*, *58*, 242-256
- Zhang, K., Kimball, J.S., Mu, Q., Jones, L.A., Goetz, S.J., & Running, S.W. (2009). Satellite based analysis of northern ET trends and associated changes in the regional water balance from 1983 to 2005. *Journal of Hydrology*, *379*, 92-110
- Zhang, Y.Q., Leuning, R., Hutley, L.B., Beringer, J., McHugh, I., & Walker, J.P. (2010). Using long-term water balances to parameterize surface conductances and calculate evaporation at 0.05° spatial resolution. *Water Resources Research*, *46*, W05512

CAPITULO 1

Using radiometric temperature for surface energy flux estimation in Mediterranean drylands from a two-source perspective

*Aceptado en *Remote Sensing of Environment* con correcciones (16/10/2012) con los siguientes autores:

Laura Morillas, Mónica García, Héctor Nieto, Luis Villagarcía, Inge Sandholt, Maria-Patricia González-Dugo, Pablo Zarco-Tejada y Francisco Domingo.

ABSTRACT

A Two-Source Model (TSM) for surface energy balance, considering explicitly soil and vegetation components, was tested under water stress conditions. The TSM evaluated estimates the sensible heat flux (H) using the surface-air thermal gradient and the latent heat flux (LE) as a residual from the surface energy balance equation. The analysis was performed in a semiarid Mediterranean tussock grassland in southeast Spain, where H is the dominant flux and LE rates are low, challenging conditions under which the TSM has not been validated before. We evaluated two different resistance schemes: series and parallel; as well as the iterative algorithm included in the TSM to disaggregate the soil-surface composite temperature into its separate components. Continuous field measurements of composite soil-vegetation surface temperature (T_R) and bare soil temperature (T_s) from thermal infrared sensors were used for model testing along with canopy temperature estimates (T'_c), derived from T_R and T_s .

Comparisons with Eddy covariance and field data showed that the TSM produced reliable estimates of net radiation (R_n) and H fluxes, with errors of $\sim 30\%$ and $\sim 10\%$, respectively, but not for LE , with errors $\sim 90\%$. Despite of lower errors ($\sim 10\%$) in estimating H using parallel resistance, the series scheme increased slightly the correlations ($R^2 = 0.78-0.80$ vs. $R^2 = 0.75-0.77$) and was also more robust in disaggregating soil and canopy fluxes. Differences between model runs using the iterative algorithm to disaggregate T_R and the simplified version that uses separate inputs of T_s and T'_c were minor. This demonstrates the robustness of the iterative procedure to disaggregate a composite soil-vegetation temperature into separate soil and vegetation components in semiarid environments with good prospects for image applications.

Keywords: Mediterranean drylands; surface temperature; two-source model; surface energy fluxes; Priestley-Taylor assumption; parallel and series resistance network.

INTRODUCTION

Land surface temperature is an integrated variable determined by the interaction between the land surface and the atmosphere (Choudhury 1992), and it is a key factor for partitioning available energy into sensible heat flux (H) and latent heat flux (LE) (Kustas and Norman 1996). Consequently, land surface temperature is one of the remote sensing variables most widely used for surface flux modelling, as shown by the large number of papers published since the 1980's (for review see Glenn et al. 2007; Kalma et al. 2008; Kustas and Anderson 2009).

Some difficulties associated with the application of remotely sensed surface temperature for land surface flux modelling have been pointed out. They include angular dependence (Rasmussen et al. 2011), atmospheric and emissivity correction requirements (Dash et al. 2002), and differences between aerodynamic and radiometric surface temperature (; Chehbouni et al. 1997; Norman and Becker 1995). These difficulties have contributed to scepticism in the research community about its operational usefulness (Cleugh et al. 2007; Hall et al. 1992). Nonetheless, great advances have been made in application of thermal infrared remote sensing to land surface flux estimation, and today, a wide range of operational remote sensing models relying on the use of surface temperature is available (Kalma et al. 2008; Kustas and Anderson 2009).

This paper focuses on physical models based on a direct estimation of the sensible heat flux, which is governed by the bulk resistance equation for heat transfer (Brutsaert 1982), and relies on the surface-to-air temperature gradient. The latent heat flux can then be estimated as the difference between the available energy minus the sensible heat flux. These models were originally designed from a one-source perspective where the soil-canopy system was represented by an ensemble surface temperature, called the "aerodynamic temperature" (T_{aero}), which determines the total sensible heat flux (Kustas and Anderson 2009). The drawback of this perspective is that the aerodynamic temperature cannot be measured by remote sensing. Therefore, in some one-source models where T_{aero} has been replaced by the radiometric surface temperature (T_R), an extra resistance, called the excess resistance (R_{ex}), has been included to account for the differences between these two temperatures (see Norman and Becker 1995 for clarification of the thermal terminology). Appropriately calibrated, one-source models have shown satisfactory estimates of surface energy fluxes in heterogeneous landscapes (Bastiaanssen et al. 1998; Kustas et al. 1996; Troufleau et al. 1997), however, they show a highly empirical

dependency which questions its operational application, particularly in areas where no field flux measurements are available.

To overcome these limitations, one-source models have evolved into a multisource formulation. Following this trend, the *Two-Source Model* (TSM) for sensible heat flux (H) designed by Norman et al. (1995), provides a more realistic representation of the turbulent and radiation exchanges over partial vegetation canopies than one-source models (Timmermans et al. 2007). The TSM accommodates the difference between T_R and T_{aero} by considering soil (H_s) and canopy (H_c) sensible heat fluxes separately, using the temperature of soil (T_s) and canopy (T_c) respectively. Since remote sensing resolution is often too coarse to distinguish between T_s and T_c , the TSM model includes an algorithm for estimating T_s and T_c from mono-angle T_R . This algorithm assumes as a first condition that canopy latent heat flux (LE_c) responds to a potential rate estimated by the Priestley-Taylor equation (Priestley and Taylor 1972). From this starting point, the iterative procedure estimates T_s and T_c and solves the soil and canopy turbulent heat fluxes by applying the surface energy balance equation to canopy and soil separately, and assuming T_c , T_s and T_R have a nonlinear relationship (see next Section for more details). Depending on the coupling assumed between soil and canopy fluxes, the TSM can be applied under two different resistance networks: the parallel approach, which assumes no interaction between sources, and series approach, which allows interaction between soil and canopy (Norman et al. 1995).

Sensitivity analyses of the TSM have shown that it is more robust than one or other two-source temperature models (Zhan et al. 1996), and generally outperforms one-source schemes in extreme climatic conditions (Kustas and Anderson 2009). In addition, the TSM allows surface energy fluxes between soil and canopy to be distinguished. This makes possible to obtain separate soil evaporation and canopy transpiration estimates, critical to understanding vegetation processes and water dynamics in drylands (Huxman et al. 2005; Reynolds et al. 2000). Such evidences suggest that the TSM is a good candidate for application to Mediterranean drylands. The effectiveness of the TSM model has been successfully proven in partially covered agricultural areas, including semiarid areas, but mainly under irrigated conditions (Colaizzi et al. 2012b; French et al. 2007; Gonzalez-Dugo et al. 2009; Kustas and Norman 1999a; Li et al. 2005). Only a few studies have tested the TSM model under natural semiarid conditions, most of them at the Walnut Gulch (AZ, USA) experimental site (Norman et al. 1995; Timmermans et al. 2007; Zhan et al. 1996), and no experimental analysis of the TSM effectiveness in Mediterranean drylands has been previously presented.

This paper explores the usefulness of the TSM for surface flux estimation in a Mediterranean tussock grassland located in southeast Spain. In these ecosystems, water availability and energy supply conditions do not coincide, resulting in extremely low evapotranspiration rates and dominant H (Rana and Katerji 2000), which makes for very challenging conditions for running the model. At the same time, two practical aspects of the TSM were analyzed for model application in these specific conditions: the most appropriate arrangement of resistances (parallel or series approach), and the behaviour of the iterative procedure included in the model to retrieve canopy and soil temperatures.

Even though parallel resistance network was originally proposed for sparsely vegetated semiarid regions, and series approach for denser vegetation cover (Kustas and Norman 1997; Norman et al. 1995), there is no agreement about which approach offers better results in semiarid sparse vegetation. Kustas and Norman (1999a) found better results using the series resistance network in an irrigated cotton crop in central Arizona, whereas Li et al. (2005) found similar results with either parallel or series formulation in corn and soy crops under a wide range of fractional vegetation cover and soil moisture conditions. Due to its greater simplicity, and based on Li et al. (2005), later work has preferably applied the parallel TSM formulation (Sánchez et al. 2008; Timmermans et al. 2007) with good results under natural semiarid ecosystems, but it has never been properly compared with the series approach under these conditions.

With regard to the iterative procedure for separating canopy and soil temperatures and fluxes, some uncertainties have previously been described concerning the best empirical value for the Priestley- Taylor constant, α_{PT} (usually $\alpha_{PT} = 1.3$) (Agam et al. 2010; Kustas and Norman 1999a). Colaizzi et al. (2012a) also reported unreliable partitioning between soil and canopy fluxes using the iterative procedure based on Priestley-Taylor in irrigated row crops. Therefore, reevaluation of the effectiveness of this iterative procedure under Mediterranean natural semiarid conditions, where potential evapotranspiration is rarely reached and iteration is strongly forced, seems highly advisable.

These two aspects of the TSM implementation in Mediterranean drylands were evaluated by: i) applying the two possible resistance approaches, series and parallel, to our field site and comparing them, and ii) comparing the results from TSM using a composite soil-vegetation temperature T_R and the iterative procedure for flux partitioning, with results using separate T_s and T_c - and hence without iteration- to evaluate uncertainties associated with the iterative procedure included in the TSM formulation.

A dataset of continuous ground measurements during 5-months was used in this assessment. This allowed the effectiveness of the TSM to be evaluated under a wide range of natural micrometeorological and water availability conditions.

MODEL DESCRIPTION

We used the TSM proposed by Norman et al. (1995) including the latest improvements proposed by Kustas and Norman (1999a). This model is based on the Surface Energy Balance equation (SEB) which can be formulated for the whole canopy-soil system (Eq.1) as well as for the canopy layer and the soil layer (designed by c and s subscripts respectively) (Eq. 2 and 3).

$$Rn = LE + H + G \quad (1)$$

$$Rn_c = H_c + LE_c \quad (2)$$

$$Rn_s = H_s + LE_s + G \quad (3)$$

where Rn is net radiation and G is soil heat flux, which includes all the fluxes in $W\ m^{-2}$. This way, all fluxes can be estimated for the canopy and soil layers with the exception of the soil heat flux (G) which was originally proposed to be estimated as a constant fraction of Rn_s (Choudhury 1987) (Eq.7).

$$Rn = Rn_c + Rn_s \quad (4)$$

$$H = H_c + H_s \quad (5)$$

$$LE = LE_c + LE_s \quad (6)$$

$$G = c_G Rn_s \quad (7)$$

More detailed methods to estimate G have been recently used to test the TSM (Colaizzi et al. 2012b; Kustas et al. 2012) based on Santanello and Friedl (2003) but showing still considerable uncertainty. Therefore, we used measured G to reduce the effect of G uncertainties over LE estimates, more sensitive to errors due to the low magnitude of LE characterizing Mediterranean drylands (Domingo et al. 2011).

A Beer's law formulation was originally proposed for partitioning net radiation between the soil and vegetation (Norman et al. 1995). However, this method results in significant systematic errors for sparse canopies with relatively hot soil surfaces and some authors only recommend it for canopies with nearly full cover (Kustas and Norman 1999b). As an alternative for sparse canopies, a more physically sound algorithm considering short-wave and long-wave components was proposed by Kustas and Norman (1999a). This method requires incoming short-wave radiation as input and considers transmission of direct and diffuse short-wave radiation, and the transmission of long-wave radiation through the canopy by the Campbell and Norman (1998) formulation. This can be expressed as in Equations 8 to 11:

$$Rn_c = Ln_c + (1 - \tau_s)(1 - \alpha_c)S \quad (8)$$

$$Rn_s = Ln_s + \tau_s(1 - \alpha_s)S \quad (9)$$

where S (W m^{-2}) is the incoming shortwave radiation, τ_s is solar transmittance through the canopy, α_s is soil albedo, α_c is the canopy albedo. Estimates of τ_s , α_s and α_c are computed following the equations 15.4 to 15.11 in (Campbell and Norman 1998) and based on LAI, the reflectances and transmittances of soil and a single leaf, and the proportion of diffuse irradiation, assuming that the canopy has a spherical leaf angle distribution.

Ln_s and Ln_c (W m^{-2}) are the net soil and canopy long-wave radiation, respectively, estimated using the following expression:

$$Ln_c = [1 - \exp(-k_L \Omega LAI)] [L_{sky} + L_s - 2L_c] \quad (10)$$

$$Ln_s = \exp(-k_L \Omega LAI) L_{sky} + [1 - \exp(-k_L \Omega LAI)] L_c - L_s \quad (11)$$

where k_L ($k_L \approx 0.95$) is the long-wave radiation extinction coefficient, which is similar to the extinction coefficient for diffuse radiation with low vegetation, i.e., Leaf Area Index (LAI) lower than 0.5 (Campbell and Norman 1998). Ω is the vegetation clumping factor proposed by Kustas and Norman (1999a) for sparsely vegetated areas, which can be set to one when measured LAI implicitly includes the clumping effect (i.e. LAI from the *Moderate Resolution*

Imaging Spectroradiometer, MODIS) (Anderson et al. 1997; Norman et al. 1995; Timmermans et al. 2007), and L_s , L_c and L_{sky} (W m^{-2}) are the long-wave emissions from soil, canopy and sky. The Stefan–Boltzman equation based on soil, canopy and air temperatures, and vapor pressure (Brutsaert 1982) can be used to compute L_s , L_c and L_{sky} .

To estimate H_c and H_s , the TSM resistance network may be considered to be either in parallel (TSM_P) or in series (TSM_S) (Fig. 1). TSM_P assumes that the air temperature above the soil surface is independent of the vegetation temperature, while TSM_S permits interaction between soil and vegetation heat fluxes, influencing the temperature in the air-canopy interface.

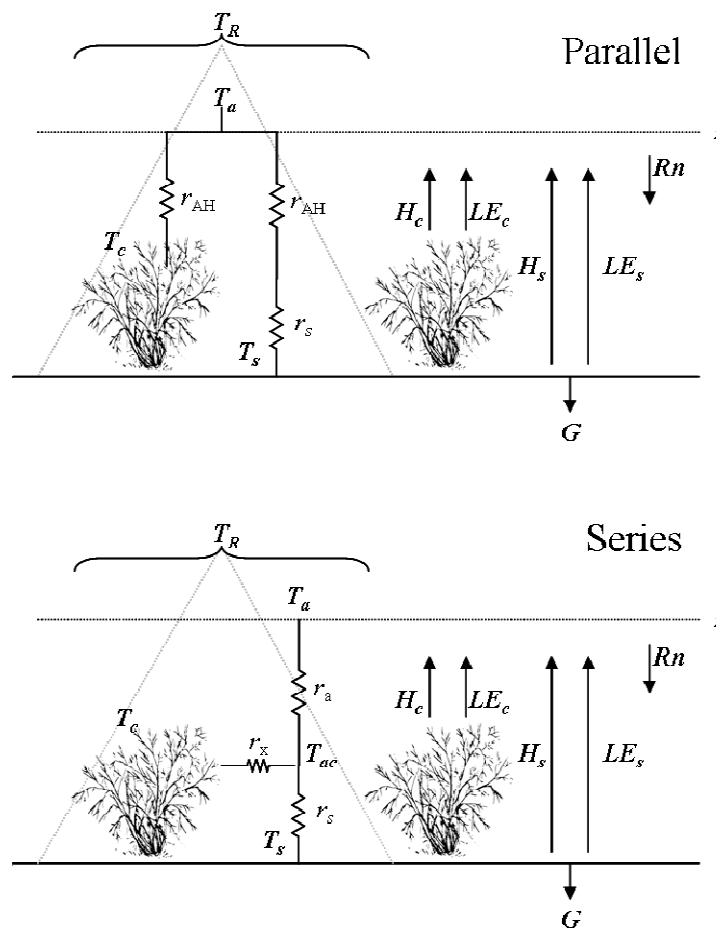


Figure 1. Resistances and flux separation for the parallel (top) and series (bottom) versions of TSM where z is reference height; T_c , T_s , and T_R are radiometric temperatures of canopy, soil and the aggregated surface of both respectively; T_a is air temperature; r_s , r_a , r_{AH} and r_x are surface, aerodynamics and total boundary layer resistances respectively (details in text) and Rn , G , LE and H are net radiation, soil heat flux, latent heat flux and sensible heat flux respectively (c and s subscripts denote soil and canopy, respectively).

The TSM_P expression for H_c and H_s is as follows:

$$H_s = \rho C_p \frac{T_s - T_a}{r_{AH} + r_s} \quad (12)$$

$$H_c = \rho C_p \frac{T_c - T_a}{r_{AH}} \quad (13)$$

where r_{AH} ($m s^{-1}$) is the aerodynamic resistance to turbulent heat transport between the canopy source/sink height (Eq. 11):

$$r_{AH} = \frac{\left[\ln\left(\frac{z-d}{z_{om}}\right) - \psi_m \right] \left[\ln\left(\frac{z-d}{z_{oh}}\right) - \psi_h \right]}{k^2 u} \quad (14)$$

where z is the height where air temperature and wind speed are measured, d (m) is the zero-plane displacement height, z_{om} (m) is the momentum roughness length, z_{oh} (m) is the heat roughness length, and ψ_m and ψ_h are the stability correction functions for sensible heat and momentum flux, respectively, which depend on the Monin-Obukhov length, L (m). The method proposed by Schaudt and Dickinson (2000) was used for d and z_{om} estimation, considering shrubland land cover type and a crown width ratio of 1. z_{oh} was estimated as a fraction of z_{om} as postulated by Garratt and Hicks (1973), i.e., $z_{oh} = z_{om}/\exp(kB^{-1})$, where $kB^{-1} \approx 2$.

r_s ($m s^{-1}$) is the resistance to heat flow in the boundary layer immediately above the soil surface. In the Kustas and Norman (1999a) updated TSM, r_s was estimated considering the effect of the surface-air temperature difference over the free convective velocity based on Kondo and Ishida (1997):

$$r_s = \frac{1}{c(T_s - T_a)^{1/3} + bu_s} \quad (15)$$

where $c = 0.0025$ and $b = 0.012$ and u_s is the wind speed (m s^{-1}) at a height above the soil surface where the effect of soil surface roughness is minimal. This can be estimated following Goudriaan (1977) (see Appendix C of Norman et al. 1995).

For the TSM_s , H_c and H_s are defined by

$$H_s = \rho C_p \frac{T_s - T_{ac}}{r_s} \quad (16)$$

$$H_c = \rho C_p \frac{T_c - T_{ac}}{r_x} \quad (17)$$

where T_{ac} (K) is the air temperature in the canopy-air space included in Eq. 18:

$$H = \rho C_p \frac{T_{ac} - T_a}{r_a} \quad (18)$$

where r_a (m s^{-1}) is computed using the same equation previously defined for r_{AH} (m s^{-1}) (Eq. 14), but with $z_{oh} = z_{om}$.

r_x (m s^{-1}) is the total boundary layer resistance of the complete canopy estimated from the wind speed within the canopy air space (see Appendix A in Norman et al. 1995).

The TSM is based on single-time surface radiometric temperature observations (T_R) which is related to the soil (T_s) and canopy (T_c) radiometric temperatures based on the fractional vegetation cover within the sensor field of view, f_c , as follows:

$$T_R = \left[f_c T_c^4 + (1 - f_c) T_s^4 \right]^{1/4} \quad (19)$$

where all temperatures are in K.

In the TSM T_c and T_s are estimated from T_R by iteration for Equations 12-13 (TSM_P) or 16-17 (TSM_S). As a starting point for determining the divergence between soil and canopy fluxes,

the iteration procedure uses the Priestley-Taylor equation (Priestley and Taylor 1972) (Eq.20) to estimate an initial LE_c .

$$LE_c = \alpha_{PT} f_G \frac{\Delta}{\Delta + \gamma} Rn_c \quad (20)$$

where α_{PT} is the Priestley-Taylor parameter (≈ 1.3), f_G is the fraction of leaf area index (LAI) that is green or actively transpiring, Δ is the slope of the saturation vapor pressure-temperature curve at T_c (kPa K^{-1}) and γ is the psychrometric constant (kPa K^{-1}).

Once the initial LE_c is obtained, an initial H_c is derived using the estimated Rn_c from Equation 2 and T_c is obtained from inversion of Equations 13 (TSM_P) or 17 (TSM_S). T_s is estimated from this initial T_c by Eq.19 and H_s by Eq. 12 or 16 (depending on the resistance approach). Finally an initial LE_s can be obtained by Eq. 3 using estimated Rn_s and G . This equation system is the basis of the iterative procedure. If the estimated LE_s is above zero, iteration stops, as a reliable solution has been reached. On the contrary, when the estimated LE_s is below zero, an unrealistic situation under daytime conditions is assumed since condensation in the soil is very unlikely to occur. This is considered a sign of water stress, and consequently LE_s is set to zero and LE_c falls from its initial potential rate. Therefore, the initial LE_c is overridden and α_{PT} is iteratively reduced until the solutions for T_c and T_s agree with measured T_R through Eq. 19 and realistic latent heat fluxes are found for both canopy and soil ($LE_s \geq 0$ and $LE_c \geq 0$ for daytime) (Norman et al. 1995; Kustas et al. 2012). Sometimes, even when LE_s and LE_c are set at zero, the resulting H_s (residually estimated from Eq. 3) exceeds the energy available to the soil ($H_s > Rn_s - G$). In such situations, the iterative procedure, originally designed to use estimated G from Eq. 7, considers unreliable the constant value of c_g used in Eq. 7 and finds a “residual solution” by inverting G from Eq. 3 to satisfy both the soil and canopy surface energy balances (Norman et al. 1995). As in our study, measured values of G were used for model running, those cases for which iteration was not able to reach the soil energy closure when $LE_s = 0$ and $LE_c = 0$ using measured G , were considered as an iteration failure and were not included in the accuracy analyses.

Iteration is not required for the TSM when T_s and T_c are known a priori. In that case H_c and H_s can be estimated directly using Eq. 12-18 and the latent heat fluxes computed as a residual of each energy balance layer (Eq. 2 and 3). This model is hereinafter referred to as *TSM without iteration*, to differentiate it from the *TSM with iteration* based on T_R measurements.

MATERIAL AND METHODS

Study site and field measurements

The Balsa Blanca field site is located 6.3 km from the coast (36°56'24.17"N; 2°1'59.55"W; elevation 196m a.m.s.l.) in Cabo de Gata National Park. The site is a tussock grassland, where the predominant species is the *Stipa tenacissima* L. (57.2%), a perennial grass, with other less abundant shrub species, such as *Thymus hyemalis* Lange (1.7%), *Chamaerops humilis* L. (1.6%), *Brachypodium retusum* (Pers.) P. Beauv (1.4%), *Ulex parviflorus* Pourr (0.5%) and *Phlomis purpurea* L. (0.2%). Because the vegetation is perennial, measured values of cover fraction ($f_c = 0.6$) and canopy height ($h_c = 0.7$ m) can be considered constant during the study period. The model was tested from January 15th, (day of year - DOY 15) to June 9th (DOY 160) 2011. This period covers the wide range of soil water availability and phenological conditions shown in Figure 2. During the study period, the volumetric soil moisture content, measured at a depth of 0.04 m in a bare soil area with a water content reflectometer (model CS616, Campbell scientific INC., USA), ranged from a minimum of 7 to a maximum of 24%, which covered the range of annual variation. The evaporative fraction, defined as the ratio of latent heat flux (LE) to available energy ($Rn-G$), ranged from 0.07 to 0.49 (at midday) (notice that the evaporative fraction never exceeded 0.5) and LAI from MODIS ranged from 0.3 to 0.7.

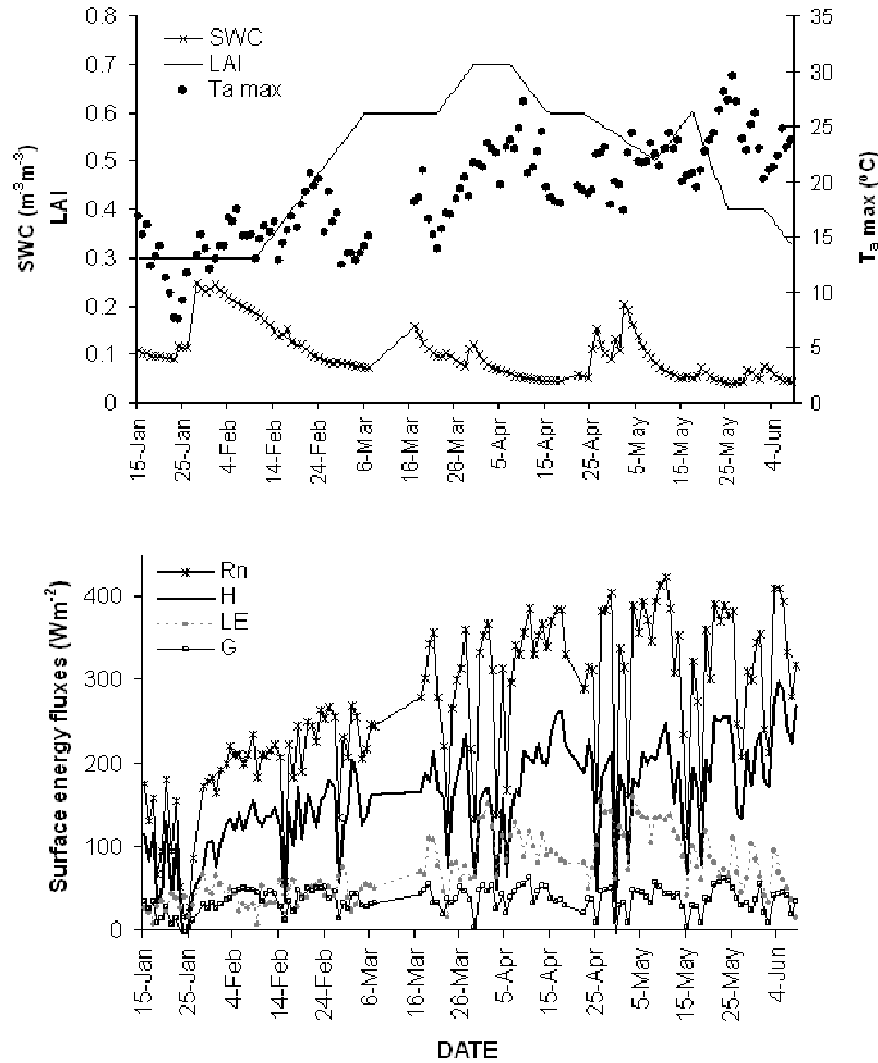


Figure 2. Variation in leaf area index (*LAI*) from MODIS over time, soil water content at midday (*SWC*) and daily maximum air temperatures (T_a max) (top) and variation in daytime averages of observed net radiation (*R_n*), soil heat flux (*G*), sensible heat flux (*H*) and latent heat flux (*LE*) (bottom panel) during the study period.

Continuous T_R and T_s measurements were acquired using Apogee IRTS-P broadband thermal infrared thermometers (Campbell Scientific Inc., USA). This broadband radiometer has a full wavelength range of 6 to 14 μm . Two IRT sensors were installed at heights of 3.5 m and 0.65 m, measuring two target surfaces at nadir, respectively: a) composite soil-vegetation surface and b) a pure bare soil surface (Fig. 3). The half field of view of 28° resulted in a soil and vegetation mixture (T_R) sampling area 3.70 m in diameter and a bare soil (T_s) sampling area 0.69m in diameter. Incoming short-wave radiation was also measured at a height of 3.5m using an LP02 Pyranometer (Campbell Scientific Inc., USA). Temperatures and radiance were

measured every minute and stored as 15-min averages on a Campbell CR1000 datalogger (Campbell Scientific Inc., USA).

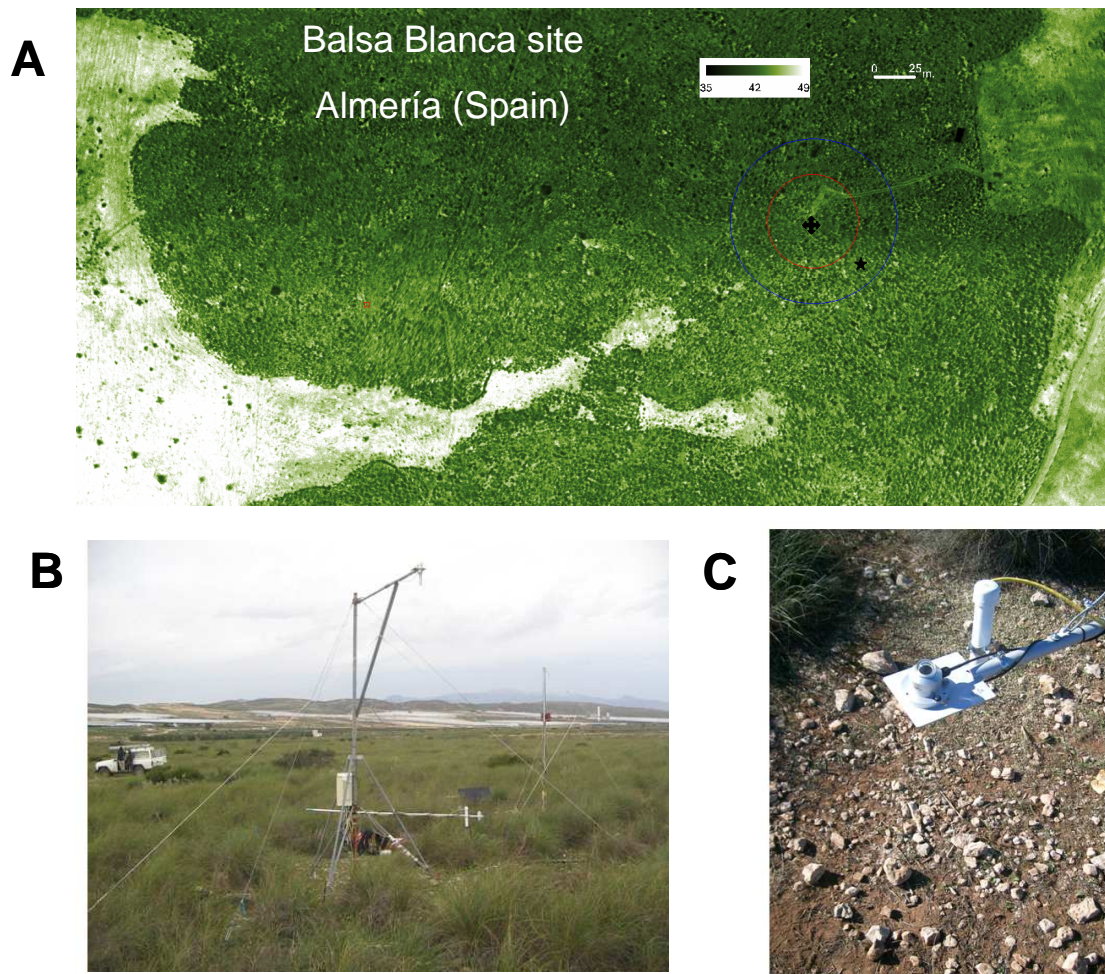


Figure 3. Field site pictures, in A unstable (red) and stable (blue) footprints of EC tower are marked in red and blue respectively, in B experimental assembly of IRTS-P sensors for T_R and T_s measurements and in C detail of bare soil temperature measurements.

Temperature and radiance measurements were acquired within the 100-m fetch of the Eddy Covariance (EC) tower located at this field site (Rey et al. 2011). The EC system for H and LE measurement included a three-dimensional sonic anemometer CSAT3 (Campbell Scientific Ltd, USA) measuring wind speed and direction, and a Li-Cor open-path infrared gas analyzer (Li7500, Campbell Scientific Ltd, USA) measuring water vapor and CO_2 concentrations. Both EC system components, located 3.5 m high and connected to the Campbell CR3000 datalogger (Campbell Scientific Ltd, USA), measured at 10 Hz, and the datalogger calculated and stored means, variances and covariances every 15 min. LE measurements were corrected for air density fluctuations from heat and water vapor flux as proposed by Webb et al. (1980), and for the

rotation of the coordinate system (Kowalski et al. 1997; McMillen 1988). Air temperature (T_a) and humidity (RH) were also measured every minute using a thermo-hygrometer (HMP45C, Campbell Scientific Ltd.) located at a height of 2.5 m (z) on the EC tower. Net radiation (Rn) was measured every minute at a height of 1.90 m over a mixture of canopy and soil surface using a net radiometer (NR-Lite; Kipp & Zonen, Campbell Scientific Ltd, USA). Rn , RH and T_a 15-min-averages were recorded by the same Campbell CR3000 datalogger used for the EC system data.

In addition, the soil heat flux (G) was calculated by the combined method (Fuchs 1986; Massman 1992) by adding the average flux measured by a soil heat flux plate at a fixed depth (in this case 0.08 m) (HFT-3; REBS, Seattle, Wa, USA) to the energy stored in the soil layer above the heat flux plate measured using two thermocouples (TCAV, Campbell Scientific Ltd.) buried at 0.02 m and 0.06 m over the flux plates. Two pairs of soil heat flux plates and their corresponding thermocouples were installed in bare soil and under plant positions for computing G_{bs} and G_{up} , respectively. Soil temperatures and fluxes were measured every minute and 15-min averages were recorded by a CR10X datalogger (Campbell Scientific Inc., USA). Representative data for G at the experimental site was computed as $G = fc G_{up} + (1-fc) G_{bs}$, where fc is the vegetation cover fraction at the site.

Satellite and airborne campaign data

LAI and f_{par} from the MODIS (Moderate Resolution Imaging Spectroradiometer) sensor were acquired as TSM model inputs. The f_{par} product was used to estimate f_g , included in Eq. 20, as the ratio between intercepted and absorbed Photosynthetic Active Radiation f_{IPAR}/f_{APAR} (Fisher et al. 2008). MODIS data from Terra, MOD15A (Collection 5), and from the Aqua satellites, MYD15A2, were used. The mean of Terra and Aqua 8-day composites (1-km pixel) for each product was linearly interpolated between observations for daily estimates.

To assess the variability of surface temperature (T_R) within the footprint of the EC tower four Very High Resolution (VHR) images of 0.4 m pixel acquired from an unmanned airborne campaign over the site in May-18th-2009 at 7:00 h, 9:10 h, 11:38h and 14:10 h (solar time) were used. The Unmanned Aerial Vehicle (UAV) platform operated was a 2-m wingspan fixed wing platform with up to 1-hour endurance at 5.8 kg take-off weight (TOW) and 63 km/h ground speed (mX-SIGHT, UAV Services and Systems, Germany) operated by the Laboratory for Research Methods in Quantitative Remote Sensing (QuantaLab, IAS-CSIC, Spain) and adapted

to carry a payload consisting on a thermal camera (Berni et al. 2009; Zarco-Tejada et al. 2012). The UAV was controlled by an autopilot (AP04, UAV Navigation, Madrid, Spain) to follow a flight plan (Berni et al. 2009).

The Miricle 307 thermal camera (Thermoteknix Systems Ltd, Cambridge, UK) was flown over the study sites with a 14.25 mm f1.3 lens, connected to a computer onboard the unmanned vehicle. The image sensor was a Focal Plane Array (FPA) based on uncooled microbolometers with a resolution of 640x480 pixels and a spectral response in the range of 8-12 μm , yielding a 25 μm pixel size. The camera delivered uncalibrated 14-bit digital raw images. Radiometric calibration was conducted in the laboratory using blackbodies under varying target and ambient temperatures to develop radiometric calibration algorithms. Atmospheric correction methods were applied to the thermal imagery based on the MODTRAN radiative transfer model to obtain surface temperature. Local atmospheric conditions were determined by air temperature, relative humidity and barometric pressure measurements at the time of flight using a portable weather station (Model WXT510, Vaisala, Finland). Atmospheric correction methods conducted with single-band thermal cameras were shown to provide successful estimation of vegetation surface temperature (Berni et al. 2009). Bouguet's image calibration procedure was applied to all imagery acquired (Berni et al. 2009), and photogrammetric techniques were used to register the frame-based imagery to map coordinates. Three of the images were co-registered a posteriori to the image acquired at 7.00h achieving a geolocation error of 4 pixels.

To assess the variability of LAI at the study site we used an ASTER (Advanced Spaceborne Thermal Emission and Reflection Radiometer) from May-6th-2003 at 11.00 UTC. ASTER, on board the Terra platform along with MODIS scans a 60 km swath on the ground every 16 days with a swath angle of $\pm 2.4^\circ$. The sensor has nine reflective bands and five bands in the thermal infrared (TIR) region. To estimate the NDVI (15 m pixel) we used the surface reflectance product (2AST07; HDFEOS version 2.8), with a spatial resolution of 15 m (VNIR) and 30 m (SWIR) and an absolute accuracy of 4% of reflectance (Abrams and Hook 2002).

Pre-processing of radiometric measurements

The Apogee IRT-P sensors, with reported accurate of $\pm 0.3^\circ\text{C}$ within a range of -10 to 55 $^\circ\text{C}$, were programmed to correct for the effect of the internal sensor temperature and the thermal mass (Bugbee et al. 1996). To ensure that the reported accuracy of IRT sensors is maintained under our extreme field conditions, they were recalibrated in the laboratory with a blackbody

calibration source (Raytek BB4000) before their installation in the field. The two IRT sensors, labelled as IRT_{soil} and $IRT_{\text{composite}}$, according to their position in the experimental field set up, were tested in a growth chamber under different combinations of black body temperatures (T_{BB}), ranging from 20 to 70°C, and air temperatures (T_a), ranging from 5 to 30°C. Temperatures were measured every 15 seconds and 5-min-averages were recorded in a Campbell CR1000 datalogger. Mean measurement errors exceeded the reported accuracy (Table 1) when target temperatures were over 50°C. Given that surface temperatures higher than 50°C have been described under semiarid conditions (Chehbouni et al. 2001), we corrected the IRT measurements following the regression line between the Apogee IRT and the blackbody temperatures over the whole range of temperatures tested in the laboratory calibration (see calibration line in Table 1).

Table 1: Results of laboratory calibration of the Apogee IRT-P sensors. Mean absolute error (MAE) in °C of each sensor in different scenarios: for all the temperature combinations tested (MAE), for the range of temperatures reported by the manufacturer* (MAE_{range}) and for the temperatures tested out of the manufacturer range (MAE_{out of range}). Air temperature (T_a) and black body temperature (T_{BB}) ranges considered for each scenario are expressed in °C. The final calibration line applied to each sensor is also shown.

GENERAL STATS	T_a range	T_{BB} range	IRT_{soil}	$IRT_{\text{composite}}$
MAE	5-30	20-70	0.42	0.42
MAE _{range}	5-30	20-50	0.26	0.31
MAE _{out range}	5-30	60-70	0.72	0.62
<i>Empirical calibration line</i>			$y = 1.01x - 0.03$	$y = 1.0x - 0.06$

*reported accuracy: ± 0.3 °C from -10 to 55°C

In addition to this calibration, emissivity and atmospheric effects were also accounted for. The radiance reaching the IRT radiometers, R_B , is the result of two main contributions: a) the radiance emitted by the surface because of its temperature, and b) the portion of downwelling long-wave sky radiation reflected by the surface (Norman and Becker 1995):

$$R_B = \varepsilon R_R + (1 - \varepsilon)L \quad (21)$$

where ε is surface emissivity, R_R is the black body surface spectral radiance according to the surface radiometric temperature (T_R), and L is the hemispheric downwelling long-wave radiance from the sky divided by π .

The IRT radiometers provide measurements as brightness temperatures (T_B) related to brightness radiance (R_B), assuming emissivity equal to 1. Therefore, in order to estimate R_R , first R_B was estimated from the IRT measurements by applying the Stefan-Boltzman equation, and second R_R was derived from Eq. 21 for each IRT sensor using known emissivity and downwelling long-wave radiance. Once the radiometric radiances, R_R , from the IRT_{soil} and IRT_{composite} sensors had been found, the T_s and T_R radiometric, or “corrected”, temperatures were found using the Stefan-Boltzman equation.

For T_s emissivity corrections we considered soil emissivity, $\varepsilon_s = 0.95$, associated with bare soils in open and closed shrublands (Trigo et al. 2008). Although some studies have shown that ε_s can vary with soil water content fluctuation (Mira et al. 2007), a constant value was used because the effects of that variation are in the same range as the Apogee IRT sensor error (Sánchez et al. 2009). For T_R emissivity corrections, the composite emissivity (ε_R) depends on the vegetation fraction cover ($fc = 0.6$), which was estimated as a linear combination of both soil and canopy emissivities, ε_s and ε_c , respectively (Sobrino et al. 2001) (Eq. 22). For ε_c we used $\varepsilon_c = 0.99$, measured in the field at a similar site for *S. tenacissima* (Villagarcía 2000).

$$\varepsilon_R = fc \varepsilon_c + (1 - fc) \varepsilon_s \quad (22)$$

The downwelling long-wave radiance L was computed by means of the Stefan-Boltzmann equation using air temperature and atmospheric emissivity. Air temperature and vapor pressure were used for estimating atmospheric emissivity following Brutsaert (1982).

Once T_R and T_s were found, T_c was estimated using Eq.19. The estimated T_c is referred to below as derived T'_c .

Model validation

Model outputs were evaluated by comparing them with the H and LE fluxes derived from the EC system. The energy closure of 15-min measurements in our field site is shown in Figure 4. The slope of the linear regression between the available energy ($Rn-G$) and the sum of the surface fluxes ($H+LE$) was 0.8, which indicates an average imbalance of about 20%, on the same order as reported by Wilson et al. (2002). However, for model evaluation, the conservation of energy equation must be satisfied (Twine et al. 2000), especially in residual models. Therefore,

the *residual-LE closure* method (Twine et al. 2000) was implemented. This method assumes that most of the EC imbalance is caused by inaccuracies in LE , and solves for LE as the residual of the energy balance equation (assuming H is measured accurately). Our choice is based on previous work suggesting that this method would be the most appropriate for validating SEB-based models using EC data (Alfieri et al. 2012; Li et al. 2005), and on studies showing that underestimation of LE by EC is greater than for H (Wang and Dickinson 2012).

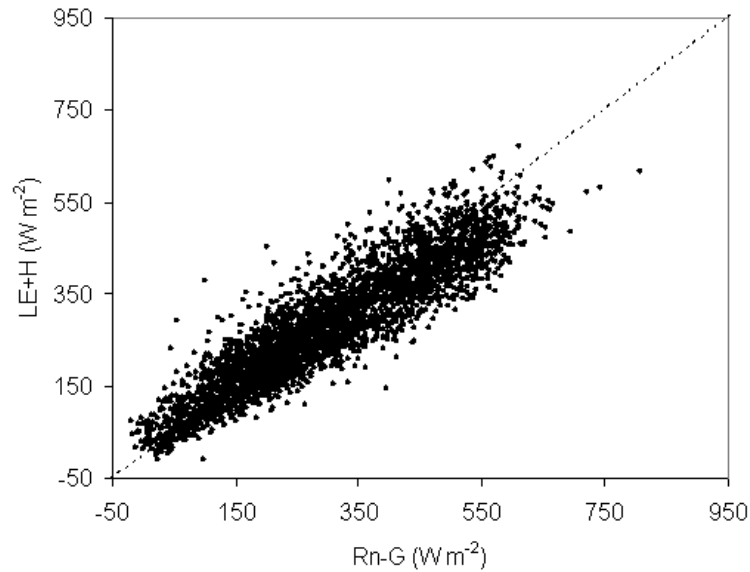


Figure 4. EC energy closure measurements of 15 min measured data (N = 2991).

For model evaluation, our dataset of continuous measurements during the study period was reduced to those 15-min daytime observations with observed Rn and LE above zero (not daytime condensation), and model Rn_s and Rn_c above zero (minimum energy supply), in order to evaluate the TSM under the conditions it was originally designed for. These criteria left a total of 2991 cases.

Analysis of spatial heterogeneity

Water-limited ecosystems are more vulnerable to a mismatch between tower flux and land surface measurements due to their heterogeneous vegetation composition (Vivoni et al. 2010). If the spatial heterogeneity is high, non-linear aggregation of state variables such as T_R and vegetation cover, might increase the differences between EC data and model outputs (Ershadi et al. 2013). In our study, model inputs from sensors with footprints different than that of the EC

systems were used. As footprints can differ in up to three orders of magnitude it is critical to perform an a priori assessment of the spatial variability of the site before running the TSM.

The aim in this Section was twofold: i) to characterize the spatial heterogeneity of the site for vegetation cover and surface temperature. ii) Assess if the composite soil-vegetation surface temperature (T_R) and LAI used as model inputs are representative of effective or the spatially-averaged variables within the footprint of the EC tower.

First, the EC footprint area was characterized using analyses from Were et al. (2010). They applied the Flux Source Area Model (FSAM) of Schmid (1994, 1997) at the site that calculates the dimensions of the source area of a given sensor as a function of sensor height, atmospheric stability and wind speed fluctuations. Were et al. (2010) considered the dimensions of the source area responsible for 50% of the total source weight calculated with FSAM. The footprints of the EC tower for unstable and stable conditions, representing 96.4% and 0.4 % of the total observations respectively, were defined as a circle of 28.8 m radius for unstable conditions and 51.1 m radius for stable conditions (Were et al. 2010) (Fig. 3).

Then, statistics for T_R derived from the UAV images (mean, standard deviation and coefficient of variation, CV) were extracted for four different sites: Apogee's footprint site (hereinafter Apogee-site) considered representative of the model input footprint, eddy covariance tower site (hereinafter EC-tower), and two EC footprints (hereinafter EC-footprint stable and EC-footprint unstable). The Apogee-site and the EC-tower regions were defined based on the error from image co-registration (1.6 m). Similarly, statistics for NDVI from the ASTER image were extracted for three regions: EC-footprint stable, EC-footprint unstable and MODIS-1km pixel (same as footprint of model input). Significant differences between mean values from the different regions were assessed using t-tests as NDVI and T_R were normally distributed. NDVI was used instead of LAI as no LAI imagery was available at high resolutions. However, NDVI is linearly related with LAI within the range of values found at the study site ($LAI < 2$ m) (Gamon et al. 1995). For assessing spatial heterogeneity of T_R within the EC footprint, the T_R from the UAV can be used as atmospheric conditions do not change within the area. The pixels (0.4 m) will include a mixture of soil and vegetation, and also some pixels of pure vegetation and bare soil due to the high spatial resolution.

RESULTS

Analyses of spatial heterogeneity

The heterogeneity of the footprint for T_R was found to be similar for unstable and stable conditions with standard deviation increasing towards the warmer afternoon hours when the H flux increases as well (Table 2).

Table 2: Spatial heterogeneity of composite soil-vegetation surface temperature (TR) within the footprint area for stable and unstable conditions of the Eddy Covariance tower derived from four UAV scenes of 0.4 m pixel. Mean is the spatially-averaged TR in the area, Std is the standard deviation, n the number of pixels in the area, and CV the coefficient of variation (%).

Footprint area	Area (m ²)	Hour (solar)	Mean	Std	n	CV (%)
Footprint stable	8203.42	7:00	28.17	1.10	60762	3.90
		9:10	37.49	1.32	60762	3.52
		11:38	41.81	1.66	60762	3.97
		14:10	40.75	1.82	60762	4.47
Footprint unstable	2605.78	7:00	28.20	1.11	15852	3.94
		9:10	37.47	1.11	15852	2.96
		11:38	41.81	1.51	15852	3.61
		14:10	40.59	1.60	15852	3.94

The T_R representative of the model footprint (Apogee-site) was not significantly different (Fig. 5) from the area-averaged T_R over the footprint area under either stable or unstable conditions after midday. However, before noon the area-averaged T_R within the footprint area was $\sim 0.8^\circ\text{C}$ lower than T_R at the Apogee site. This could have a small impact on modeled fluxes, producing H overestimates (Timmermans et al. 2007). Additionally, despite of the fact that the location of the IRT at the Apogee-site is distant from the tower EC-site, T_R from both sites are not significantly different at any time of the day.

The area-averaged NDVI within the footprint of the EC tower under unstable conditions, dominant at the site, was not significantly different from that within the MODIS 1km pixel (see Table 3) its Coefficient of Variation (CV) was three times greater. However, there is a great deal of published evidence showing that the relationship between surface reflectance is linear across the range of spatial scales of most sensors and atmospheric conditions (Moran et al. 1997). This suggests that using the NDVI from MODIS at 1 km pixel is equivalent to using the area-averaged NDVI value within the footprint.

Table 3: Spatial heterogeneity of NDVI within the footprint (stable and unstable conditions) of the Eddy Covariance tower using and the MODIS 1 km pixel region derived from ASTER (15 m pixel). Mean is the spatially-averaged NDVI in the area, Std is the standard deviation and CV the coefficient of variation (%) Significant differences between means at $p < 0.05$ were indicated by different letters.

	Area (m ²)	Mean	Std	n	CV (%)	Significant differences
Footprint stable	8203.42	0.36	0.012	36	3.4	a
Footprint unstable	2605.78	0.36	0.013	16	3.7	ab
MODIS-1km pixel	1000000	0.37	0.049	4434	13.2	b

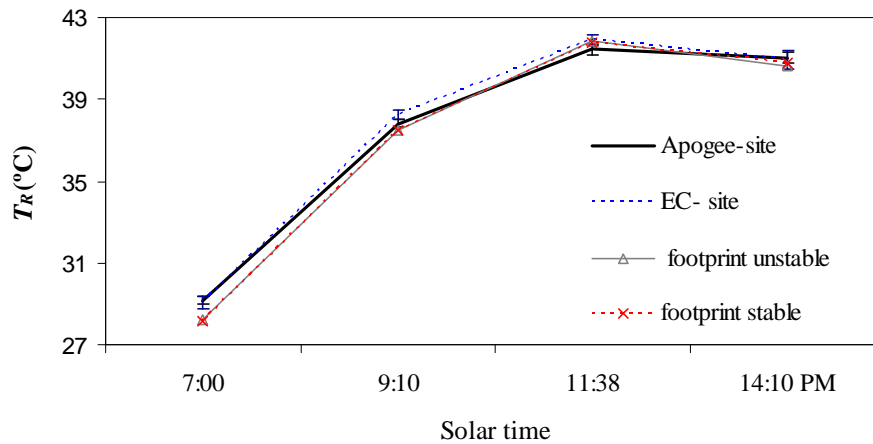


Figure 5. Comparison of spatially-averaged T_R at the IRT Apogee site, at the Eddy Eovariance site, and within the footprint regions defined for stable and unstable conditions. T_R were derived from High Resolution Images from airborne flights at four different times on May-18th -2009. Error bars represent the confidence interval for significant differences ($p < 0.05$).

Series vs. parallel original TSM version

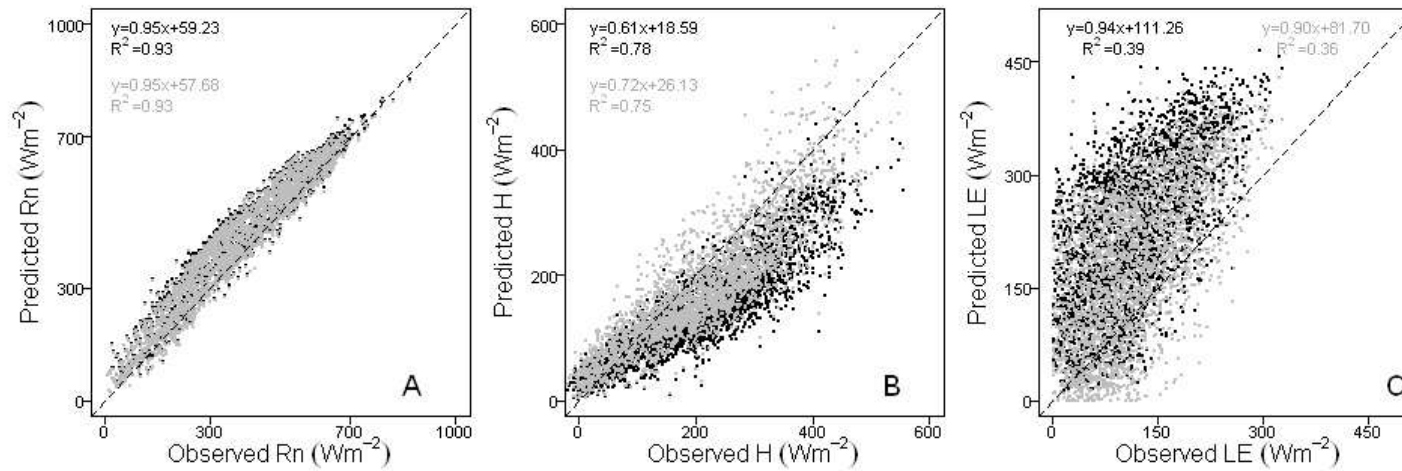
No significant differences were found between TSM_P and TSM_S outputs using the TSM in our semiarid site (Fig. 6). Statistics comparing model outputs with EC derived fluxes shown in Table 4, have lower errors with the parallel approach, but explained variance is slightly higher with the series approach.

TSM_P and TSM_S were equally successful in estimating R_n with slopes close to 1 and $R^2 = 0.93$ for all approaches (Fig. 6A and D), and low Mean Absolute Percentage Errors (MAPE) of 12-13 % (Table 4). However, a tendency to overestimate is observed (Fig. 6A and D).

Differences in parallel and series model versions were more significant for H than for R_n (Fig. 6B and E). Both resistance networks showed a better capacity for estimating low H than high H values, with similar accuracy when H was low. At high values of H , the TSM_S showed a

clear tendency to underestimate, whereas TSM_p behaviour was more irregular especially using the TSM *with iteration* (Fig. 6B and E). As a result, mean average errors for H were slightly lower with the parallel approach, with MAE values of 51- 48 $W m^{-2}$ (25-23% of MAPE) using the TSM *with* or *without iteration* respectively, than with the series which showed MAE values of 69-71 Wm^{-2} (33-34% of MAPE) respectively. However slightly better correlation ($R^2 = 0.78-0.80$ vs. $R^2 = 0.75-78$) and lower scatter (Fig. 6B and E) using the series approach was found.

TSM with iteration (using T_R)



TSM without iteration (using T_s and T_c)

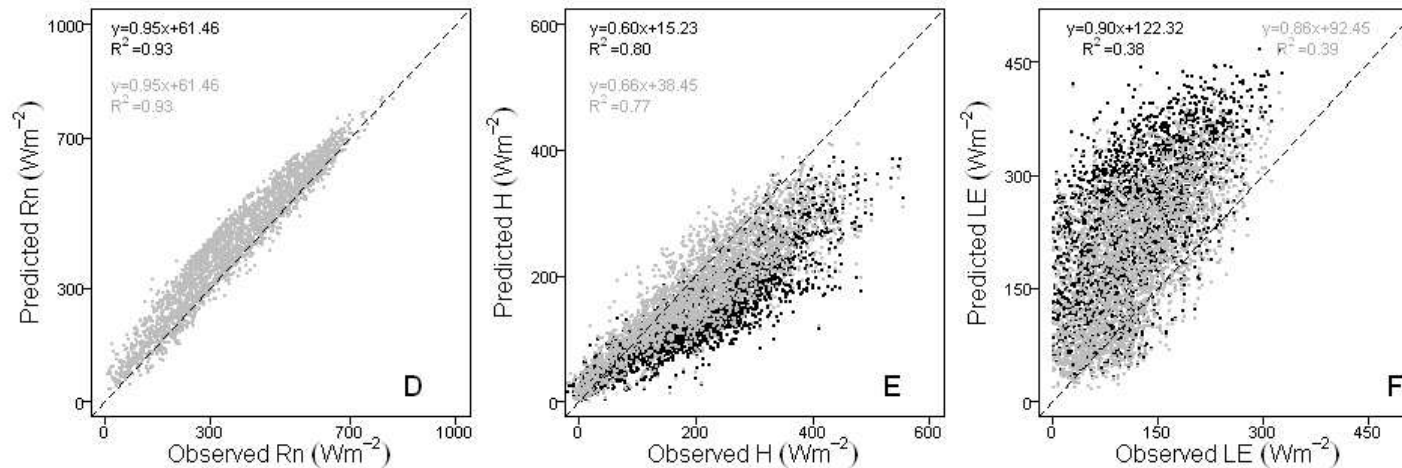


Figure 6. Linear regressions between the surface energy fluxes estimated by the TSM with iteration (using T_R) (in A,B and C panels) and by the TSM without iteration (using T_s and T_c) (in D,E and F panels) versus their corresponding ground measurements: R_n , H , and LE for full dataset analysed ($N = 2991$). In grey, TSM model with parallel resistance approach (TSM_P) and in black, series resistance approach (TSM_S). Dashed line is the 1:1 line.

Under the semiarid conditions studied, the TSM showed large relative errors in the latent heat flux, LE , with MAE values of 84-115 W m⁻² and MAPE in the order of 73-99% (Table 4). The lower errors were found using the TSM_P (73-74%). Linear regressions between modelled and observed LE showed a larger scatter (Fig. 6C and F), with R^2 below 0.40 for all approaches and despite of LE was mostly overestimated, slope values were close to one (Table 4), denoting greater importance of non-systematic rather than systematic errors.

TSM_P and TSM_S tackle the partitioning of the turbulent fluxes between soil and canopy in a different way. Although no separate measurements of soil and canopy fluxes were available for a proper evaluation of this partitioning by TSM_P and TSM_S , the comparison of measured and estimated T_s (Fig. 7) showed a general tendency to overestimate T_s , especially at high temperatures. This tendency, denoting that the TSM would be overestimating H_s flux, was more pronounced with the TSM_P (RMSE = 3.37 °C) than with the TSM_S (RMSE = 1.67 °C).

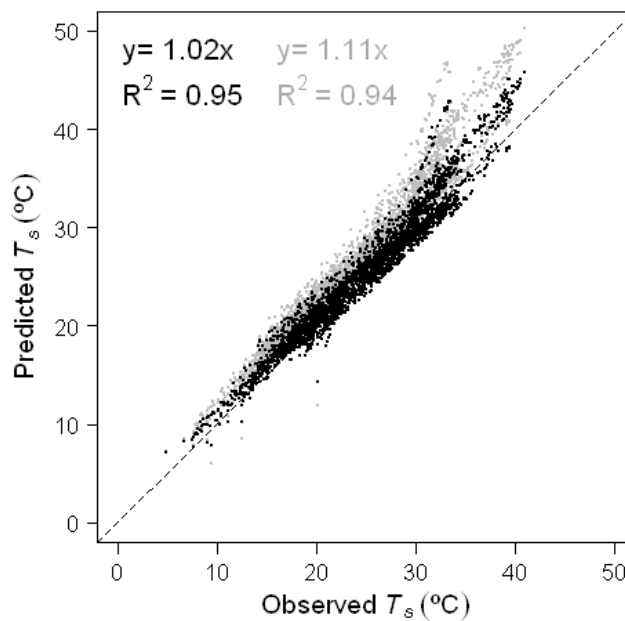


Figure 7. Comparison of soil surface temperature ground observations and TSM with iteration output. In grey, T_s predicted by the TSM model with the parallel resistance approach (TSM_P) and in black, T_s predicted by the TSM model with the series resistance approach (TSM_S) (N = 2991). The dashed line is the 1:1 reference line. Root Mean Squared Error (RMSE) was 3.27°C and 1.67°C for TSM_P and TSM_S results, respectively.

Table 4. Statistics comparing net Radiation (Rn), sensible heat (H) and latent heat (LE) fluxes observed and predicted by TSM using T_R and the iteration procedure (left) and using T_s and T'_c without iteration (right). Results of the TSM model with parallel (TSM_P) and series resistance (TSM_S) approaches are shown (N= 2991).

Flux	Resistance approach	TSM with iteration (using T_R)							TSM without iteration (using T_s and T'_c)					
		$\langle O \rangle$ W m ⁻²	$\langle P \rangle$ W m ⁻²	RMSE ^a W m ⁻²	MAE ^b W m ⁻²	MAPE ^c %	R ² -	slope -	$\langle P \rangle$ W m ⁻²	RMSE ^a W m ⁻²	MAE ^b W m ⁻²	MAPE ^c %	R ² -	slope -
Rn	TSM_P	375	412	58	46	12	0.93	0.95	418	62	49	13	0.93	0.95
	TSM_S		416	61	48	13	0.93	0.95						
H	TSM_P	209	176	64	51	25	0.75	0.72	176	64	48	23	0.77	0.66
	TSM_S		146	84	69	33	0.78	0.61	142	87	71	34	0.80	0.60
LE	TSM_P	115	185	105	86	74	0.36	0.90	192	105	84	73	0.39	0.86
	TSM_S		220	130	110	95	0.39	0.94	227	135	115	99	0.38	0.90

^a $\langle O \rangle$ is the observed average

^b $\langle P \rangle$ is the predicted average

^c Mean absolute error $MAE = \left(\sum_{i=1}^n |P_i - O_i| / n \right)$

^d Root mean square error $RMSE = \left[\left(\sum_{i=1}^n (P_i - O_i)^2 / n \right) \right]^{1/2}$

^e Mean absolute percentage error $MAPE = \frac{100}{\langle O \rangle} \left(\sum_{i=1}^n |P_i - O_i| / n \right)$, where P_i is the model prediction, and O_i is the observation

Evaluating the iteration procedure included in the original TSM

No significant changes in the scatterplots were found between the TSM *with iteration* (Fig. 6A-C) and the TSM *without iteration* (Fig. 6D-F), and statistics were similar (Table 4).

Nonetheless, some minor differences in H estimates depending on the model version (*with* or *without iteration*) are detected (Fig. 6B and E). These differences were more obvious with the TSM_P approach, which increased in bias when T_s and T'_c were used (slope = 0.66 vs. slope = 0.72) despite of a slight increase of explained variance ($R^2 = 0.77$ vs. $R^2 = 0.75$) and decrease of percentage errors (MAPE = 23% vs. MAPE = 25%) compared to the TSM_P using iteration. The TSM_S presented a very similar behaviour using iteration or not, showing the same tendency to underestimate high values of H as well as similar correlations ($R^2 = 0.80$ vs. $R^2 = 0.78$), slopes (0.60 and 0.61 respectively) and overall errors (MAPE = 34% and MAPE = 33%). These differences on estimation of H using T_s and T'_c did not significantly affected estimates of LE . The scatter plots continued to show wide dispersion for both TSM_P and TSM_S (Fig. 6C and F) and only the slopes were reduced from 0.90 to 0.86, using TSM_P , and from 0.94 to 0.90, using TSM_S , when iteration was not used (see Table 4).

In view of these results (Fig. 6 and Table 4), no strong differences between TSM performance using T_s and T'_c or T_R and iteration can be confirmed under natural semiarid conditions. Nonetheless, it is important to consider that the iterative procedure failed in a certain number of cases, not included or discussed in previous analyses. Iteration was not able to achieve energy closure for soil layer using measured G values for those failed cases (see Model Description Section). These iteration failures were more common using TSM_P , $N = 668$, than TSM_S , $N = 292$. In those cases when iteration failed, the TSM worked properly using observed T_s and T'_c . In Figure 8, predicted fluxes from the TSM *with iteration* and *without iteration* can be compared for only such cases. When the iteration procedure failed both in series and in parallel, TSM_P and TSM_S , iteration clearly overestimated H (predicted LE was always zero). However, without iteration, H was estimated better and was in good agreement, close to the 1:1 line. The iteration failed when using TSM_S mostly with low energy supply ($Rn < 300 \text{ W m}^{-2}$), whereas TSM_P iteration failed under a wider range of energy supply conditions (Rn between 0 - 600 W m^{-2}).

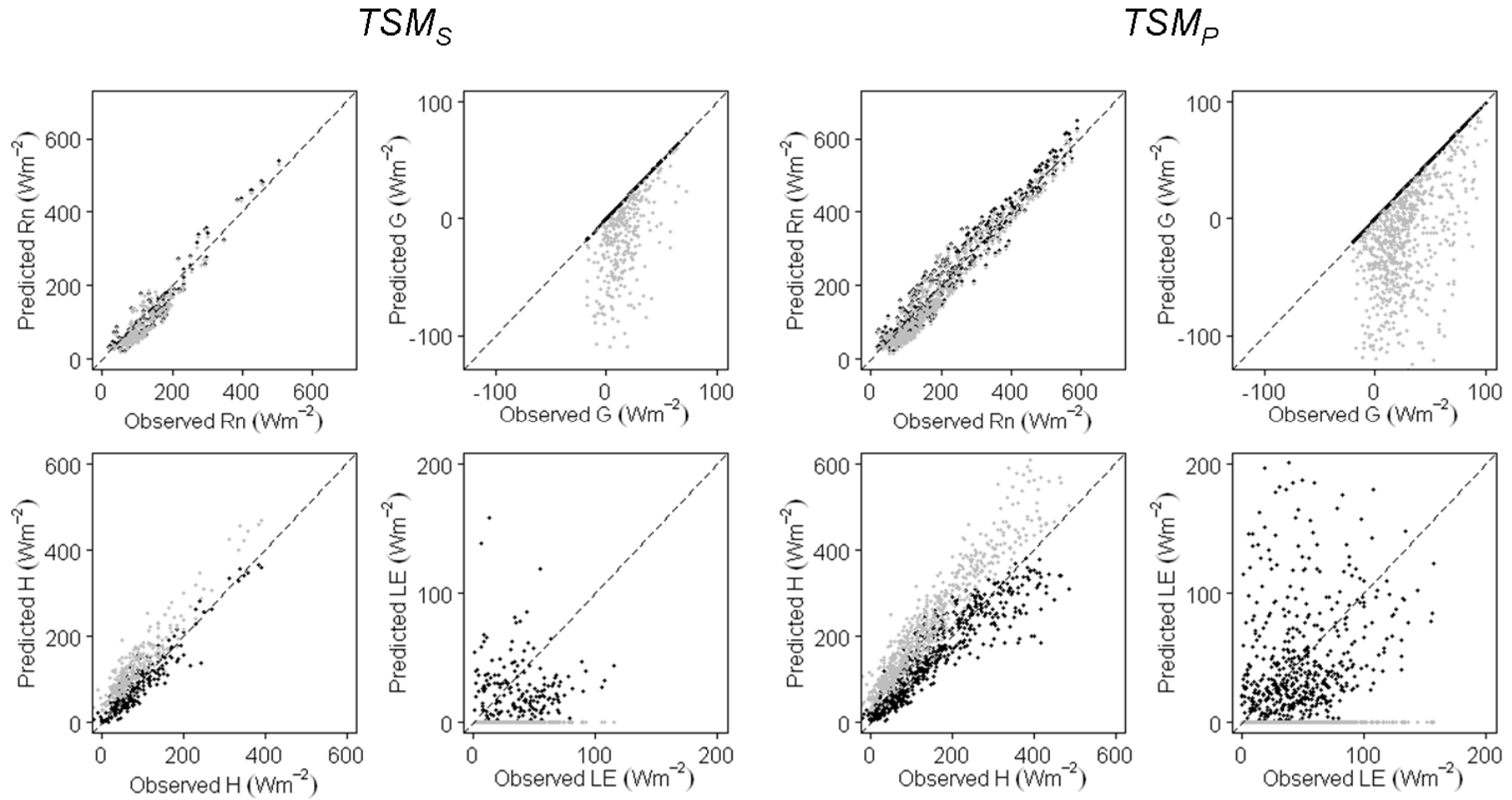


Figure 8. Linear regressions of estimated surface fluxes by TSM_P (left) and TSM_S (right) using measured T_s and derived T'_c without iteration (in black) and using T_R and with iteration (in grey) over their corresponding ground measurements: a) R_n , b) G , c) H , d) LE for those observations when iteration failed using TSM_P ($N = 668$) or using TSM_S ($N = 292$). Dashed line is the 1:1 line.

DISCUSSION

Accuracy of the TSM for surface flux estimation under Mediterranean semiarid conditions

Accurate estimation of surface fluxes in semiarid and sparsely vegetated areas is a particularly challenging task, more so when the latent heat flux is very low due to the strong water limitations (Fig. 2), such as in Mediterranean drylands (Domingo et al. 2011). Our results showed that under these conditions, the TSM of Norman et al. (1995) was accurate for estimating R_n and H fluxes, but not for LE even using measured G to reduce uncertainties affecting residually estimated LE .

Agreement between R_n ground observations and TSM model estimates was similar for the four TSM versions tested (parallel and series; with and without iteration) with overestimates showing a mean absolute percentage error (MAPE) of 12-13% (Table 4). This level of accuracy is satisfactory considering that only field measurements of incoming irradiance were used, and that the uncertainty of field measurements of R_n is from 5 to 10% (Kustas and Norman 1996). Similar level of accuracy has been reported by others authors (13%) in semiarid cotton croplands (Colaizzi et al. 2012c) who included specific modifications for radiation modelling in row crops (Colaizzi et al. 2012b) and in semiarid shrublands using ASTER reflectance for clear-sky conditions with errors below 8% (Garcia et al. 2008).

H estimated accuracy ranged from 23 to 34% depending on the model version (Table 4). This error is not unreasonable, bearing in mind the mismatch between the footprint of the infrared radiometers and the flux measurement area, with a spatial heterogeneity within the footprint area in T_R and vegetation greenness around 4% for both variables. Despite of that, it is remarkable that the error in H is not significantly higher than the 10% to 30% uncertainty affecting turbulent flux measurement by Eddy Covariance (Twine et al. 2000) which happens to be 20% in our study site (Fig. 4). This level of accuracy in H is similar to that found by Li et al. (2005), who applied the TSM in soy and corn croplands under different vegetation cover and water availability conditions, with mean relative errors of from 34 to 38%. Our errors were slightly higher than the range of errors reported by previous authors in a semiarid rangeland in Arizona (19-24%) (Norman et al. 1995; Timmermans et al. 2007; Zhan et al. 1996). However, it is important to highlight that some of these studies tested the TSM under semiarid conditions only during the wet season (Zhan et al. 1996), or using data only for short periods (3 days) (Timmermans et al. 2007). The reported tendency of the TSM to underestimate for high H at our field site (Fig. 6B and E) was observed at times when H was higher than LE , which was also

reported by Zhan et al. (1996) for H over 300 W m^{-2} . We observed this TSM behaviour both with and without iteration (known T_s and T'_c). This shows that the tendency to underestimate is not related to limitations in the iteration approach, but could be interpreted as an indicator of an overall limitation of the TSM when H is the dominant flux and also an effect to compensate for the overestimates in Rn . It is also likely that when H is the dominant flux and conditions become warmer, the surface heterogeneity within the footprint increases as was shown in Table 2, using a diurnal UAV campaign, increasing the likelihood of a mismatch between surface fluxes measured by the EC system and estimated by the TSM model (Vivoni et al. 2010).

The TSM showed a high MAE in LE of 84 W m^{-2} (73%) to 115 W m^{-2} (99%), and low linear agreement with R^2 always below 0.4 (see Fig. 6C and F). French et al. (2003) also found higher errors in LE estimates using the TSM in bare soils and patchy pasture lands (53% and 30% of relative error MAPE, respectively) than in more uniform pastures (10-16%). Agam et al. (2010) also reported high MAE of around 65 W m^{-2} in LE estimates under natural semiarid conditions with high vapor pressure deficit and low LAI using an initial α_{PT} of 1.3. They suggested that the reduction of the initial value of α_{PT} used in the iteration could be consider as a possible solution to reduce LE errors in the TSM under such conditions. However, our results show that similar errors affecting LE were found using the TSM *without iteration* with no Priestley-Taylor assumption. This points out that other factors different to those related with the iteration should be causing the TSM derived LE errors. Modelling LE at Mediterranean water-stressed sites like ours, where 15- min LE observations are within the range of EC closure errors during several days is challenging. As the TSM estimates LE as a residual of the energy balance equation, biases from H , Rn and G might accumulate in the LE estimates and higher non-systematic errors could be expected (Kalma et al. 2008). In the present work measurements of G flux were here used to reduce uncertainties affecting LE , because modelled G from Eq. 7, even using a site calibrated c_g value ($c_g = 0.16$), resulted in considerable errors ($R^2=0.52$ and MAPE of 30%, results not shown). Even though, the effect of a slight overestimation of Rn and underestimation of H strongly affected LE predictions which were hence overestimated in our semiarid site. Furthermore, a *residual-LE closure* was used for validation following the conclusions of previous authors (see Material and Methods Section, Model Validation Subsection). Therefore, uncertainty of observed LE on one hand and errors in estimating Rn and H on the other could explain the wide scatter in the LE scatterplots (Fig. 6C and F). Other models tested to estimate daily LE at the same field site also provide low correlations: R^2 of 0.33

to 0.49 using a Penman-Monteith model (Capítulo 3) and $R^2 = 0.57$ using a Priestley-Taylor mod.

Practical aspects for use of the TSM in Mediterranean drylands

Even though the parallel resistances version of the TSM (TSM_P) was originally recommended for sparsely vegetated semiarid regions and the series resistances version (TSM_S) for more densely vegetated regions (Kustas and Norman 1999b; Norman et al. 1995), results of testing both versions under a variety of conditions have been ambivalent (Kustas and Norman 1997, 1999a; Li et al. 2005; Zhan et al. 1996). Therefore, there is not yet a general agreement on which TSM version should be selected in each case. In this paper, the two resistance approaches to estimate surface energy fluxes under natural semiarid Mediterranean conditions were compared, and in agreement with Li et al. (2005) and Zhan et al. (1996), no strong differences were found between fluxes from the two approaches. However, the overall errors for H and LE fluxes were slightly lower (~10% and ~20% respectively) with the parallel resistance approach than the series (Table 4) for the TSM *with* and *without iteration*. Some differences between the series and parallel approaches were only noticeable with TSM *with iteration* (Fig. 6B and E). In this case, the series approach showed a stronger tendency to underestimate H , whereas the parallel schemes sometimes also overestimated H , showing a better general tendency (slope = 0.61 vs. slope = 0.72), but slightly lower explained variance than the series approach ($R^2 = 0.75$ vs. $R^2 = 0.78$) (Table 4 and Fig. 6). Underestimates of H have also been found in agricultural areas toward the end of the wet season using the series version of the TSM when non-transpiring plant components or senescent leaves increased (Colaizzi et al. 2012a; French et al. 2007). Limitations affecting the design of the TSM_S for partitioning of soil-canopy fluxes based on the Priestley-Taylor assumption under high senescent vegetation conditions were suggested by these authors as possible explanation. Considering that accumulation of senescent leaves in the canopy is a typical characteristic of perennial grasslands like our field site, in the present study we accounted for the variation of the green canopy fraction (f_G) and the reduction of α_{PT} was allowed in the iterative procedure (see Model Description Section). However systematic underestimation of H flux from TSM_S was still observed at high observed H rates, when senescent components are expected to be higher, and similar tendency was also observed using the TSM_S run *without iteration*. Colaizzi et al. (2012c) also obtained overestimates of evapotranspiration, which should be derived from underestimates of H , for both TSM versions *with* or *without iteration* when canopy contained non transpiring elements. They used an

alternative to the Priestley-Taylor equation based on Penman-Monteith and despite of the fact that uncertainties were reduced, overestimates in LE were still found. They attributed those errors to downward bias in measurements of T_R and T_c with field infrared thermometers viewing a greater proportion of the top and greener part of the canopy colder than the whole canopy contained a higher proportion of non transpiring elements. In our study similar errors could be affecting producing T_R underestimates and possible upward bias of T_s , as it is measured in an area slightly less shaded than the portion of bare soil area in the footprint area of T_R .

However, overestimates of H using TSM_P and *iteration* are related to the thermal gradient considered in the parallel resistance approach (driven by T_s-T_a and T_c-T_a), which is higher than with series resistance (driven by T_s-T_{ac} and T_c-T_{ac}). This higher thermal gradient in the parallel approach results in more frequent overestimation of H (Fig. 6B) and in some $LE = 0$ predictions, despite observed LE being of almost 150 W m^{-2} . Predicted $LE = 0$ were also found by Kustas and Norman (1997), who attributed them to outliers in H retrievals. In this regard, the series approach, due to the moderating effect of the air temperature in the canopy interface (T_{ac}), was more effective in limiting an unrealistic rise in T_s , and thereby, possible overestimates of H_s (see detailed analysis in Li et al. 2005). In our study, the series resistance was also more robust than the parallel resistance, regardless of whether the model was run *with iteration* or *without* (Fig. 6B and E). This agrees with previous analyses, in which it has been claimed that TSM_S is more robust, and that it can therefore be applied to a wider range of environmental conditions (Kustas and Norman 1999a; Li et al. 2005).

The comparison of T_s estimated from *iteration* and observed can also provide some insights into the accuracy of turbulent soil and canopy flux partitioning by the two resistance approaches. Partitioning seems to have been adequate with both TSM approaches when soil temperatures were below 30°C (Fig. 7), but turned out to be more problematic at higher T_s conditions, with both resistance schemes showing a tendency to overestimate T_s , and presumably H_s , with the TSM_S presenting better fit and a lower T_s bias. This seems to indicate that the series approach allowed more accurate partitioning of turbulent fluxes in our semiarid Mediterranean conditions, which might also be indicated by a higher R^2 than for the parallel version. Compared to other studies, the overall errors for T_s estimation *with iteration* at our site (3.37°C and 1.67°C RMSE for TSM_P and TSM_S , respectively) were lower than in previous studies on soybean and corn crops (RMSE~ 4°C) (Li et al. 2005) although in those cases T_s came from the TSM run using T_R from satellite remote sensing images.

Minor differences between TSM performance *with and without iteration* were found in our field site when the iteration worked properly. Those differences were more noticeable using TSM_P than TSM_S , which could indicate weaker effectiveness of iteration for flux partitioning with the parallel resistance approach. More noticeable differences between observed and predicted LE from the original TSM and the simplified TSM version using measured T_s and T_c , (~10% of difference on MAPE), were shown by Colaizzi et al. (2012c) using the series resistance scheme in a irrigated cotton crop area. However, several differences between the their work and ours regarding water availability (dryland vs. irrigated cropland), ecosystem type (grassland vs. cotton cropland), methodology used to measure T_s and T_c and model design (Priestley-Taylor assumption vs. Penman Monteith assumption for the initial estimation of T_c) make it difficult to discern the reason behind different model performance.

Finally, in evaluating the iteration procedure proposed by Norman et al. (1995), it is also important to consider failed iteration in a certain number of cases in which the TSM was accurate using T_s and T'_c (Fig. 8). This iteration failures could be related with the unsuitability of $\alpha_{PT}=1.3$ used to initialize the iteration in natural semiarid areas (Agam et al. 2010). The unreliability of this value could cause overestimates of initial LE_c resulting in $LE_s = 0$ and overestimates of H_s from the overall energy balance which will force the iteration to reduce G flux to unreliable values ($G \ll 0$) (Fig. 8). The fact that iteration failed more often using TSM_P and in a wider range of energy supply conditions ($0 < Rn < 600 \text{ W m}^{-2}$) than TSM_S (mostly $Rn < 300 \text{ W m}^{-2}$) can also be attributed to the moderating effect of the air temperature in the canopy interface (T_{ac}) using TSM_S reducing H_s overestimations.

CONCLUSIONS

Our analysis using aggregated soil-vegetation radiometric temperatures showed that the TSM can be applied operationally, producing reliable estimates of sensible heat flux, H , and net radiation, Rn , fluxes with error levels of $\sim 30\%$ and $\sim 10\%$ respectively, under the wide range of environmental conditions typical of Mediterranean semiarid perennial grasslands. However, latent heat flux, LE , estimates were not accurate and errors ranged from 73 to 99%. The residual estimation of LE in the TSM has also been shown to be problematic in areas where the magnitude of the LE flux is as low (average daytime LE of 70 W m^{-2}) as in our Mediterranean field site. Under these conditions, inaccuracies associated with Rn and H fluxes from the TSM, especially the latter, showed a strong impact on LE estimates. Reduction of uncertainties of temperature measurements should be addressed in order to reduce errors affecting H flux and improve LE estimates from the TSM under semiarid natural conditions. Methods with a lower sensitivity of surface temperature uncertainties as the Dual-Temperature-Difference (DTD) method (Kustas et al. 2012) can also be a promising alternative which will be compared in future works with the TSM.

The choice of parallel or series resistance for the TSM was revealed to be unimportant for the overall TSM performance in semiarid areas, as no significant differences between model approaches were found at our field site, nor at other natural semiarid areas tested. However, despite having slightly lower errors in H ($\sim 10\%$) and LE ($\sim 20\%$) estimates when using the parallel approach, there is some evidence of better suitability of series resistance. It seems that the effect of considering air temperature in the canopy interface with the series approach was appreciably better than with the parallel approach for separating total fluxes into canopy and soil, and also reduced the number of cases of algorithm failure. Nonetheless, in order to establish the best resistance approach for accurate partitioning of total turbulent fluxes under semiarid Mediterranean conditions, comparisons with soil and canopy fluxes measured separately must be evaluated. Regarding the effect of using a composite soil-vegetation temperature with iteration or separate canopy and soil temperatures directly, our H estimates presented lower the scatter without iteration under the parallel approach ($R^2 = 0.77$ vs. $R^2 = 0.74$) and a 2% of reduction in MAPE, while in the series approach the results were more robust as they did not change significantly with or without iteration. These results show the robustness of the iteration procedure, especially under the series scheme, to disaggregate composite a soil-vegetation temperature into its separate soil and vegetation components in semiarid grasslands providing good prospects for up-scaling using mono-angle remote sensing data.

REFERENCES

- Abrams, M., & Hook, S. (2002). ASTER user handbook version. Jet Propulsion Laboratory, California Institute of Technology, pp 135.
- Agam, N., Kustas, W.P., Anderson, M.C., Norman, J.M., Colaizzi, P.D., Howell, T.A., Prueger, J.H., Meyers, T.P., & Wilson, T.B. (2010). Application of the Priestley-Taylor approach in a two-source surface energy balance model. *Journal of Hydrometeorology*, 11, 185-198
- Alfieri, J.G., Kustas, W.P., Prueger, J.H., Hipps, L.E., Evett, S.R., Basara, J.B., Neale, C.M.U., French, A.N., Colaizzi, P., Agam, N., Cosh, M.H., Chavez, J.L., & Howell, T.A. (2012). On the discrepancy between eddy covariance and lysimetry-based surface flux measurements under strongly advective conditions. *Advances in Water Resources*, 50, 62-78
- Anderson, M.C., Norman, J.M., Diak, G.R., Kustas, W.P., & Mecikalski, J.R. (1997). A two-source time-integrated model for estimating surface fluxes using thermal infrared remote sensing. *Remote Sensing of Environment*, 60, 195-216
- Bastiaanssen, W.G.M., Menenti, M., Feddes, R.A., & Holtslag, A.A.M. (1998). A remote sensing surface energy balance algorithm for land (SEBAL): 1. Formulation. *Journal of Hydrology*, 212-213, 198-212
- Berni, J.A.J., Zarco-Tejada, P.J., Suarez, L., & Fereres, E. (2009). Thermal and Narrowband Multispectral Remote Sensing for Vegetation Monitoring From an Unmanned Aerial Vehicle. *IEEE Transactions on Geoscience and Remote Sensing*, 47, 722-738
- Brutsaert, W. (1982). Evaporation into the atmosphere-Theory, history, and applications. Dordrecht, Holland: D. Reidel Publishing Company, pp.299.
- Bugbee, B., Monje, O., & Tanner, B. (1996). Quantifying energy and mass transfer in crop canopies: Sensors for measurement of temperature and air velocity. *Advances in Space Research*, 18, 149-156
- Campbell, G. S., & Norman, J. M. (1998). An introduction to environmental biophysics. New York: Springer, pp 286.
- Cleugh, H.A., Leuning, R., Mu, Q., & Running, S.W. (2007). Regional evaporation estimates from flux tower and MODIS satellite data. *Remote Sensing of Environment*, 106, 285-304
- Colaizzi, P.D., Evett, S.R., Howell, T.A., Gowda, P.H., O'Shaughnessy, S.A., Tolck, J.A., Kustas, W.P., & Anderson, M.C. (2012a). Two-source energy balance model: Refinements and lysimeter tests in the southern high plains. *Transactions of the ASABE*, 55, 551-562
- Colaizzi, P.D., Evett, S.R., Howell, T.A., Li, F., Kustas, W.P., & Anderson, M.C. (2012b). Radiation model for row crops: I. Geometric view factors and parameter optimization. *Agronomy Journal*, 104, 225-240
- Colaizzi, P.D., Kustas, W.P., Anderson, M.C., Agam, N., Tolck, J.A., Evett, S.R., Howell, T.A., Gowda, P.H., & O'Shaughnessy, S.A. (2012c). Two-source energy balance model estimates of evapotranspiration using component and composite surface temperatures. *Advances in Water Resources*, 50, 134-151
- Chehbouni, A., LoSeen, D., Njoku, E.G., Lhomme, J.P., Monteny, B., & Kerr, Y.H. (1997). Estimation of sensible heat flux over sparsely vegetated surfaces. *Journal of Hydrology*, 189, 855-868

- Chehbouni, A., Nouvellon, Y., Lhomme, J.P., Watts, C., Boulet, G., Kerr, Y.H., Moran, M.S., & Goodrich, D.C. (2001). Estimation of surface sensible heat flux using dual angle observations of radiative surface temperature. *Agricultural and Forest Meteorology*, 108, 55-65
- Choudhury, B.J. (1987). Relationships between vegetation indices, radiation absorption, and net photosynthesis evaluated by a sensitivity analysis. *Remote Sensing of Environment*, 22, 209-233
- Choudhury, B.J. (1992). Multispectral satellite observations for arid land studies. *ISPRS Journal of Photogrammetry and Remote Sensing*, 47, 101-126
- Dash, P., Götsche, F.M., Olesen, F.S., & Fischer, H. (2002). Land surface temperature and emissivity estimation from passive sensor data: Theory and practice-current trends. *International Journal of Remote Sensing*, 23, 2563-2594
- Domingo, F., Serrano-Ortiz, P., Were, A., Villagarcía, L., García, M., Ramírez, D.A., Kowalski, A.S., Moro, M.J., Rey, A., & Oyonarte, C. (2011). Carbon and water exchange in semiarid ecosystems in SE Spain. *Journal of Arid Environments*, 75, 1271-1281
- Ershadi, A., McCabe, M.F., Evans, J.P., & Walker, J.P. (2013). Effects of spatial aggregation on the multi-scale estimation of evapotranspiration. *Remote Sensing of Environment*, 131, 51-62
- Fisher, J.B., Tu, K.P., & Baldocchi, D.D. (2008). Global estimates of the land-atmosphere water flux based on monthly AVHRR and ISLSCP-II data, validated at 16 FLUXNET sites. *Remote Sensing of Environment*, 112, 901-919
- French, A.N., Hunsaker, D.J., Clarke, T.R., Fitzgerald, G.J., Luckett, W.E., & Pinter Jr, P.J. (2007). Energy balance estimation of evapotranspiration for wheat grown under variable management practices in central Arizona. *Transactions of the ASABE*, 50, 2059-2071
- French, A.N., Schmugge, T.J., Kustas, W.P., Brubaker, K.L., & Prueger, J. (2003). Surface energy fluxes over El Reno, Oklahoma, using high-resolution remotely sensed data. *Water Resources Research*, 39, SWC31-SWC312
- Fuchs, M. (1986). Heat flux. In: A. Kute (Ed), *Methods of Soil Analysis Part I Physical and Meteorological Methods* (pp. 957-968). Madison, USA: American Society of Agronomy
- Gamon, J.A., Field, C.B., Goulden, M.L., Griffin, K.L., Hartley, A.E., Joel, G., Penuelas, J., & Valentini, R. (1995). Relationships between Ndvi, Canopy Structure, and Photosynthesis in 3 Californian Vegetation Types. *Ecological Applications*, 5, 28-41
- García, M., Oyonarte, C., Villagarcía, L., Contreras, S., Domingo, F., & Puigdefabregas, J. (2008). Monitoring land degradation risk using ASTER data: The non-evaporative fraction as an indicator of ecosystem function. *Remote Sensing of Environment*, 112, 3720-3736
- Garratt, J., & Hicks, B. (1973). Momentum, heat and water vapor transfer to and from natural and artificial surfaces. *Quarterly Journal of the Royal Meteorological Society*, 99, 680 - 687
- Glenn, E.P., Huete, A.R., Nagler, P.L., Hirschboeck, K.K., & Brown, P. (2007). Integrating remote sensing and ground methods to estimate evapotranspiration. *Critical Reviews in Plant Sciences*, 26, 139-168
- Gonzalez-Dugo, M.P., Neale, C.M.U., Mateos, L., Kustas, W.P., Prueger, J.H., Anderson, M.C., & Li, F. (2009). A comparison of operational remote sensing-based models for estimating crop evapotranspiration. *Agricultural and Forest Meteorology*, 149, 1843-1853
- Goudriaan, J. (1977). *Crop Micrometeorology: A simulation study*. Wageningen, The Netherlands: Center for Agricultural Publishing and Documentation, pp.257.

- Hall, F.G., Huemmrich, K.F., Goetz, S.J., Sellers, P.J., & Nickeson, J.E. (1992). Satellite remote sensing of surface energy balance: success, failures, and unresolved issues in FIFE. *Journal of Geophysical Research*, 97, 19,061-019,089
- Huxman, T.E., Wilcox, B.P., Breshears, D.D., Scott, R.L., Snyder, K.A., Small, E.E., Hultine, K., Pockman, W.T., & Jackson, R.B. (2005). Ecohydrological implications of woody plant encroachment. *Ecology*, 86, 308-319
- Kalma, J.D., McVicar, T.R., & McCabe, M.F. (2008). Estimating land surface evaporation: A review of methods using remotely sensed surface temperature data. *Surveys in Geophysics*, 29, 421-469
- Kondo, J., & Ishida, S. (1997). Sensible heat flux from the Earth's surface under natural convective conditions. *Journal of the Atmospheric Sciences*, 54, 498-509
- Kowalski, A.S., Anthoni, P.M., Vong, R.J., Delany, A.C., & Maclean, G.D. (1997). Deployment and evaluation of a system for ground-based measurement of cloud liquid water turbulent fluxes. *Journal of Atmospheric and Oceanic Technology*, 14, 468-479
- Kustas, W.P., Alfieri, J.G., Anderson, M.C., Colaizzi, P.D., Prueger, J.H., Evett, S.R., Neale, C.M.U., French, A.N., Hipps, L.E., Chávez, J.L., Copeland, K.S., & Howell, T.A. (2012). Evaluating the Two-Source Energy Balance Model using local thermal and surface flux observations in a strongly advective irrigated agricultural area. *Advances in Water Resources*, 50, 120-133
- Kustas, W., & Anderson, M. (2009). Advances in thermal infrared remote sensing for land surface modeling. *Agricultural and Forest Meteorology*, 149, 2071-2081
- Kustas, W.P., Humes, K.S., Norman, J.M., & Moran, M.S. (1996). Single- and dual-source modeling of surface energy fluxes with radiometric surface temperature. *Journal of Applied Meteorology*, 35, 110-121
- Kustas, W.P., & Norman, J.M. (1996). Use of remote sensing for evapotranspiration monitoring over land surfaces. *Hydrological Sciences Journal*, 41, 495-516
- Kustas, W.P., & Norman, J.M. (1997). A two-source approach for estimating turbulent fluxes using multiple angle thermal infrared observations. *Water Resources Research*, 33, 1495-1508
- Kustas, W.P., & Norman, J.M. (1999a). Evaluation of soil and vegetation heat flux predictions using a simple two-source model with radiometric temperatures for partial canopy cover. *Agricultural and Forest Meteorology*, 94, 13-29
- Kustas, W.P., & Norman, J.M. (1999b). Reply to comments about the basic equations of dual-source vegetation-atmosphere transfer models. *Agricultural and Forest Meteorology*, 94, 275-278
- Li, F., Kustas, W.P., Prueger, J.H., Neale, C.M.U., & Jackson, T.J. (2005). Utility of remote-sensing-based two-source energy balance model under low- and high-vegetation cover conditions. *Journal of Hydrometeorology*, 6, 878-891
- Massman, W.J. (1992). Correcting errors associated with soil heat flux measurements and estimating soil thermal properties from soil temperature and heat flux plate data. *Agricultural and Forest Meteorology*, 59, 249-266
- McMillen, R.T. (1988). An eddy correlation technique with extended applicability to non-simple terrain. *Boundary-Layer Meteorology*, 43, 231-245

- Mira, M., Valor, E., Boluda, R., Caselles, V., & Coll, C. (2007). Influence of soil water content on the thermal infrared emissivity of bare soils: Implication for land surface temperature determination. *Journal of Geophysical Research F: Earth Surface*, *112*(4), F04003
- Moran, M.S., Humes, K.S., & Pinter, P.J. (1997). The scaling characteristics of remotely-sensed variables for sparsely-vegetated heterogeneous landscapes. *Journal of Hydrology*, *190*, 337-362
- Norman, J.M., & Becker, F. (1995). Terminology in thermal infrared remote sensing of natural surfaces. *Agricultural and Forest Meteorology*, *77*, 153-166
- Norman, J.M., Kustas, W.P., & Humes, K.S. (1995). Source approach for estimating soil and vegetation energy fluxes in observations of directional radiometric surface temperature. *Agricultural and Forest Meteorology*, *77*, 263-293
- Priestley, C.H.B., & Taylor, R.J. (1972). On the assessment of surface heat flux and evaporation using large-scale parameters. *Monthly Weather Review*, *100*, 81-92
- Rana, G., & Katerji, N. (2000). Measurement and estimation of actual evapotranspiration in the field under Mediterranean climate: A review. *European Journal of Agronomy*, *13*, 125-153
- Rasmussen, M.O., Göttsche, F.M., Olesen, F.S., & Sandholt, I. (2011). Directional effects on land surface temperature estimation from meteosat second generation for savanna landscapes. *IEEE Transactions on Geoscience and Remote Sensing*, *49*, 4458-4468
- Rey, A., Pegoraro, E., Oyonarte, C., Were, A., Escribano, P., & Raimundo, J. (2011). Impact of land degradation on soil respiration in a steppe (*Stipa tenacissima* L.) semi-arid ecosystem in the SE of Spain. *Soil Biology and Biochemistry*, *43*, 393-403
- Reynolds, J.F., Kemp, P.R., & Tenhunen, J.D. (2000). Effects of long-term rainfall variability on evapotranspiration and soil water distribution in the Chihuahuan Desert: A modeling analysis. *Plant Ecology*, *150*, 145-159
- Sánchez, J.M., Caselles, V., Niclós, R., Coll, C., & Kustas, W.P. (2009). Estimating energy balance fluxes above a boreal forest from radiometric temperature observations. *Agricultural and Forest Meteorology*, *149*, 1037-1049
- Sánchez, J.M., Kustas, W.P., Caselles, V., & Anderson, M.C. (2008). Modelling surface energy fluxes over maize using a two-source patch model and radiometric soil and canopy temperature observations. *Remote Sensing of Environment*, *112*, 1130-1143
- Santanello, J.A., & Friedl, M.A. (2003). Diurnal covariation in soil heat flux and net radiation. *Journal of Applied Meteorology*, *42*, 851-862
- Sobrino, J.A., Raissouni, N., & Li, Z.L. (2001). A comparative study of land surface emissivity retrieval from NOAA data. *Remote Sensing of Environment*, *75*, 256-266
- Schaudt, K.J., & Dickinson, R.E. (2000). An approach to deriving roughness length and zero-plane displacement height from satellite data, prototyped with BOREAS data. *Agricultural and Forest Meteorology*, *104*, 143-155
- Schmid, H.P. (1994). Source areas for scalars and scalar fluxes. *Boundary-Layer Meteorology*, *67*, 293-318
- Schmid, H.P. (1997). Experimental design for flux measurements: Matching scales of observations and fluxes. *Agricultural and Forest Meteorology*, *87*, 179-200

- Timmermans, W.J., Kustas, W.P., Anderson, M.C., & French, A.N. (2007). An intercomparison of the Surface Energy Balance Algorithm for Land (SEBAL) and the Two-Source Energy Balance (TSEB) modeling schemes. *Remote Sensing of Environment*, 108, 369-384
- Trigo, I.F., Peres, L.F., DaCamara, C.C., & Freitas, S.C. (2008). Thermal land surface emissivity retrieved from SEVIRI/Meteosat. *IEEE Transactions on Geoscience and Remote Sensing*, 46, 307-315
- Troufleau, D., Lhomme, J.P., Monteny, B., & Vidal, A. (1997). Sensible heat flux and radiometric surface temperature over sparse Sahelian vegetation. I. An experimental analysis of the kB-1 parameter. *Journal of Hydrology*, 188-189, 815-838
- Twine, T.E., Kustas, W.P., Norman, J.M., Cook, D.R., Houser, P.R., Meyers, T.P., Prueger, J.H., Starks, P.J., & Wesely, M.L. (2000). Correcting eddy-covariance flux underestimates over a grassland. *Agricultural and Forest Meteorology*, 103, 279-300
- Villagarcía, L. (2000). Reformulación, parametrización y validación de un modelo de evapotranspiración para la vegetación dispersa. Tesis Doctoral. Almería. Universidad de Almería, pp. 216
- Vivoni, E.R., Watts, C.J., Rodriguez, J.C., Garatuza-Payan, J., Mendez-Barroso, L.A., & Saiz-Hernandez, J.A. (2010). Improved land-atmosphere relations through distributed footprint sampling in a subtropical scrubland during the North American monsoon. *Journal of Arid Environments*, 74, 579-584
- Wang, K., & Dickinson, R.E. (2012). A review of global terrestrial evapotranspiration: Observation, modeling, climatology, and climatic variability. *Reviews of Geophysics*, 50, RG2005
- Webb, E.K., Pearman, G.I., & Leuning, R. (1980). Correction of flux measurements for density effects due to heat and water vapor transfer. *Quarterly Journal Royal Meteorological Society*, 106, 85-100
- Were, A., Serrano-Ortiz, P., Moreno De Jong, C., Villagarcía, L., Domingo, F., & Kowalski, A.S. (2010). Ventilation of subterranean CO₂ and eddy covariance incongruities over carbonate ecosystems. *Biogeosciences*, 7, 859-867
- Wilson, K., Goldstein, A., Falge, E., Aubinet, M., Baldocchi, D., Berbigier, P., Bernhofer, C., Ceulemans, R., Dolman, H., Field, C., Grelle, A., Ibrom, A., Law, B.E., Kowalski, A., Meyers, T., Moncrieff, J., Monson, R., Oechel, W., Tenhunen, J., Valentini, R., & Verma, S. (2002). Energy balance closure at FLUXNET sites. *Agricultural and Forest Meteorology*, 113, 223-243
- Zarco-Tejada, P.J., Gonzalez-Dugo, V., & Berni, J.A.J. (2012). Fluorescence, temperature and narrow-band indices acquired from a UAV platform for water stress detection using a micro-hyperspectral imager and a thermal camera. *Remote Sensing of Environment*, 117, 322-337
- Zhan, X., Kustas, W.P., & Humes, K.S. (1996). An intercomparison study on models of sensible heat flux over partial canopy surfaces with remotely sensed surface temperature. *Remote Sensing of Environment*, 58, 242-256

CAPITULO 2

Environmental factors affecting the accuracy of surface fluxes from a two-source model in Mediterranean drylands: upscaling instantaneous to daytime estimates

*Enviado a *Agricultural and Forest Meteorology* con los siguientes autores:
Laura Morillas, Luis Villagarcía, Mónica García, Héctor Nieto, Olga Uclés y Francisco Domingo.

ABSTRACT

The temperature-based Two-Source Model (TSM) of Norman et al. (1995) has not been properly evaluated under the water stress conditions typical of natural Mediterranean drylands. In such areas, the asynchrony between precipitation and energy supply, strongly reduces evapotranspiration E (or latent heat flux if expressed in energy terms,) making sensible heat flux (H) the dominant turbulent heat flux. We present a detailed analysis of the main environmental factors affecting the TSM effectiveness under such challenging conditions. The accuracy of the TSM, evaluated via errors in 15-min H estimates, was proved to have a diurnal variation. Accuracy was clearly reduced for solar elevation angles lower than 25° and during marginal hours of daytime, before 10 am and after 3 pm. The surface to air temperature difference, ($T_R - T_a$) and the wind speed were the two environmental factors showing the strongest effect on the TSM accuracy. In contrast with results observed in other ecosystems, in a Mediterranean tussock grassland the TSM accuracy was not clearly reduced by cloudiness and it was improved under higher water stress and stressed vegetation conditions. The parallel resistances scheme of the TSM (TSM_P) showed overall lower errors and a lower tendency to underestimate at high H values but the TSM_S reduced model errors under some specific conditions such low energy supply conditions and atmospheric neutral conditions.

Two extrapolation methods to obtain daytime turbulent fluxes from 15-min estimates from the TSM were compared: i) averaging the total daytime instantaneous fluxes derived from the TSM (Averaging method) and ii) assuming the constancy of midday values of the evaporative and the non evaporative fraction derived from TSM along the daytime period (EF or NEF method). Daytime estimates of H , and E were more accurate using the Averaging method than with the EF or NEF method. Moreover, daytime estimates of H and E were better when using instantaneous fluxes from the TSM_P than from the TSM_S . Thus, reliable daytime estimates of H were obtained from the TSM_P in a Mediterranean dryland, with mean errors of 20% and high correlations ($R^2=0.85$). However, daytime E was strongly overestimated (125%) using the TSM although a good correlation with eddy covariance measurements was found ($R^2=0.84$).

Keywords: turbulent heat fluxes, temperature-based two source model, model effectiveness, diurnal behavior, time extrapolation methods, Mediterranean dryland.

INTRODUCTION

A two-source energy balance model was proposed by Norman et al. (1995) for modelling the surface energy fluxes over sparse vegetated areas consisting of a more realistic and physically sound design than one-source models (OSM) (French et al. 2005; Timmermans et al. 2007). This model, known as the TSM, considers the surface to air temperature gradient as the key driver of the turbulent fluxes coming from soil and vegetation surfaces. The TSM, under a multilayer perspective, models the land surface as a resistance network between energy sources from soil, vegetation and the overlying atmosphere (French et al. 2005). Depending on the coupling assumed between temperatures of canopy and soil, the resistance network of the TSM can be considered *in series* (TSM_S), when interaction between canopy and soil temperatures is assumed or, *in parallel* (TSM_P) assuming no thermal interaction exist between both layers (Kustas and Norman 1999b). To account for the partitioning of turbulent fluxes between soil and canopy layers by the TSM, radiometric temperatures from soil (T_s) and canopy (T_c) are necessary. However, the spatial resolution of most of the surface temperature (T_R) data provided by remote sensing is commonly too coarse to distinguish between them. The TSM faces this issue applying an iterative procedure based on two main assumptions. First a simple linear contribution of the soil and canopy emitted radiances, proportional to vegetation cover, to the remotely sensed radiance measured by the temperature sensor is assumed (see Capítulo 1). The second assumption considers an initial canopy latent heat flux (LE_c) responding to a potential rate estimated by the Priestley-Taylor equation (Priestley and Taylor 1972). This initial LE_c value is iteratively overridden until the surface energy balance equation on both soil and canopy layers is met. Thus, the TSM retrieves H and LE estimates of soil and canopy layers using single measurements of T_R , meteorological variables (air temperature, vapor pressure deficit, wind speed, and solar irradiance) and ancillary information about the vegetation (leaf area index, vegetation height and cover fraction) (Colaizzi et al. 2012b). A detailed description of the TSM formulation can be found in Capítulo 1.

Many studies have tested the utility of the TSM and subsequent improvements over a broad range of vegetation cover and climate conditions (see a summary in Wang and Dickinson 2012). Nonetheless, the TSM model has been particularly recommended for clear sky conditions, high thermal difference between soil and canopy (Wang and Dickinson 2012) and no presence of senescent vegetation (Colaizzi et al. 2012a; Norman et al. 1995). Kustas and Anderson (2009) evaluated the TSM performance (in comparison with OSM) under extreme scenarios simulated by the Cupid model, a complex soil-vegetation-atmosphere transfer (SVAT) model, and they did

not found special limitations for their water stressed vegetation scenario. However, model performance has not been properly in-situ evaluated under strong water limited conditions where H represents a significantly greater proportion of the available energy as it occurs in Mediterranean drylands (García et al. 2007). In Capítulo 1 the TSM behaviour under the natural water-limited conditions characterizing Mediterranean drylands was presented during an extensive time period (5 months including the growing season) for the first time in studies of TSM. Those results showed that the TSM produces reliable estimates of the dominant turbulent flux H , with errors around 30%, despite of the fact that significant variability was still found ($R^2 = 0.75-0.78$). However, poor accuracy was found for the LE flux with errors up to ~90%. These results highlighted the need of clarifying under which environmental conditions the TSM effectiveness is reduced in natural arid and semiarid areas. This is a prior step before further model development and improvement in natural arid and semiarid ecosystems can be undertaken.

The TSM was originally designed to estimate the surface energy fluxes using instantaneous surface temperature retrievals from remote sensing sensors (Norman et al. 1995). The model is designed to be applied during daytime conditions and is based on parameterizations optimized for a period encompassing few hours around solar noon (Kustas and Anderson 2009). Even though, when continuous T_R measurements have been available, the TSM has been applied for the complete daytime period (Colaizzi et al. 2012b; Norman et al. 2000; Sánchez et al. 2008). Nonetheless, the diurnal behaviour of the TSM has not been discussed yet, despite of the fact that other temperature-based models have shown weakness during marginal hours of daytime period (Su 2002). This has important practical implications for potential users of the TSM, especially when data from sun synchronous satellites, limited to the time of the satellite overpass, are going to be used for model running.

The majority of studies in relation to the TSM have analyzed model accuracy just for instantaneous fluxes. However, daily or daytime estimates of turbulent fluxes are required for water resources monitoring and ecological management purposes (Glenn et al. 2007; Kalma et al. 2008). Some papers have shown acceptable results when estimating daily E using the TSM in irrigated agricultural areas (Colaizzi et al. 2012a; Colaizzi et al. 2012b; French et al. 2007; Gonzalez-Dugo et al. 2009). Nevertheless, no references exist in the bibliography about the possibilities to obtain daytime turbulent fluxes using the TSM in Mediterranean semiarid natural areas where it is expected a reduced daily LE and increased daytime H fluxes (Domingo et al. 2011).

The objective of this work is to clarify some of the issues previously described regarding TSM performance under Mediterranean natural semiarid conditions. Specifically, three issues have been evaluated in the present work: i) the diurnal behaviour of the TSM to estimate the dominant H flux, ii) the main environmental factors affecting model accuracy for estimating the H flux in semiarid areas and iii) the capacity of the TSM to obtain daytime values of H and E at Mediterranean semiarid sites. To perform these analyses we used a dataset including in-situ flux measurements and 15 minute TSM model outputs from both series and parallel schemes of surface energy fluxes (Capítulo 1). The analysis performed here should provide new insights on the effectiveness and sensitivity of the two resistance schemes of the TSM under a wide range of environmental conditions and set the basis for estimating diurnal surface fluxes from instantaneous estimates from satellite images in Mediterranean semiarid grasslands.

EXPERIMENTAL DATASET AND FIELD SITE MEASUREMENTS

This study was performed in a Mediterranean semiarid field site called Balsa Blanca located in southeast Spain ($36^{\circ}56'24.17''\text{N}$; $2^{\circ}1'59.55''\text{O}$). The vegetation of the site is sparse and it is dominated by the perennial tussock grass *Stipa tenacissima* (L.) showing a cover fraction (fc) estimated on the field of 0.6. The climate is Mediterranean semiarid with a mean annual rainfall of 200 mm and a mean annual temperature of 18°C . More detailed information about the site can be found in Rey et al. (2012).

This field site was equipped with an Eddy Covariance (EC) system located at 3.5 m height for measuring H and LE fluxes from an homogeneous and representative area at 10 Hz frequency (further details in Capítulo 1). Averaged values of H and LE every 15 min were recorded in a datalogger (Campbell Scientific Inc., USA) and considered here as instantaneous fluxes. In order to assure the energy closure of our EC derived measurements, which presented an imbalance of ~20%, the *residual-LE* closure method was applied (Twine et al. 2000) as previous authors suggested (Alfieri et al. 2012; Li et al. 2005)

Measurements of surface temperature (T_R) for model running and additional measurements of bare soil temperature (T_s) were acquired within the 100m fetch of the EC tower using broadband thermal infrared thermometers, Apogee IRTS-P (Campbell Scientific Inc., USA). T_R was measured with a sensor placed at 3.5m height observing the ground at nadir over a sampling area of 3.70 m in diameter, which is a representative mixture of soil and vegetation. T_s was on the other hand measured at 0.65m height over a sampling bare soil area of 0.69 m in diameter.

Incoming short-wave radiation (S) was also measured at 3.5 m height using a LP02 Pyranometer (Campbell Scientific Inc.,USA). Temperatures and radiances were measured every minute and stored as 15-min averages in a datalogger (Campbell Scientific Inc.,USA). Brightness temperatures sensed by the IRT-P sensors were transformed into radiometric temperatures (see Norman and Becker 1995 for terminology clarification) by correction of emissivity and atmospheric effects (details of temperature pre-processing can be found in Capítulo 1). Air temperature (T_a) and relative humidity of the air (HR) were also measured at 2.5 m every minute with a thermo-hygrometer (HMP45C, Campbell Scientific Inc.,USA) and 15- min averages were also stored. Leaf area index (LAI) was acquired from the *Moderate Resolution Imaging Spectroradiometer* (MODIS) onboard the Terra and Aqua satellites with 1-km pixel resolution (see more details in Capítulo 1). Additionally, the Soil Water Content (SWC) was measured from a water content reflectometer (model CS616, Campbell Scientific INC., USA) located at 0.04 m depth in bare soil. SWC was used in present work to characterize water availability conditions. Soil profile temperature was measured with two thermocouples (TCAV) at 0.02 and 0.06 depth, which they were later used to correct soil temperature variations on SWC measurements by applying the calibration standard quadratic equation detailed by the manufacturer (Campbell Scientific INC., USA).

In order to accomplish the objectives of this work we used a complete dataset including 15-min measurements (EC derived) and predictions of the H and LE fluxes derived from the original TSM presented by Norman et al. (1995) and including the latest improvements proposed by Kustas and Norman (1999a). The detailed description of the main equations can be found in Capítulo 1. Predictions of H and LE from the two possible resistance arrangements of the TSM, parallel (TSM_P) and series (TSM_S), were included. The study time period was from January 15th (day of year - DOY 15) to June 9th (DOY 160) 2011, covering a wide range of environmental conditions (see observed ranges in Table 2). The dataset evaluated included those observations for which H and LE estimates were obtained from the TSM with a correct behaviour of the iterative procedure (N= 2991) (see more details in Capítulo 1).

METHODS

Analyzing the diurnal behaviour of the TSM

To study the diurnal behaviour of the TSM, we have assessed the relationship between the accuracy of the instantaneous H estimates and the two main factors related with solar energy supply that change during the daytime period: the time of the day and the solar elevation angle, reflecting a seasonal component. The time of day is the most common factor considered in evaluations of the diurnal behaviour of models because of its implications when using sun-synchronous satellite data, usually reduced to one daily acquisition, for model running. However, the solar energy supply, the main factor controlling the surface energy fluxes, is mainly driven by the solar elevation angle. For instance, incoming solar radiation at one specific time of day clearly differs between wintertime and summertime due to a higher solar elevation angle in summer. Consequently, the accuracy of the TSM can be expected to change depending on these two factors, time of the day and solar elevation along the year.

In order to analyze the effect that these two non-independent factors have over the TSM accuracy, a sequential analysis was performed. First, we evaluated the evolution of the TSM accuracy under a linear gradient of observed solar elevation angles (SE) (see ranges of SE in Table 1) using the entire 15-min dataset ($N=2991$). By doing so we established the minimum solar angle conditions necessary for the TSM to success along the year. Secondly, the evolution of the TSM accuracy during daytime hours was analyzed hour by hour between 7 am to 4 pm by using a data subset in which those solar elevation conditions with reduced the TSM accuracy based on the previous analysis were removed ($N=2667$). In this way, this second analysis will show only the effects due to time of the day regardless of the solar elevation effects. From this sequential analysis the range of minimum solar elevation angle and time of day under which a robust behaviour of the TSM can be found in our semiarid conditions along the year will be determined.

The TSM accuracy was quantified using the *Mean Absolute Percentage Error* (MAPE) and the coefficient of determination (R^2), between observed and TSM predicted H . The coefficient of determination (R^2) was selected as an indicator of the proportion of variance explained by the model. MAPE was computed by Eq. 1 where O_i and P_i represent observed and predicted values respectively. This statistic normalizes the absolute error to the magnitude of the observed flux, making it possible to compare model accuracy under conditions in which the magnitude of the modelled flux can strongly differ as it happens along the day.

$$MAPE = \frac{100}{n} \left(\sum_{i=1}^n |P_i - O_i| / O_i \right) \quad (1)$$

Additionally, to determine the ranges of *SE* and Time of day for which the accuracy of the model differed significantly (p-value < 0.05) Tukey HSD tests were performed (Sokal and Rohlf 2012).

Assessing model response to environmental factors

In order to identify the conditions under which the TSM performance reduces its effectiveness and assess the factors showing a stronger effect on model performance, the effect of nine factors on model accuracy was evaluated. Those factors were chosen in order to reflect different conditions of energy supply, water availability, vegetation status and state of the boundary layer.

Three factors were related to the energy supply: solar irradiance (*S*), cloud sky cover represented by a cloud factor (*clf*), and the surface to-air temperature difference ($T_R - T_a$).

The cloud factor was estimated as Crawford and Duchon (1999) proposed (Eq. 2). *clf* ranges from a totally clear sky is represented by *clf*=0 to a totally covered sky conditions represented by *clf*=1.

$$clf = 1 - s \quad (2)$$

where *s* is the ratio between solar irradiance (*S*) and potential clear sky irradiance at the ground (R_{so}). R_{so} was estimated by Eq.3, an approach proposed by Allen et al. (1998) based on Beer's Law.

$$R_{so} = R_a \exp\left(\frac{0.0018P}{Kt \sin \phi}\right) \quad (3)$$

where R_a (MJ m^{-2}) is the extraterrestrial solar irradiance that depends on the day of the year, latitude and solar time, *Kt* is a turbidity coefficient whose value is assumed in our study to

be 1 reflecting clean air conditions; P is the atmospheric pressure (kPa) and ϕ is the angle of the solar elevation angle (rad).

Two factors were selected to represent water availability conditions: soil water content (*SWC*) measured at 0.04 m depth in a bare soil area and vapor pressure deficit (*VPD*). Two factors were mostly related to vegetation status: leaf area index (*LAI*) and the difference between soil and surface radiometric temperature ($T_s - T_R$). T_R can be used as an indirect indicator of the vegetation status so that when ($T_s - T_R$) is high, vegetation should be colder than soil, suggesting possibly high transpiration rates, while when ($T_s - T_R$) is low or even negative, this suggests that vegetation is inactive and/or is strongly water stressed.

Finally the two factors related to boundary layer conditions were wind speed (*WS*) and the stability index z_s/L (Monteith and Unsworth 1990), where z_s is the effective height of the flux measurement system and L is the Monin-Obukhov length. Based on this stability index, the atmospheric conditions can be divided in stable ($z_s/L > 0.01$), neutral ($-0.01 < z_s/L < 0.01$) and unstable conditions ($z_s/L < -0.01$).

To study the *TSM* effectiveness over the observed range of variation of the nine factors, we used a data subset that included only those observations for which the accuracy of the *TSM* was not significantly affected by the solar elevation and the time of day conditions according to the analysis previously exposed of the diurnal behavior of the *TSM* (see previous Section). In this way the effect of the factors over the *TSM* was studied controlling for two previously studied factors: *SE* and Time of day. The observed range of variation of each factor was divided in 5 classes (See Table 2) and model accuracy was quantified for each class established with a minimum number of observations ($n > 11$). Four statistics were used to quantify model accuracy over *H*: *Mean Absolute Percentage Error* (MAPE, Eq. 1), *Mean Percentage Error* (MPE, Eq. 4), the *slope* of the regression between observed and predicted *H* and the coefficient of determination (R^2).

$$MPE = \frac{100}{n} \left(\sum_{i=1}^n P_i - O_i / O_i \right) \quad (4)$$

These four statistics were calculated for each of the five classes within each environmental factor.

Extrapolation from instantaneous to daytime fluxes

We evaluated two methods to extrapolate daytime turbulent fluxes, H_D and LE_D , from instantaneous estimates of TSM, (H_i , LE_i and AE_i): i) using midday estimates of the *evaporative fraction (EF)* and the *non evaporative fraction (NEF)* derived from TSM and assuming that those remain constant during the daytime period (*EF method* or *NEF method* respectively) and ii) by averaging all the estimates of H_i and LE_i available during daytime (*Averaging method*).

The *EF* or *NEF method* is based on the assumption that both *EF*, which is the portion of available energy ($AE = Rn - G$) dissipated as latent heat flux ($EF=LE/AE$), and its complementary *NEF*, the portion of available energy dissipated as sensible heat flux ($NEF=H/AE$), remain constant along the daytime period (Crago 1996). Based on this assumption, H_D and LE_D can be estimated from instantaneous values of EF_i or NEF_i and daytime averages of the available energy (AE_D) as it is presented in Eq. 5 and 6 (with i and D subscripts referring instantaneous and daytime averages respectively).

$$\frac{LE_i}{AE_i} = \frac{LE_D}{AE_D} \Leftrightarrow EF_i = EF_D \Rightarrow LE_D = EF_i \times AE_D \quad (5)$$

$$\frac{H_i}{AE_i} = \frac{H_D}{AE_D} \Leftrightarrow NEF_i = NEF_D \Rightarrow H_D = NEF_i \times AE_D \quad (6)$$

Traditionally, midday estimates of NEF_i or EF_i have been used in Eq. 5 and 6 (Lhomme and Elguero 1999; Bastiaanssen et al. 1998). In the present work, we computed midday values of NEF_i and EF_i by averaging the 15-min estimates of *NEF* and *EF* between 12am to 1pm (solar time) in order to reduce the variability inherent to flux modelling at 15-min time steps,. Estimates of AE_D were computed as the daytime average of the 15min available energy (AE_i) estimated from Capítulo 1.

The *EF* or *NEF method* and the *Averaging method* were applied to estimate H_D and LE_D for those days for which both measurements and estimates of H_i and LE_i were available during the entire daytime period (with $Rn > 55 \text{ W m}^{-2}$). This resulted in a data subset of only 24 days, including clear sky and cloudy days, randomly distributed during the complete study period.

A prior step in the *EF* or *NEF method*, was to study baseline errors derived from the assumption of daytime self preservation of *EF* and *NEF*. For this purpose, H_D and LE_D were

estimated for the same 24 days data subset by using EF , NEF and AE_D from the EC data, rather than from TSM outputs. This allowed to characterize the proportion of error intrinsic to this temporal up-scaling method in our Mediterranean semiarid conditions and for discussing the reliability of the self preservation assumption under such conditions.

While the daytime values of H_D were presented in energy terms (Wm^{-2}), the daytime values of LE_D were transformed in total E values ($mm\ day^{-1}$) to facilitate the comparison with other studies following Eq. 7.

$$E_D = \frac{\Delta t}{\rho\lambda} LE_D \quad (7)$$

where Δt is the number of seconds comprised in the daytime period, λ is the latent heat of vaporization (Jg^{-1}) and ρ is the density of water ($1000\ g\ m^{-3}$).

RESULTS

Diurnal behaviour of the TSM

The TSM performance under different ranges of solar elevation (*SE*), using the entire analysis data set (N= 2991), is shown in Table 1. A significant influence of *SE* on the accuracy of *H* estimates from both model versions, *TSM_P* and *TSM_S*, was found by the Tukey test (p-values < 0.05). High percentages of error were found for *H* under conditions of solar elevation lower than 25° (MAPE>100%). Similar results were found for *TSM_P* and *TSM_S* (Fig. 1A). However, accuracy at solar elevations higher than 25° was rather constant with errors around 26% for *TSM_P* and a 33% for *TSM_S* and no significant differences in the MAPE values (see letters from Tukey test in Table 1). The correlation between observed and predicted values, represented by R², did not change significantly either for parallel (R²~0.45) or series (R²~0.48) when solar elevation was higher than 25°. Therefore a robust behaviour of the two resistance versions of the TSM can be considered only for solar elevation conditions higher than 25°, although still a high standard deviation (*std*) of MAPE values was found for *SE* conditions between 25-35°.

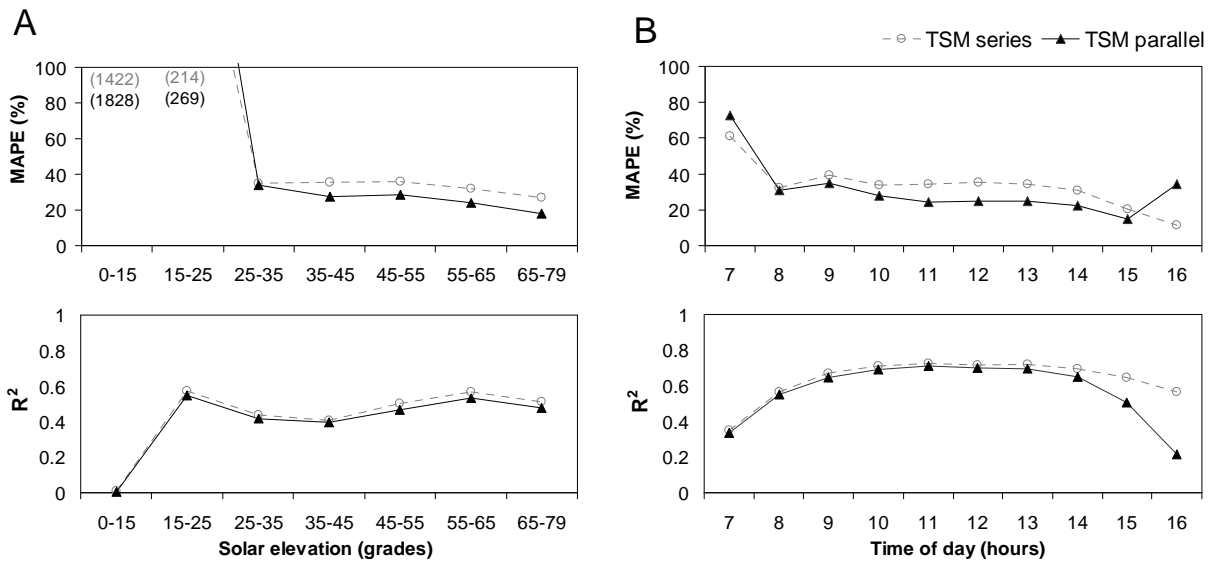


Figure 1. Evolution of the accuracy statistics of the TSM, mean absolute percentage error (MAPE) and coefficient of determination (R²), using the parallel (black line with filled triangles) or series (grey dashed line with hollow circles) resistance network, under different ranges of solar elevation (N=2991) (A) and along daytime hours (N= 2677) (B). In brackets statistics found out of scale. Tabulated values and related additional analyses are shown in Table 1.

The analysis of the effect of the time of day was performed excluding data with solar elevation conditions lower than 25° , under which the TSM clearly failed, resulting in a subset of $N=2677$. The time of day factor still presented a significant effect (p -value < 0.05 in ANOVA test) and results in Table 1 show that a significant increase of errors was observed using 7am data both for TSM_P and TSM_S (73% and 61% MAPE values respectively), but errors remained lower than 40 % for the rest of the daytime (Fig. 1B). The TSM_P scheme did not presented significant differences in mean MAPE at all times of day between 8am to 4pm, with errors ranging from 15% to 35% and R^2 values ~ 0.65 except at 4pm when R^2 decreased to 0.22. The TSM_S scheme did not presented significant differences in MAPE from 8am to 2pm with values ranging from 20% to 39% and R^2 values ~ 0.69 , but a significantly better accuracy was found during the early afternoon (4 pm) (11% of error). Despite of this, standard deviation, *std*, of the mean absolute percentage errors remained high respect to MAPE values for TSM_P and for TSM_S until 10am (Table 1).

Therefore this sequential analysis revealed that a robust behaviour of the TSM, for both parallel and series resistances schemes, was found in our semiarid site only for solar elevation conditions higher than 25° and a time of the day between 10 and 3pm (both included). Under such conditions the accuracy of H estimates from the TSM remained lower than 36% (with reduced standard deviations) and the R^2 was higher than 0.5 for both model versions, TSM_P and TSM_S .

Table 1. Statistic of the TSM performance for specific conditions of two factors (solar elevation and time of day). Mean absolute percentage error (MAPE) and standard deviation of MAPE (*std*), letters from Tukey test and coefficient of determination (R^2) are shown for each factor-range. Different letters from Tukey test show significant differences between mean MAPE values of the TSM in the different ranges within each factor.

Factor		<i>TSM_P</i>				<i>TSM_S</i>			
Solar elevation	N	MAPE (%)	<i>std</i> (%)	Tukey test	R^2	MAPE (%)	<i>std</i> (%)	Tukey test	R^2
0° - 15°	35	1828	3604	<i>c</i>	0.00	1422	2864	<i>c</i>	0.01
15° - 25°	279	269	1867	<i>b</i>	0.55	214	1541	<i>b</i>	0.57
25° - 35°	620	34	90	<i>a</i>	0.41	35	73	<i>a</i>	0.44
35° - 45°	712	27	33	<i>a</i>	0.40	36	24	<i>a</i>	0.40
45° - 55°	543	29	54	<i>a</i>	0.47	36	41	<i>a</i>	0.50
55° - 65°	489	24	15	<i>a</i>	0.53	32	14	<i>a</i>	0.57
65° - 80°	313	18	12	<i>a</i>	0.48	27	13	<i>a</i>	0.51
Total N:	2991								
Time of day	N	MAPE (%)	<i>std</i> (%)	Tukey test	R^2	MAPE (%)	<i>std</i> (%)	Tukey test	R^2
7:00	72	73	246	<i>c</i>	0.34	61	203	<i>d</i>	0.35
8:00	210	31	44	<i>ab</i>	0.55	32	33	<i>ac</i>	0.57
9:00	317	35	81	<i>b</i>	0.64	39	60	<i>a</i>	0.67
10:00	403	28	22	<i>ab</i>	0.69	34	17	<i>a</i>	0.71
11:00	386	24	13	<i>ab</i>	0.71	34	13	<i>a</i>	0.72
12:00	388	25	13	<i>ab</i>	0.70	35	13	<i>a</i>	0.72
13:00	382	25	15	<i>ab</i>	0.69	34	16	<i>a</i>	0.72
14:00	309	22	14	<i>ab</i>	0.65	31	14	<i>abc</i>	0.69
15:00	157	15	19	<i>a</i>	0.51	20	13	<i>bc</i>	0.64
16:00	53	34	26	<i>ab</i>	0.22	11	10	<i>b</i>	0.56
Total N:	2677								

TSM response under different environmental conditions

The five classes in which the nine factors were binned are shown in Table 2. These different factors and classes with their corresponding modelling error are depicted in Figure 2. This analysis was done using a data subset comprising only daytime data with a robust behaviour of the TSM based on previous analysis (solar elevation conditions higher than 25° and data from 10am to 3pm), leading a total number of cases of N=2025.

Table 2. Range of values included in each factor's class. Total observed range is presented for each environmental factor. N is the number of observations included in each class. Only cases when solar elevation is higher than 25° and between 9am and 3pm time of day were included in this analysis (N=2025).

<i>S</i> (W m^{-2})			<i>clf</i> (-)			$T_R - T_a$ ($^{\circ}\text{C}$)		
class	ranges	N	class	ranges	N	class	ranges	N
I	140 - 350	48	I	0.00 (clear sky)	1355	I	< 2.2	20
II	350 - 550	263	II	0.00 - 0.17	287	II	2.2 - 4.4	1015
III	550 - 750	800	III	0.17 - 0.35	217	III	4.4 - 6.6	764
IV	750 - 950	805	IV	0.3 - 0.52	114	IV	6.6 - 8.8	162
V	> 950	109	V	>0.52	52	V	> 8.8	64
Observed range: [140 , 1173]			Observed range: [0.00 , 0.70]			Observed range: [1.4 , 10.7]		
<i>SWC</i> (vol/vol)			<i>VPD</i> (kPa)			<i>LAI</i> (-)		
class	ranges	N	class	ranges	N	class	ranges	N
I	0.03 - 0.07	663	I	0.0 - 0.4	51	I	0.30 - 0.38	417
II	0.07 - 0.11	727	II	0.4 - 0.8	577	II	0.38 - 0.46	246
III	0.11 - 0.15	296	III	0.8 - 1.2	697	III	0.46 - 0.54	372
IV	0.15 - 0.19	147	IV	1.2 - 1.6	373	IV	0.54 - 0.62	580
V	>0.19	192	V	>1.6	327	V	>0.62	410
Observed range: [0.03 , 0.24]			Observed range: [0.08 , 3.4]			Observed range: [0.30 , 0.70]		
$T_s - T_R$ ($^{\circ}\text{C}$)			<i>WS</i> (m s^{-1})			Stability index (z_0/L)		
class	ranges	N	class	ranges	N	class	ranges	N
I	< 0.0	21	I	0.0-1.5	70	I	> -0.010 (neutral)	43
II	0.0-2.0	424	II	1.5-3.0	309	II	-0.010 , -0.340	1901
III	2.0 - 4.0	1022	III	3.0-4.5	596	III	-0.340 , -0.670	56
IV	4.0 - 6.0	494	IV	4.5-6.0	447	IV	-0.670 , -1.000	14
V	> 6.0	64	V	>6.0	603	V	< -1.000	11
Observed range: [-1.1 , 7.2]			Observed range: [0.04 , 12.3]			Observed range: [-4.050 , -0.003]		

The conditions for which the *TSM* presented the strongest decrease in accuracy were related to a low energy supply: $S < 300 \text{ W m}^{-2}$ (class I) and $(T_R - T_a) < 2.2 \text{ }^{\circ}\text{C}$ (class I). The highest MAPE values observed in those cases (class I) coincided with *H* overestimates (high and positive MPE values) and low correlation and slopes (Fig. 2). It is noticeable that under these conditions of reduced energy supply the errors were significantly lower using the *TSM_S* although the correlation was still poor. The surface to-air temperature difference ($T_R - T_a$) was the factor showing the strongest effect over MAPE values among all the analyzed factors. A progressive improvement of the *TSM* accuracy was observed as long as the $(T_R - T_a)$ increased (from classes I to V). Thus, both resistance versions of the *TSM* showed the highest accuracy for class V of $(T_R - T_a)$ factor ($T_R - T_a > 8.8^{\circ}\text{C}$), with 13% and 22% MAPE values for parallel and series schemes respectively. However the linear agreement was poor (low R^2 and *slope* values) for

class V of $(T_R - T_a)$. For the other factor indirectly related to energy supply, the cloud factor clf , the TSM showed lower MAPE and MPE values at medium classes of clf factor (classes III and IV) than for clear sky class (class I) and the parallel and series resistance schemes of the TSM presented a different response when sky was strongly covered. While TSM_P presented a clear decrease in accuracy with $MAPE > 50\%$ and overestimates of H (positive and high MPE values $\sim 50\%$) when cloudiness was high, $clf > 0.52$ (class V), the TSM_S did not increase the percentage errors substantially under such conditions.

MAPE values of the TSM slightly increased when water availability was high (see evolution of MAPE values along the SWC gradient Fig.2), and the linear agreement between observed and predicted H values was clearly better (higher R^2 and $slope$) at low ranges of SWC showing a progressively deterioration to higher SWC conditions. In agreement with that, the TSM accuracy was slightly better when VPD was high (see evolution of MAPE values along VPD gradient) and the linear agreement improved, specially the $slope$, at high VPD classes (Fig. 3). Furthermore, a similar response to variations on SWC and VPD was found for TSM_P and TSM_S .

Regarding to the influence of factors related to the vegetation state, it is remarkable that high R^2 values and $slope$ values close to one, were found for low LAI levels (classes I and II) dropping for higher LAI values ($LAI > 0.46$) although no strong variation of the TSM model errors (MPE and MAPE) was found for the five LAI classes. In the same direction, a worse TSM performance was found when temperature differences between T_s and T_R were high reflecting more active vegetation. The $(T_s - T_R)$ factor showed higher errors (MPE and MAPE) and lower linear correlation from classes I to V (Fig. 3). This suggests that the TSM works more accurately when differences between soil and vegetation temperatures are low or even negative which is usually related with less active vegetation in accordance to a better performance at lower rather than high LAI values.

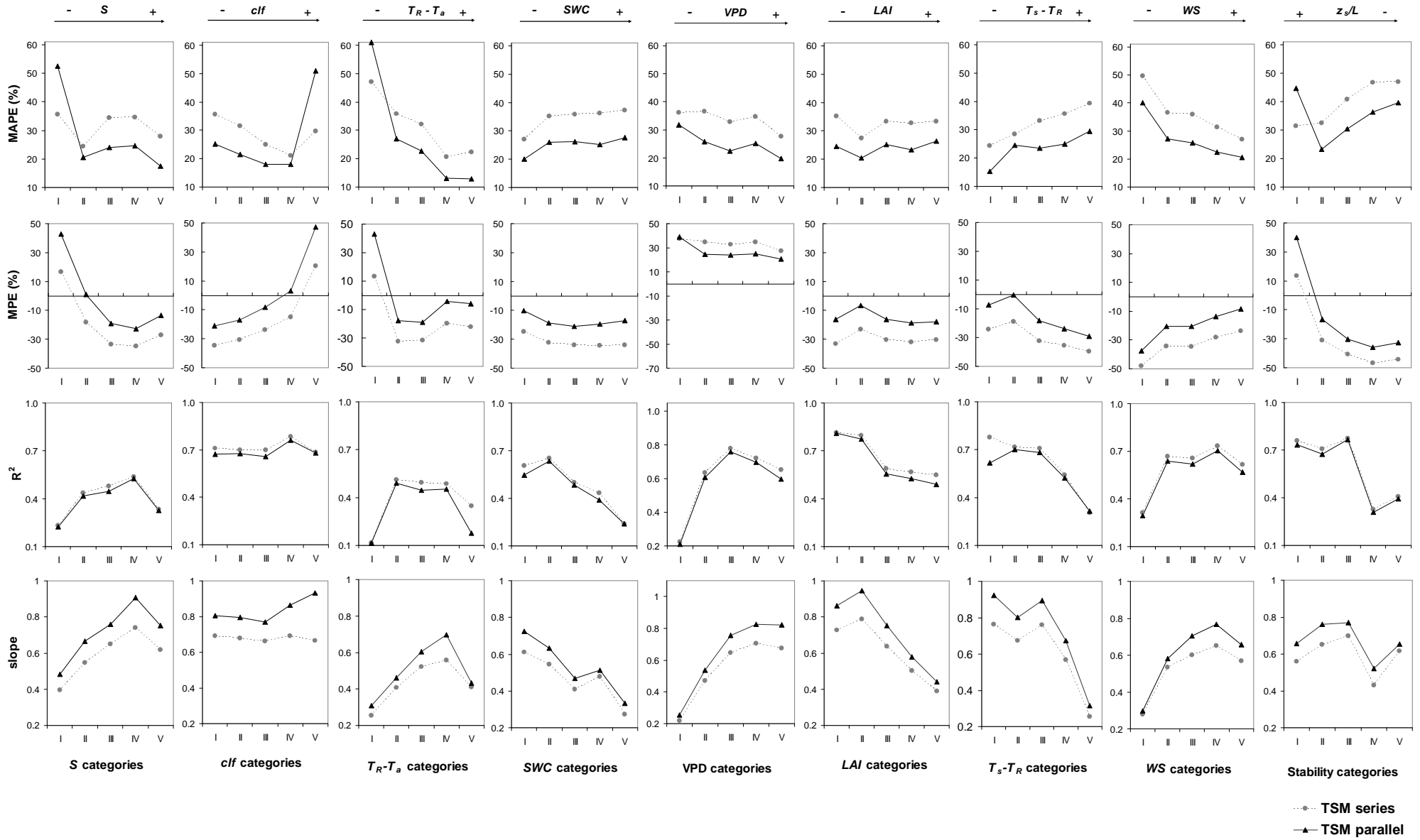


Figure 2. Evolution of the TSM accuracy statistics: mean absolute percentage error (MAPE), mean percentage error (MPE), coefficient of determination (R^2), and slope of the linear regression between the observed and predicted values of H , for the five classes of each analyzed factor (Table 2). Only observations with solar elevation $>25^\circ$ and time of day between 10am and 3pm were included in this analysis (N=2025).

Finally, the analysis of the factors related to the boundary layer state, WS and stability index z_s/L , showed that the TSM accuracy clearly improved under higher wind speed conditions. A progressive reduction of MAPE and MPE with increasing wind speed was found as well as a better linear agreement. Figure 2 shows clearly that under neutral stability conditions (class I), the TSM presented very high errors (MAPE and MPE) when using the parallel resistance scheme, TSM_P . However, when using the TSM_S , lower errors occur under neutral conditions than under unstable conditions. Within the gradient of unstable conditions (classes II to V) all error statistics seemed to increase to more unstable conditions, both for TSM_P and TSM_S , but the unequal number of observations included within unstable classes (Table 2), makes difficult to asseverate this last idea.

Additionally, it is notable that the TSM_P showed lower overall errors (MAPE and MPE) and *slope* values closer to 1 with similar R^2 values than the TSM_S . However, the TSM_S showed a slightly more robust behaviour than the TSM_P reducing the model percentage errors under some specific conditions related with low energy supply (class I of S factor, class V of clf factor, class I of $(T_R - T_a)$ factor) and with atmospheric neutral conditions (class I of the z_s/L factor).

As general highlights we can indicate that the effectiveness of the TSM, under the two possible resistance schemes, clearly decreased when the $(T_R - T_a)$ was lower than 2.2°C and when WS was lower than 1.5 ms^{-1} . For those conditions the TSM presented $\text{MAPE} > 40\%$, $R^2 < 0.4$ and $\text{slope} < 0.4$. The conditions under which the TSM performance was better, coinciding lower errors (MAPE and MPE) and high values of *slope* and R^2 , were conditions characterized by low SWC, low LAI, and reduced thermal differences between soil and total surface.

Daytime fluxes extrapolation from instantaneous values

Our results showed that, despite of both temporal up-scaling methods, *Averaging* and *NEF* methods, produced underestimates of H_D using instantaneous estimates from the TSM (Fig. 3), the *Averaging method* presented lower errors (20-36% vs. 31-43%) and substantially better R^2 values (0.85-0.86 vs. 0.41-0.50) than the *NEF method* (Table 3). It is also remarkable that H_D estimates were always more underestimated using instantaneous estimates from TSM_S .

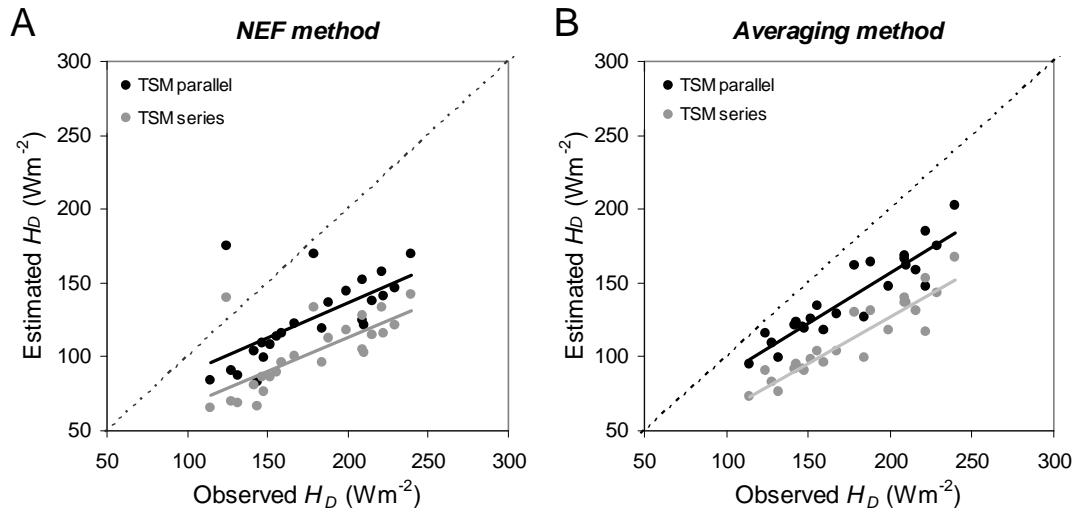


Figure 3. Scatterplots between estimated and observed daytime H_D , obtained by the *NEF method* (A) and the *Averaging method* (B) respectively both applied using *TSM* outputs for instantaneous fluxes, versus observed (eddy covariance measured) H_D . (N=24 days). Dashed line is the 1:1 line.

Daytime E was strongly overestimated with any of the two temporal up-scaling methods (Fig. 4). Estimates of daytime E showed MAEs ranging from 1.27 to 1.80 mm day^{-1} which represent more than the 100% of the mean observed E (1.02 mm day^{-1}) (Table 3). However it is important to notice that the correlation was high for all methods showing R^2 values between 0.82-0.85. The *Averaging method* presented lower MAPE values (125-162% using TSM_P and TSM_S respectively) than the *EF method* (146-177%) and the scatter between the observed and predicted was lower for the *Averaging method* at low values of daytime E ($E < 1 \text{ mm day}^{-1}$) (Fig. 4).

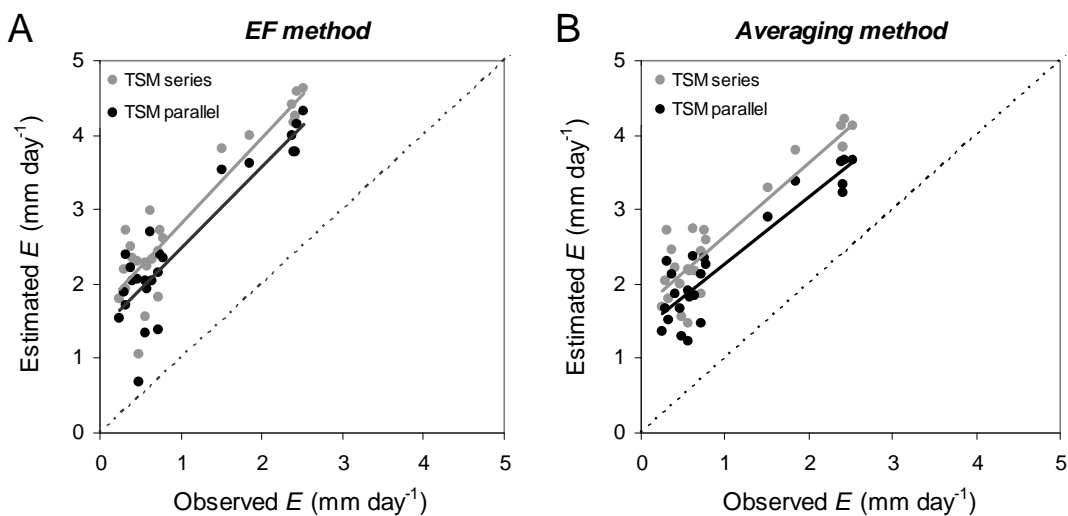


Figure 4. Scatterplots between estimated and observed daytime E , obtained by the *EF method* (A) and the *Averaging method* (B) respectively both applied from *TSM* derived instantaneous fluxes, versus observed daytime E . (N=24 days). Dashed is the 1:1 line.

Despite of the fact that daytime estimates of turbulent fluxes using the *EF* or *NEF method* were less accurate than with the *Averaging method* when using TSM estimates, the *EF* or *NEF method* seems highly efficient when using the retrieved EC fluxes instead (Fig. 5). The assumption of daytime self-preservation of *EF* and *NEF* only resulted in a mean absolute error of 13.2 W m^{-2} , which represents a percentage error of only 8% and 16% of the daytime measured H_D and LE_D respectively. This fact shows evidence that errors affecting daytime estimates of H_D and E obtained by the *EF* or *NEF method* using TSM derived fluxes, were mainly related to inaccuracies affecting the TSM instantaneous fluxes.

Table 3. Statistics showing the accuracy of the estimated daytime averaged H , H_D , and daytime E , E_D , obtained by the *EF* or *NEF method* and the *Averaging method* respectively based on instantaneous estimates from the TSM under the two resistance approaches in parallel (TSM_P) and in series (TSM_S). Root mean squared error (RMSE), mean absolute error (MAE), in brackets the percentage that MAE represents to the mean measured flux and determination coefficient R^2 are showed (N=24 days for all cases).

Flux	Scaling method	RMSE (Wm^{-2})		MAE (Wm^{-2})		R^2	
		TSM_P	TSM_S	TSM_P	TSM_S	TSM_P	TSM_S
H_D	<i>NEF method</i>	58	78	55 (31%)	75 (43%)	0.41	0.50
	<i>Averaging method</i>	39	66	35 (20%)	63 (36%)	0.85	0.86
E_D		RMSE (mm day^{-1})		MAE (mm day^{-1})		R^2	
		TSM_P	TSM_S	TSM_P	TSM_P	TSM_P	TSM_S
E_D	<i>EF method</i>	1.54	1.85	1.48 (146%)	1.80 (177%)	0.82	0.84
	<i>Averaging method</i>	1.31	1.69	1.27 (125%)	1.65 (162%)	0.84	0.85

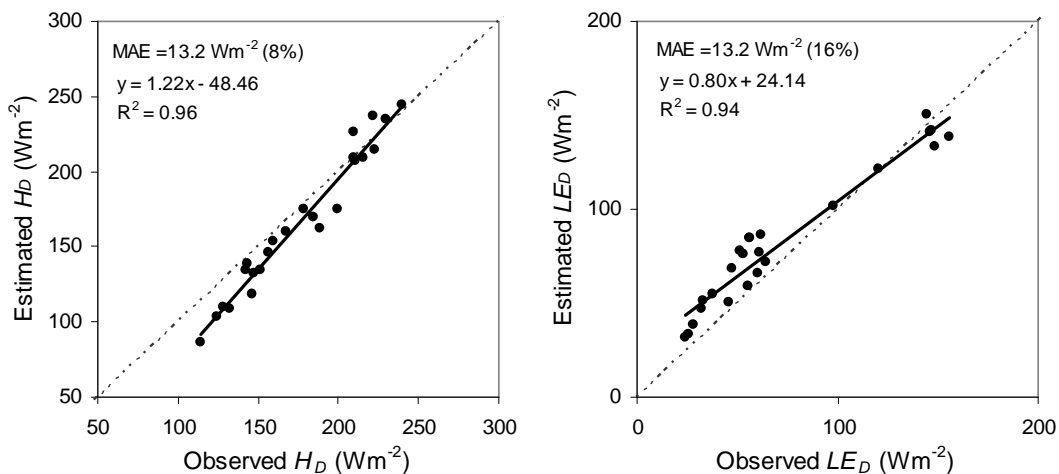


Figure 5. Scatterplots between the estimated daytime H_D , (left panel) and LE_D , (right panel) obtained when applying the *NEF method* and *EF method* respectively using measured values of midday NEF, EF and AE_D versus the observed H_D and LE_D (N=24 days). Dashed line is the 1:1 line. Mean absolute error (MAE) is shown and in brackets.

DISCUSSION

Diurnal behaviour of the TSM

Our analysis of the diurnal behaviour of the TSM showed that the TSM accuracy was clearly affected by the solar elevation and the time of the day. The TSM effectiveness was clearly reduced at solar elevation angles lower than 25° and also at marginal hours of the daytime period (before 10am and after 3pm) even at $SE > 25^\circ$ (Fig. 1 and Table 1). A similar increase on errors affecting modelled H at marginal daytime hours was pointed out by Su (2002) using a Surface Energy Balance System (SEBS). They found the highest model errors, around $40\text{-}50 \text{ W m}^{-2}$, during marginal daytime hours and proposed as main explanation failures in stability corrections affecting these transition periods from nighttime stable conditions to daytime unstable conditions (Su 2002). We think that, in the case of the TSM, an additional factor is responsible for the decrease of model accuracy under marginal time of day hours. Kustas and Norman et al. (1997) showed that the uncertainty affecting the surface to air temperature difference estimates, ($T_R - T_a$), largely affects the accuracy of H using TSM (uncertainties of $\pm 3^\circ\text{K}$ in $T_R - T_a$ leads $> 50\%$ variation in H). We also found that model accuracy decreased when ($T_R - T_a$) was low even around midday (Fig. 2). Therefore, we consider that the uncertainty associated to the IRT sensors (Kustas et al. 2012) can cause stronger errors on $T_R - T_a$ when temperatures are low, i.e at around sunrise or sunset when the solar elevation angles are low. This fact could explain the decrease of the TSM effectiveness under such conditions. From our results, it can be stated that a robust behaviour of TSM can be expected under solar elevation angles higher than 25° for the daytime period between 10am and 3 pm (both included) under natural semiarid conditions. Consequently, we would only recommend applying the TSM using satellite data over natural semiarid areas when they are acquired within this range of daytime and solar elevation angle conditions.

TSM response under different environmental conditions

The TSM has been particularly recommended for conditions of clear sky, high thermal difference between soil and canopy (Wang and Dickinson 2012) and no presence of senescent vegetation (Colaizzi et al. 2012a; Norman et al. 1995). However, these recommendations are mainly derived from studies on irrigated semiarid agricultural areas. The analysis presented in this paper revealed a different response of the TSM under natural semiarid conditions. Under the range of conditions observed in our Mediterranean tussock grassland, the TSM presented the highest limitations when the surface-air thermal gradient was low ($T_R - T_a < 2.2^\circ\text{C}$). Under these

conditions, TSM clearly overestimated H (Fig. 2). Norman et al. (2000) also found high errors affecting H estimates using TSM when $T_R - T_a$ was low. They showed that the Dual Temperature Difference method (DTD), which mainly reduces model sensitivity to errors associated with absolute values of T_R and T_a , offered a clear improvement of H estimates when $(T_R - T_a)$ was low. This is proving that TSM errors when $(T_R - T_a)$ is low are related to uncertainties affecting temperature measurements. As a practical aspect, it is important to enhance that our results showed the TSM_S clearly reduced errors when $(T_R - T_a) < 2.2^\circ\text{C}$ in comparison with the TSM_P . This is because of the air temperature in the canopy interface (T_{ac}), which is considered in TSM_S , partially reduces the sensitivity to absolute errors T_R and T_a (Capítulo 1).

Other factor analyzed in the present study, which affects the TSM accuracy but has not been deeply studied before, is the cloudiness, represented here by the cloud factor, clf . It is important to notice that most of the previous TSM analyses were restricted to clear-sky conditions, because of the absence of satellite data retrievals for cloudy days (French et al. 2005; Li et al. 2005) or just because cloudy conditions were removed from the analysis to ensure relatively steady-state energy fluxes (Colaizzi et al. 2012a). Kustas et al. (2002) found that H retrievals, from a temperature based one source model, presented a high sensitivity to high fluctuations in T_R derived from intermittent cloudy conditions in a riparian site. Our analysis showed on the contrary that under natural semiarid conditions the TSM accuracy was not reduced under medium covered sky conditions ($0 < clf < 0.52$) founding even lower percentages of error (MAPE and MPE) than for clear sky conditions for both resistance schemes (Fig. 2). This different response could be related with the different factors driving the water and energy fluxes in well-watered ecosystems, as riparian areas, controlled by energy supply, versus in water-limited ecosystems, as in our Mediterranean semiarid grassland, controlled by water availability. However, further analyses would be necessary to determine the reasons of that different response of the TSM under the two different scenarios. The decrease of the TSM performance under the maximum cloud cover sky conditions observed ($clf > 0.52$), more noticeable when using the TSM_P , could be more related to the effect of uncertainties of temperature measurements since temperatures when cloudiness is high can be expected lower (exposed earlier) than with clear skies.

The limitations previously found for the TSM performance under conditions of high fraction of senescent vegetation (Colaizzi et al. 2012a; French et al. 2007; Kustas and Norman 1997; Norman et al. 1995) were not observed under our natural semiarid conditions. Our results on the contrary showed that a better model performance was found under conditions of low or

even negative ($T_s - T_R$), low LAI, and low SWC. However, under our natural semiarid conditions a new factor showing an important effect over the TSM accuracy, was identified, the wind speed. The TSM offered better H estimates, when wind speed was high and clearly reduced its accuracy at low wind speeds. Neutral stability conditions (class I of the z_s/L factor) showed as well an important decrease of the TSM accuracy, but only using the parallel resistance scheme.

Daytime fluxes extrapolation from instantaneous values

Daytime retrievals of turbulent heat fluxes under natural semiarid conditions were found in this study to be more accurate for H , with minimum errors of 20% and $R^2=0.85$, whereas higher errors were found for daytime values of E with minimum errors of 125% but high correlations, $R^2=0.84$ (Table 3). Previous studies have shown clearly a better capacity of the TSM to estimate daytime E (Kustas et al. 2012; Kustas and Norman 1997) or daily (24h) E (Colaizzi et al. 2012b; Gonzalez-Dugo et al. 2009) than that found in our conditions, with errors ranging from 5 to 25%. However, it is important to consider that all those studies were performed in areas (irrigated agricultural semiarid sites and grass tall prairies), where the latent heat flux was the dominant turbulent heat flux, whereas in our Mediterranean natural semiarid site the dominant flux was H . Indeed H_D was 71% of measured daytime available energy for the 24 days that were included in our daytime analysis. Therefore, the percentage of error found for daytime estimates of the dominant turbulent heat flux in our site (H) was within the range of errors of the dominant turbulent heat flux in other sites. However, with regard to daytime E , other two source models that have been tested in this specific field site have shown better accuracies, with errors ranging between 30-35% although they explained a lower percentage of the flux variability (with R^2 between 0.47 and 0.57) (Capítulo 3; Capítulo 4).

Comparison of the two methods to up-scale the instantaneous estimates of turbulent heat fluxes to daytime values, better estimates were found using the *Averaging method* (Table 3). This is because in the *Averaging method* the overestimation found at marginal daytime hours, when S is reduced, and the underestimation found at midday, when S is high (Fig. 2), were compensated by the averaging procedure. This evidences a higher potential of geostationary satellites such as MSG-SEVIRI or GOES or ground sensors as preferential data sources to estimate daytime fluxes by mean of TSM in natural semiarid sites compared to polar-orbiting satellites such as MODIS or ASTER, which will depend on the *EF* or *NEF method* to obtain daytime fluxes. Nonetheless, despite of the lower accuracy found by the *EF* or *NEF method* to estimate daytime values using instantaneous TSM outputs, this method proved to be efficient

when using instantaneous EC fluxes (Fig. 5). Gentine et al. (2011) stated recently that the diurnal behaviour of the EF (and therefore its complementary NEF) exhibits daytime self-preservation only under limited conditions of clear skies, humid air, and strong solar radiation based on a deep study performed in an irrigated wheat crop at a semiarid site. However we found that the self-preservation assumption only resulted in percentage errors of 8% and 16% for H_D and LE_D respectively, even when including cloudy days (10 of 24 tested days presented cloudiness). Similar agreement was found for cloudy than for clear sky days (results not shown) using measured instantaneous fluxes. This indicates that cloudiness did not affect the daytime self-preservation of EF or NEF under our conditions. This agrees with the results from Farah et al. (2004) who pointed out no effect of clouds on the diurnal cycle of EF in semiarid areas and stated a fairly stable behaviour of daytime EF pattern for areas with high available energy, moderate to dry surface conditions and high surface resistance. Thus, the EF or NEF method was not operational in our conditions because of inaccuracies affecting to TSM retrievals but our results showed that it could be operational if improvements on those estimates were achieved.

Finally, our analyses also showed that better estimates of daytime E and H_D were found using the parallel version of the TSM than the series one, despite of a slight decrease in the correlations (Table 3). From the TSM_S , H_D was systematically more underestimated by the two temporal up-scaling methods (Fig. 3) and consequently daytime E was more overestimated (Fig. 4) than with the TSM_P . A previous study also found better daytime estimates of LE from the parallel than from the series version of the TSM when soil and canopy temperatures derived from dual angle surface temperature was used in a tall grass prairie (Kustas and Norman 1997). This seems to indicate that despite of the more robust behaviour of TSM_S at instantaneous time scales; the TSM_P presents a clear advantage to estimate daytime turbulent heat fluxes.

CONCLUSIONS

A detailed analysis has been performed to evaluate the main factors affecting the TSM effectiveness under water stress conditions typical of Mediterranean drylands. By means of a sequential analysis, we proved that the TSM was affected by the two factors associated with variations in solar irradiance along the daytime period and also seasonal course: solar elevation and time of day. Our results proved that a robust behaviour of the TSM can only be expected for conditions with solar elevation angles higher than 25° and during daytime hours from 10 am to 3 pm (both conditions simultaneously). It was also proved that, under natural semiarid conditions here evaluated, the TSM was not sensitivity to some environmental factors, such as cloudiness or vegetation status, which indeed did affected the model performance in other sites without water stress. Thus, in our study the TSM accuracy was not reduced under medium cloudiness conditions ($0 < clf < 0.52$) with TSM accuracy even being improved with respect to clear sky conditions. Furthermore, when a high portion of senescent vegetation is expected, with higher water stress (low *SWC* and high *VPD*) and very stressed vegetation (low or even negative values of $T_R - T_s$), the TSM effectiveness was not just reduced but instead increased in our semiarid site. The environmental factors that affected more strongly the TSM performance in our site were the surface to air temperature difference ($T_R - T_a$) and the wind speed, with an increase of accuracy when both factors were high. In general, the TSM_P showed overall lower errors and a lower tendency to underestimate at high *H* values, but the TSM_S reduced model errors under low energy supply conditions and atmospheric neutral conditions.

Finally, the ability of the TSM to estimate daytime turbulent fluxes was only demonstrated for the dominant sensible heat flux, H_D , despite of a systematic tendency to underestimate. Daytime *E* values were strongly overestimated using the TSM, but a high portion of its variability could be explained. Using instantaneous fluxes from the TSM, the *Averaging method* together with the parallel version of TSM provided better daytime estimates than the *EF* or *NEF method*. This implies that data from geostationary satellites such as MSG-SEVIRI or from ground located sensors should be used as preferential data sources to estimate daytime fluxes using the TSM rather than polar orbiting sensors such as MODIS.

REFERENCES

- Alfieri, J.G., Kustas, W.P., Prueger, J.H., Hipps, L.E., Evett, S.R., Basara, J.B., Neale, C.M.U., French, A.N., Colaizzi, P., Agam, N., Cosh, M.H., Chavez, J.L., & Howell, T.A. (2012). On the discrepancy between eddy covariance and lysimetry-based surface flux measurements under strongly advective conditions. *Advances in Water Resources*, 50, 62-78
- Allen, R.G., Pereira, L.S., Raes, D., & Smith, M. (1998). Crop evapotranspiration: Guidelines for computing crop requirements. Roma, Italy: FAO Irrigation and Drainage Paper N° 56, pp. 300.
- Bastiaanssen, W.G.M., Menenti, M., Feddes, R.A., & Holtslag, A.A.M. (1998). A remote sensing surface energy balance algorithm for land (SEBAL): 1. Formulation. *Journal of Hydrology*, 212-213, 198-212
- Colaizzi, P.D., Evett, S.R., Howell, T.A., Gowda, P.H., O'Shaughnessy, S.A., Tolck, J.A., Kustas, W.P., & Anderson, M.C. (2012a). Two-source energy balance model: Refinements and lysimeter tests in the southern high plains. *Transactions of the ASABE*, 55, 551-562
- Colaizzi, P.D., Kustas, W.P., Anderson, M.C., Agam, N., Tolck, J.A., Evett, S.R., Howell, T.A., Gowda, P.H., & O'Shaughnessy, S.A. (2012b). Two-source energy balance model estimates of evapotranspiration using component and composite surface temperatures. *Advances in Water Resources*, 50, 134-151
- Crago, R.D. (1996). Conservation and variability of the evaporative fraction during the daytime. *Journal of Hydrology*, 180, 173-194
- Crawford, T.M., & Duchon, C.E. (1999). An improved parameterization for estimating effective atmospheric emissivity for use in calculating daytime downwelling long-wave radiation. *Journal of Applied Meteorology*, 38, 474-480
- Domingo, F., Serrano-Ortiz, P., Were, A., Villagarcía, L., García, M., Ramírez, D.A., Kowalski, A.S., Moro, M.J., Rey, A., & Oyonarte, C. (2011). Carbon and water exchange in semiarid ecosystems in SE Spain. *Journal of Arid Environments*, 75, 1271-1281
- Farah, H.O., Bastiaanssen, W.G.M., & Feddes, R.A. (2004). Evaluation of the temporal variability of the evaporative fraction in a tropical watershed. *International Journal of Applied Earth Observation and Geoinformation*, 5, 129-140
- French, A.N., Hunsaker, D.J., Clarke, T.R., Fitzgerald, G.J., Luckett, W.E., & Pinter Jr, P.J. (2007). Energy balance estimation of evapotranspiration for wheat grown under variable management practices in central Arizona. *Transactions of the ASABE*, 50, 2059-2071
- French, A.N., Jacob, F., Anderson, M.C., Kustas, W.P., Timmermans, W., Gieske, A., Su, Z., Su, H., McCabe, M.F., Li, F., Prueger, J., & Brunsell, N. (2005). Surface energy fluxes with the Advanced Spaceborne Thermal Emission and Reflection radiometer (ASTER) at the Iowa 2002 SMACEX site (USA). *Remote Sensing of Environment*, 99, 55-65
- García, M., Villagarcía, L., Contreras, S., Domingo, F., & Puigdefábregas, J. (2007). Comparison of three operative models for estimating the surface water deficit using ASTER reflective and thermal data. *Sensors*, 7, 860-883
- Gentine, P., Entekhabi, D., & Polcher, J. (2011). The diurnal behavior of evaporative fraction in the soil-vegetation-atmospheric boundary layer continuum. *Journal of Hydrometeorology*, 12, 1530-1546

- Glenn, E.P., Huete, A.R., Nagler, P.L., Hirschboeck, K.K., & Brown, P. (2007). Integrating remote sensing and ground methods to estimate evapotranspiration. *Critical Reviews in Plant Sciences*, 26, 139-168
- Gonzalez-Dugo, M.P., Neale, C.M.U., Mateos, L., Kustas, W.P., Prueger, J.H., Anderson, M.C., & Li, F. (2009). A comparison of operational remote sensing-based models for estimating crop evapotranspiration. *Agricultural and Forest Meteorology*, 149, 1843-1853
- Kalma, J.D., McVicar, T.R., & McCabe, M.F. (2008). Estimating land surface evaporation: A review of methods using remotely sensed surface temperature data. *Surveys in Geophysics*, 29, 421-469
- Kustas, W.P., Alfieri, J.G., Anderson, M.C., Colaizzi, P.D., Prueger, J.H., Evett, S.R., Neale, C.M.U., French, A.N., Hipps, L.E., Chávez, J.L., Copeland, K.S., & Howell, T.A. (2012). Evaluating the two-source energy balance model using local thermal and surface flux observations in a strongly advective irrigated agricultural area. *Advances in Water Resources*, 50, 120-133
- Kustas, W., & Anderson, M. (2009). Advances in thermal infrared remote sensing for land surface modeling. *Agricultural and Forest Meteorology*, 149, 2071-2081
- Kustas, W.P., & Norman, J.M. (1997). A two-source approach for estimating turbulent fluxes using multiple angle thermal infrared observations. *Water Resources Research*, 33, 1495-1508
- Kustas, W.P., & Norman, J.M. (1999a). Evaluation of soil and vegetation heat flux predictions using a simple two-source model with radiometric temperatures for partial canopy cover. *Agricultural and Forest Meteorology*, 94, 13-29
- Kustas, W.P., & Norman, J.M. (1999b). Reply to comments about the basic equations of dual-source vegetation-atmosphere transfer models. *Agricultural and Forest Meteorology*, 94, 275-278
- Kustas, W.P., Prueger, J.H., & Hipps, L.E. (2002). Impact of using different time-averaged inputs for estimating sensible heat flux of riparian vegetation using radiometric surface temperature. *Journal of Applied Meteorology*, 41, 319-332
- Lhomme, J.P., & Elguero, E. (1999). Examination of evaporative fraction diurnal behaviour using a soil-vegetation model coupled with a mixed-layer model. *Hydrology and Earth System Sciences*, 3, 259-270
- Li, F., Kustas, W.P., Prueger, J.H., Neale, C.M.U., & Jackson, T.J. (2005). Utility of remote-sensing-based two-source energy balance model under low- and high-vegetation cover conditions. *Journal of Hydrometeorology*, 6, 878-891
- Monteith, J.L., & Unsworth, M.H. (1990). Principles of Environmental Physics. London, UK: Edward Arnold, pp.291.
- Norman, J.M., & Becker, F. (1995). Terminology in thermal infrared remote sensing of natural surfaces. *Agricultural and Forest Meteorology*, 77, 153-166
- Norman, J.M., Kustas, W.P., & Humes, K.S. (1995). Source approach for estimating soil and vegetation energy fluxes in observations of directional radiometric surface temperature. *Agricultural and Forest Meteorology*, 77, 263-293
- Norman, J.M., Kustas, W.P., Prueger, J.H., & Diak, G.R. (2000). Surface flux estimation using radiometric temperature: A dual-temperature-difference method to minimize measurement errors. *Water Resources Research*, 36, 2263-2274

- Priestley, C.H.B., & Taylor, R.J. (1972). On the assessment of surface heat flux and evaporation using large-scale parameters. *Monthly Weather Review*, *100*, 81-92
- Rey, A., Belelli-Marchesini, L., Were, A., Serrano-ortiz, P., Etiope, G., Papale, D., Domingo, F., & Pegoraro, E. (2012). Wind as a main driver of the net ecosystem carbon balance of a semiarid Mediterranean steppe in the South East of Spain. *Global Change Biology*, *18*, 539-554
- Sánchez, J.M., Kustas, W.P., Caselles, V., & Anderson, M.C. (2008). Modelling surface energy fluxes over maize using a two-source patch model and radiometric soil and canopy temperature observations. *Remote Sensing of Environment*, *112*, 1130-1143
- Sokal, R.R., & Rohlf, F.J. (2012). *Biometry: the principles and practice of statistics in biological research*. New York, USA.: W. H. Freeman and Co, pp.937.
- Su, Z. (2002). The Surface Energy Balance System (SEBS) for estimation of turbulent heat fluxes. *Hydrology and Earth System Sciences*, *6*, 85-99
- Timmermans, W.J., Kustas, W.P., Anderson, M.C., & French, A.N. (2007). An intercomparison of the Surface Energy Balance Algorithm for Land (SEBAL) and the Two-Source Energy Balance (TSEB) modeling schemes. *Remote Sensing of Environment*, *108*, 369-384
- Twine, T.E., Kustas, W.P., Norman, J.M., Cook, D.R., Houser, P.R., Meyers, T.P., Prueger, J.H., Starks, P.J., & Wesely, M.L. (2000). Correcting eddy-covariance flux underestimates over a grassland. *Agricultural and Forest Meteorology*, *103*, 279-300
- Wang, K., & Dickinson, R.E. (2012). A review of global terrestrial evapotranspiration: Observation, modeling, climatology, and climatic variability. *Reviews of Geophysics*, *50*, RG2005

CAPITULO 3

Improving evapotranspiration estimates in Mediterranean drylands: the role of soil evaporation

*Aceptado en *Water Resources Research* con correcciones (25/01/2013) con los siguientes autores:

Laura Morillas, Ray Leuning, Luis Villagarcía, Mónica García, Penélope Serrano-Ortiz, Francisco Domingo.

ABSTRACT

An adaptation of a simple model for evapotranspiration (E) estimations in drylands based on remotely sensed leaf area index and the Penman-Monteith equation (PML model) (Leuning et al. 2008) is presented. Three methods for improving the consideration of soil evaporation influence in total evapotranspiration estimates for these ecosystems are proposed. The original PML model considered evaporation as a constant fraction (f) of soil equilibrium evaporation. We propose an adaptation that considers f as a variable primarily related to soil water availability. In order to estimate daily f values, the first proposed method (f_{swc}) uses rescaled soil water content measurements, the second (f_{Zhang}) uses the ratio of 8 days antecedent precipitation and soil equilibrium evaporation, and the third (f_{drying}), includes a soil drying simulation factor for periods after a rainfall event. E estimates were validated using E measurements from eddy covariance systems located in two functionally-different sparsely vegetated drylands sites: a littoral Mediterranean semiarid steppe and a dry-subhumid Mediterranean montane site. The method providing the best results in both areas was f_{drying} (mean absolute error of 0.17 mm day^{-1}) which was capable of reproducing the pulse-behavior characteristic of soil evaporation in drylands strongly linked to water availability. This proposed model adaptation, f_{drying} , improved the PML model performance in sparsely vegetated drylands where a more accurate consideration of soil evaporation is necessary.

Keywords: evapotranspiration, canopy conductance, soil evaporation, LAI, optimization, soil water content, soil potential evaporation

INTRODUCTION

Evapotranspiration (E), which is the sum of evaporation from soil (E_s) and plant canopies (E_c) including rainfall interception, is the largest term in the terrestrial water balance after precipitation. E determines the balance between recharge and discharge from aquifers (Huxman et al. 2004; Huxman et al. 2005) and in drylands around 90 to 100% of annual precipitation returns to the atmosphere from the surface (Glenn et al. 2007) by mean of this process. Concurrently, latent heat flux (LE), the energetic equivalent of E , plays an important role in the surface energy balance affecting terrestrial weather dynamics and vice versa.

Accurate regional estimation of E is necessary for many operational applications: irrigation planning, management of watersheds and aquifers, meteorological predictions and detection of droughts and climate change. Remote sensing is the only feasible technique for E estimation at regional scales with a reasonable degree of accuracy (Guerschman et al. 2009; Kustas and Norman 1996). Many methods have been developed for estimating regional E in the last decades, including those based on remotely sensed surface temperature (see reviews by Glenn et al. 2007; Kalma et al. 2008; Wang and Dickinson 2012). However, there are some difficulties associated with using surface temperature for regional E estimation, mainly differences between aerodynamic and radiometric temperature (Stewart et al. 1994) or complexity of using instantaneous thermal data for flux estimation at larger time scales (Cleugh et al. 2007). This has motivated development of other methodologies. In this context, Cleugh et al. (2007) presented a method for E estimation based on regional application of the Penman-Monteith (PM) equation (Monteith 1964) using leaf area index (LAI) from MODIS (Moderate Resolution Imaging Spectrometer) and gridded meteorological data. This work stimulated a number of later studies (Leuning et al. 2008; Mu et al. 2007; Mu et al. 2011; Zhang et al. 2010; Zhang et al. 2008) that have demonstrated the potential of the PM equation as a robust, biophysically based framework for E estimation using remote sensing inputs (Leuning et al. 2008).

The key parameter of the PM equation is the surface conductance (G_s), which defines the facility of the soil-canopy system to lose water. A simple linear relationship between G_s and LAI was proposed by Cleugh et al. (2007) for estimating E at two field sites in Australia. Mu et al. (2007) took one step forward with separate estimation of evaporation from soil (E_s) and canopy (E_c) and a more detailed formulation for E_c considering the effects of vapor pressure deficit (D_a) and air temperature (T_a) on canopy conductance (G_c). Based on these studies, Leuning et al. (2008) developed a less empirical formulation for G_s to apply the PM equation at regional scale.

This new formulation considers both soil and canopy evaporation. For G_c a biophysical algorithm based on radiation absorption and D_a was proposed, whereas soil evaporation was estimated as a constant fraction, f , of soil equilibrium evaporation (Priestley and Taylor 1972) defined as the evaporation rate under ideal conditions of water availability and saturated atmosphere controlled exclusively by energy supply. Application of the *Penman-Monteith-Leuning*, PML model, as it was named by Zhang et al. (2010), requires commonly available meteorological data, *LAI* data from MODIS or other remote-sensing platforms and two main parameters, considered by Leuning et al. (2008) to be constants: g_{sx} , maximum stomatal conductance of leaves at the top of the canopy and f , representing the ratio of soil evaporation to the equilibrium rate. The original PML model was evaluated using data from 15 Fluxnet sites located across a wide range of climatic conditions and vegetation types with good general results (average systematic root-mean-square error in daytime mean E of 0.27 mm day^{-1}). Nonetheless the model has not been tested in conditions of strong aridity as Mediterranean drylands.

In drylands, where water availability is the main controlling factor of biological and physical processes (Noy-Meir 1973), evaporation from soil can exceed 80% of total E (Mu et al. 2007). Soil water availability is highly variable in these ecosystems and assuming f is a constant as in the original PML model is inadequate. Leuning et al. (2008) acknowledged this limitation and recommended that remote-sensing or other techniques be developed to treat f as a variable instead of a parameter, especially for sparsely vegetated sites ($LAI < 3$). To estimate f as a temporal variable Zhang et al. (2010) used the ratio between precipitation and equilibrium evaporation rate as an indicator of soil water availability. Preliminary results of PML model performance at an Australian tropical savannah site showed an improvement of the results for E estimation when the *Global Vegetation Moisture Index* (GVMI) (Ceccato et al. 2002) was used to estimate f as a temporal variable (C. Hensley, unpublished data, 2011).

While these studies are promising, the PML model has not as yet been tested under strong water stress conditions characteristic of Mediterranean drylands. In this work we evaluated the PML model for estimating daily E in sparsely vegetated semiarid areas using three different methods to estimate the temporal variation of f : i) direct soil water content measurements; ii) Zhang's et al. (2010) method adapted for daily application; and iii) a simple model for soil drying after rain. We analyzed the three proposed adaptations of PML in two different Mediterranean drylands: i) a littoral semiarid steppe; and ii) a shrubland montane site. Both sites are characterized by sparse vegetation ($LAI < 1$) and annual precipitation $< 350 \text{ mm year}^{-1}$ during the study period. A whole year of E measurements from eddy covariance systems installed at

each field site were used to test the adapted PML model to determine the most robust method to evaluate f in the studied conditions.

MODEL DESCRIPTION

Penman-Monteith-Leuning model (PML) description

Not considering for simplicity the canopy rainfall interception, Evapotranspiration (E) is the sum of canopy transpiration (E_c) and soil evaporation (E_s):

$$E = E_c + E_s \quad (1)$$

The fluxes of latent heat associated with E_c and E_s were written by Leuning et al. (2008) as

$$\lambda E = \frac{\varepsilon A_c + (\rho c_p / \gamma) D_a G_a}{\varepsilon + 1 + G_a / G_c} + f \frac{\varepsilon A_s}{\varepsilon + 1} \quad (2)$$

where the first term is the PM equation written for the plant canopy and the second term is the flux of latent heat from the soil. The variables A_c and A_s are the energy absorbed by the canopy and soil respectively. G_a and G_c are the aerodynamic and canopy conductances, as defined below. ε is the slope (s) of the curve relating saturation water vapor pressure to temperature divided by the psychrometric constant (γ), ρ is air density, c_p is the specific heat of air at constant pressure, and D_a is the vapor pressure deficit of the air, computed as the difference between the saturation vapor pressure at air temperature, e_{sat} , and the actual vapor, e ($D_a = e_{sat} - e$). The factor f in the second term of Eq. 2 modulates potential evaporation rate at the soil surface $E_{eq,s} = \varepsilon A_s / (\varepsilon + 1)$, by $f = 0$ when the soil is dry, to $f = 1$ when the soil is completely wet. Changes in energy stored in the soil and plant canopy are negligible on a daily basis and hence can be ignored when calculating $A_s = A\tau$, where $\tau = \exp(-k_A LAI)$ and k_A is the extinction coefficient for total available energy A . Energy absorbed by the canopy is $A_c = A(1-\tau)$ (Hu et al. 2009; Leuning et al. 2008; Zhang et al. 2010). When eddy covariance data are used for validation, $A = H + \lambda E$ can be assumed in order to ensure internal consistency in relation to eddy covariance closure error (Leuning et al. 2008). Kustas and Norman (1999) have questioned the

reliability of this simple Beer-Lambert law in sparse vegetation but a sensitivity analysis showed that E_s was insensitive to alternative estimates of A_s (not shown). Of far greater importance is correctly estimating f , as discussed below.

Aerodynamic conductance G_a is estimated using (Monteith and Unsworth 1990)

$$G_a = \frac{k^2 u}{\ln[(z_r - d)/z_{om}] \ln[(z_r - d)/z_{ov}]} \quad (3)$$

where k is Von Karman's constant (0.40), u is wind speed, d is zero plane displacement height, z_{om} and z_{ov} , are roughness lengths governing transfer of momentum and water vapor and z_r is the reference height where u is measured. In this version of Eq. 3 the influence of atmospheric stability conditions over G_a has been neglected for two reasons: i) in dry surfaces where $G_c \ll G_a$, E is relatively insensitive to errors in G_a (Leuning et al. 2008); and ii) in semiarid areas, where highly negative temperature gradients between surface and air temperature are found, correction for atmospheric stability can cause more problems than it solves for estimating G_a (Villagarcía et al. 2007). The variables d , z_{om} and z_{ov} were estimated via the canopy height (h) (Allen 1986): $d = 0.66h$, $z_{om} = 0.123h$ and $z_{ov} = 0.1h$. Because E is insensitive to G_a in arid conditions, we have used these empirical relations even though they were developed for crops and may not apply strictly to sparse vegetation (Berni et al. 2009).

Canopy conductance was estimated using (Isaac et al. 2004; Leuning et al. 2008):

$$G_c = \frac{g_{sx}}{k_Q} \ln \left[\frac{Q_h + Q_{50}}{Q_h \exp(-k_Q LAI) + Q_{50}} \right] \left[\frac{1}{1 + D_a / D_{50}} \right] \quad (4)$$

where k_Q , is the extinction coefficient of visible radiation, g_{sx} is the maximum conductance of the leaves at the top of the canopy, Q_h is the visible radiation reaching the canopy surface that can be approximated as $Q_h = 0.8A$ Leuning et al. (2008) and Q_{50} and D_{50} are values of visible radiation flux and water deficit respectively when the stomatal conductance is half of its maximum value. We used $Q_{50} = 30 \text{Wm}^{-2}$, $D_{50} = 0.7 \text{kPa}$, $k_Q = k_A = 0.6$ (Leuning et al. 2008).

The PML model (Eqs. 2 – 4) includes factors controlling soil evaporation and canopy transpiration but accurate estimation of g_{sx} and f is crucial for model success. Three methods for estimating f , with increasing complexity, are presented next.

Methods for f estimation

f as a function of soil water content data (f_{swc})

Evaporation from drying soil is largely controlled by moisture content near the surface and thus we used volumetric soil water content measured at 0.04 m to estimate f . A maximum water content threshold, θ_{max} , at which soil is considered to evaporate at the equilibrium rate ($f = 1$), and a minimum water content threshold, θ_{min} , at which soil evaporation is considered negligible ($f = 0$) were experimentally determined for each field site in order to rescale observed soil water content (θ_{obs}) from 0 to 1 as follows:

$$f_{swc} \left\{ \begin{array}{ll} = 1 & \text{when, } \theta_{obs} > \theta_{max} \\ = 0 & \text{when, } \theta_{obs} < \theta_{min} \\ = \frac{\theta_{obs} - \theta_{min}}{\theta_{max} - \theta_{min}} & \text{when } \theta_{min} \leq \theta_{obs} \leq \theta_{max} \end{array} \right. \quad (5)$$

f as function of precipitation and equilibrium evaporation ratio (f_{Zhang})

We adapted and tested a method for estimating f presented by Zhang et al. (2010) who varied f by the ratio of accumulated values of precipitation (P) and $E_{eq,s}$, over N days. Zhang et al. (2010) estimated f using $N = 32$ covering 16 days prior and 16 days after the current day i , but here we set $N = 8$ between day i and seven preceding days ($i-7$) to match the time resolution of LAI from MODIS. The final expression for f_{Zhang} is

$$f_{Zhang} = \min \left(\frac{\sum_{i-7}^i P_i}{\sum_{i-7}^i E_{eq,s,i}}, 1 \right) \quad (6)$$

where P_i is the accumulated daily precipitation and $E_{eq,s,i}$ is the daily soil equilibrium evaporation rate for day i .

f as a function of soil drying after precipitation (f_{drying})

Mediterranean areas are characterized by irregular precipitation which causes rapid increases in soil moisture during rain followed by extended drying periods. Thus and we propose to model this pulsed pattern to improve the time resolution of f compared with the f_{Zhang} method.

The formulation for f_{drying} is given by

$$f_{drying} \left\{ \begin{array}{ll} = \min \left(\frac{\sum_{i-15}^i P_i}{\sum_{i-15}^i E_{eq,s,i}}, 1 \right) & \text{when } P_i > P_{min} \\ = f_{LP} \exp(-\omega \Delta t) & \text{when } P_i \leq P_{min} \end{array} \right. \quad (7)$$

where f_{LP} is the f value for the last effective precipitation day ($P_i > P_{min} = 0.5 \text{ mm day}^{-1}$), Δt is number of days between this and the current day i and ω is a parameter controlling the rate of soil drying, higher ω values reflecting higher soil drying speed. For simplicity ω was considered a constant estimated by optimization, even though it is known that ω is related to air temperature, vapor pressure deficit, wind speed and soil hydraulic properties (Ritchie 1972).

MATERIAL AND METHODS

Validation field sites and measurements

The PML model was evaluated at two experimental sites located in southeast Spain characterized by Mediterranean climate (see Table 1) with stronger aridity conditions than where the PML model has previously been tested (Leuning et al. 2008).

Balsa Blanca is a steppe located in Cabo de Gata Natural Park at 196 m a.s.l. and 6.3 km from the coast (36°56'24.17"N; 2°1'59.55"W) showing a Mediterranean semiarid climate. During the study period 2006 to 2008 the site experienced a mean annual temperature of 17°C and mean precipitation of 319 mm yr⁻¹, falling mostly during autumn and winter, with very dry summers. Vegetation in Balsa Blanca has a fraction cover of 60%. The mean canopy height is 0.7 m ($h = 0.7$ m) and is strongly dominated by perennial grass *Stipa tenacissima* L. (57.2%) though other shrub species can be found in lower proportions: *Thymus hyemalis* Lange (1.7%), *Chamaerops humilis* L. (1.6%), *Brachypodium retusum* (Pers.) P. Beauv (1.4%), *Ulex parviflorus* Pourr (0.5%), *Phlomis purpurea* L. (0.2%). Soil has a depth of around 0.15 - 0.25 m and a measured daily mean soil water content at 0.04 m depth that ranges between 0.04 m³ m⁻³ in summer and 0.25 m³ m⁻³ after intense rain events.

Llano de los Juanes is a shrubland plateau located in the Sierra de Gádor at 1600 m elevation and 25 km from the coast (36°55'41.7''N; 2°45'1.7''W), with mean annual temperatures of 13°C and mean precipitation of 326 mm yr⁻¹ during the study period from 2005 to 2007. The climate is subhumid montane Mediterranean with irregular precipitation patterns mostly in autumn and winter when it may fall as snow. The vegetation is sparse with a cover fraction of 50% and a mean canopy height of 0.5 m ($h = 0.5$ m) dominated by three main species: *Festuca scariosa* (Lag.) Hackel (19%), *Genista pumila* ssp *pumila* (11.5%) y *Hormatophylla spinosa* (L). P. Küpfer, (6,3%) (Serrano-Ortiz 2008; Serrano-Ortiz et al. 2009). Soil depth is highly variable (between 0.15 m and 1 m) with medium sized stones and outcropping rocks (30–40% rock fragment content (Serrano-Ortiz et al. 2007). Measured soil water content at 0.04 m depth ranged between a minimum of 0.08 m³ m⁻³ in summer and 0.40 m³ m⁻³ after intense rain events.

Table 1. Details of validation field sites used in this study.

Field site name	Latitude and Longitude	Measurements dataset used	Elevation (m)	Vegetation classification (IGBP Class)	Dominant species	Mean annual precipitation (mm)	Temperature (°C)		
							Max	Mean	Min
Balsa Blanca	36°56'24.17"N ; 2°1'59.55"W	October 2006 - December 2008	196		<i>Stipa tenacissima</i>	319	33	17	4
Llano de los Juanes	36°55'41.7"N; 2°45'1.7"W	April 2005- December 2007	1600	Closed shrubland	<i>Festuca scariosa</i> , <i>Genista pumila</i> , <i>Hormatophiylla spinosa</i>	326	31	13	-7

Water vapor fluxes were measured at each site using eddy covariance (EC) systems consisting of a three axis sonic anemometer (CSAT3, Campbell Scientific Inc., USA) for wind speed and sonic temperature measurement and an open-path infrared gas analyzer (Li-Cor 7500, Campbell Scientific Inc., USA) for variations in H₂O density. EC sensors were located above horizontally uniform vegetation at 3.5 m at Balsa Blanca and at 2.5 m at Llano de los Juanes ($z_r = 3.5$ and $z_r = 2.5$ respectively). Data were sampled at 10 Hz and fluxes were calculated and recorded every 30 min. Corrections for density perturbations (Webb et al. 1980) and coordinate rotation (Kowalski et al. 1997; McMillen 1988) were carried out in post-processing, as was the conversion to half-hour means following Reynolds' rules (Moncrieff et al. 1997). The slope of the linear regressions between available energy ($R_n - G$) and the sum of the surface fluxes ($H + LE$) for both sites (see Fig. 1) yields a slope ~ 0.8 in Balsa Blanca and ~ 0.7 in Llano de los Juanes. This is consistent with the 20% underestimate found in the FLUXNET network (Wilson et al. 2002).

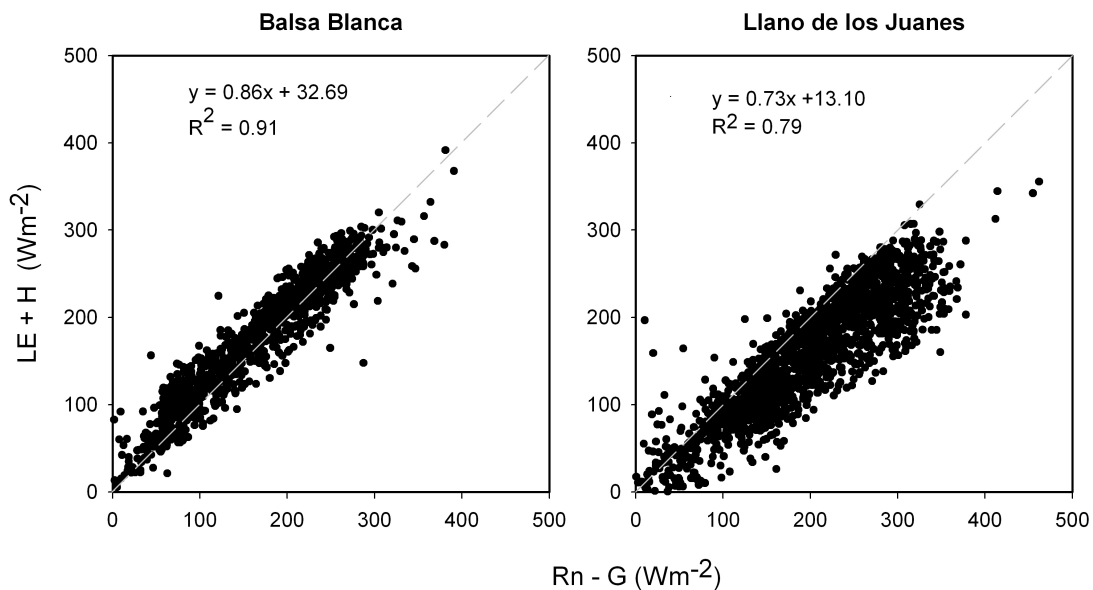


Figure 1. Scatterplots of measured $\lambda E + H$ versus $R_n - G (=A)$ for each field site used in this analysis (daytime averages). Linear relation and R^2 values are shown. In grey line 1:1 for reference.

Complementary meteorological measurements were also made at each field site. An NR-Lite radiometer (Kipp & Zonen, The Netherlands) measured net radiation over representative surfaces at 1.9 m height at Balsa Blanca and 1.5 m at Llano de los Juanes. Soil heat flux was calculated at both sites following the combination method (Fuchs 1986; Massman 1992), as the sum of averaged soil heat flux measured by two flux plates (HFT-3; REBS) located at 0.08 m depth, plus heat stored in upper soil measured by two thermocouples (TCAV; Campbell Scientific LTD) located at two depths 0.02 m and 0.06 m. Air temperature and relative humidity were measured by thermohygrometers located at 2.5 m height at Balsa Blanca field site and 1.5 m at Llano de los Juanes (HMP45C, Campbell Scientific Ltd., USA). A 0.25 mm resolution pluviometer (model ARG100 Campbell Scientific INC., USA) was used to measure precipitation at Balsa Blanca and a 0.2 mm resolution pluviometer was used at Llano de los Juanes (model 785, Davis Instruments Corp. Hayward, California, USA). Soil water content was measured at both sites using water content reflectometers (model CS616, Campbell Scientific INC., USA) located at 0.04 m depth. Due to the high soil heterogeneity, three randomly located sensors were averaged to obtain a representative SWC value at Llano de los Juanes, while at Balsa Blanca one sensor located in bare soil was used. All complementary measurements were recorded every 30 min using dataloggers (Campbell CR1000 and Campbell CR3000 dataloggers, Campbell Scientific Inc., USA) and daytime averages were used.

Remotely sensed data

LAI estimates were level 4 Moderate Resolution Imaging Spectrometers (MODIS) products provided by the ORNL-DAAC (<http://daac.ornl.gov/>): ii) MOD15A (collection 5) from the Terra satellite; and ii) MYD15A2 from the Aqua satellite, both with a temporal resolution of 8 days. The averaged value of *LAI* reported from MOD15A and MYD15A2 for the 3 km x 3 km area centered on each EC tower was computed. Filtering was performed according to MODIS quality assessment (QA) flags to eliminate poor quality data which were replaced by the average of previous and subsequent values when they were available. It was also checked that the land cover class assigned by MODIS for *LAI* estimation in the study field sites, closed and open shrublands, was consistent with the actual vegetation.

Model performance evaluation

Average daytime E measurements were used to validate daily estimates of E derived from the PML model run using average daytime micrometeorological data (Cleugh et al. 2007; Leuning et al. 2008; Zhang et al. 2010). The measurement datasets were divided into an *optimization period* to estimate locally specific g_{sx} and ω values and a *validation period* of PML model outputs at both field sites (Table 2). The estimation of optimized parameters g_{sx} and ω was performed by searching for values that minimized the cost function F for the total sample number (N) using the *rgenoud package* for the R software environment (Mebane and Sekhon 2009).

$$F = \frac{\sum_{i=1}^N |E_{est,i} - E_{obs,i}|}{N} \tag{8}$$

where $E_{est,i}$ is estimated E for day i and $E_{obs,i}$ is observed E for same day.

Table 2. Optimization and validation periods used in both field sites.

Experimental field site	Optimization period	Validation period
Balsa Blanca	18 October 2006	19 October 2007
	18 October 2007 (N=365 days)	31 December 2008 (N = 440 days)
Llano de los Juanes	27 March 2007	4 April 2005
	31 December 2007 (N=279 days)	24 March 2006 (N = 355 days)

Standardized Major Axis Regression (SMA) type II (Warton et al. 2006) was used for comparing daily measurements and model estimates of E during the validation period. SMA regression attributes error in the regression line to both the X and Y variables, a method which is recommended when the X variable is subject to measurement errors, as is assumed for the EC system measurements used in this work. Slope (a), intercept (b) and coefficient of determination (R^2) computed using SMA regression are reported in XY plots. *Mean absolute errors* (MAE) (Willmott and Matsuura 2005) are used for quantitative evaluation of PML model results, while *root mean square errors* (RMSE) are also presented for comparison with previous works. Systematic and unsystematic components of RMSE (Willmott 1982) are also reported. A low systematic error indicates that model structure adequately captures the system dynamics (Choler et al. 2010).

RESULTS

While the two field sites are both Mediterranean drylands with sparse vegetation, the temporal pattern in phenology (*LAI*) is very different. At Balsa Blanca intermittent rainfall throughout the year cause *SWC* and *E* to fluctuate more than at Llano de los Juanes which has distinct wet and dry seasons. The *E* and *SWC* patterns at Balsa Blanca are strongly linked whereas phenology is the main factor controlling *E* at Llano de los Juanes (Fig. 2).

The three methods proposed for estimating *f* yielded different levels of accuracy for estimating daily *E*. For f_{SWC} , experimental thresholds θ_{max} and θ_{min} at Balsa Blanca were, $0.20 \text{ m}^3 \text{ m}^{-3}$ and $0.05 \text{ m}^3 \text{ m}^{-3}$ respectively. At Llano de los Juanes, the same values were $0.35 \text{ m}^3 \text{ m}^{-3}$ and $0.10 \text{ m}^3 \text{ m}^{-3}$ respectively. Using f_{SWC} and f_{Zhang} in the PML model resulted in strong overestimations of *E* following heavy rainfall at both field sites (Fig. 2C and D), whereas use of f_{drying} gave closer agreement with observations. All three methods for estimating *f* overestimated *E* when observed *E* was lower than 0.2 mm day^{-1} at Balsa Blanca field site, but systematically underestimated *E* at the beginning of the dry season at Llano de los Juanes mountain site coinciding with great part of the growing season (April to July of 2005). Reasons for this are discussed in the next section.

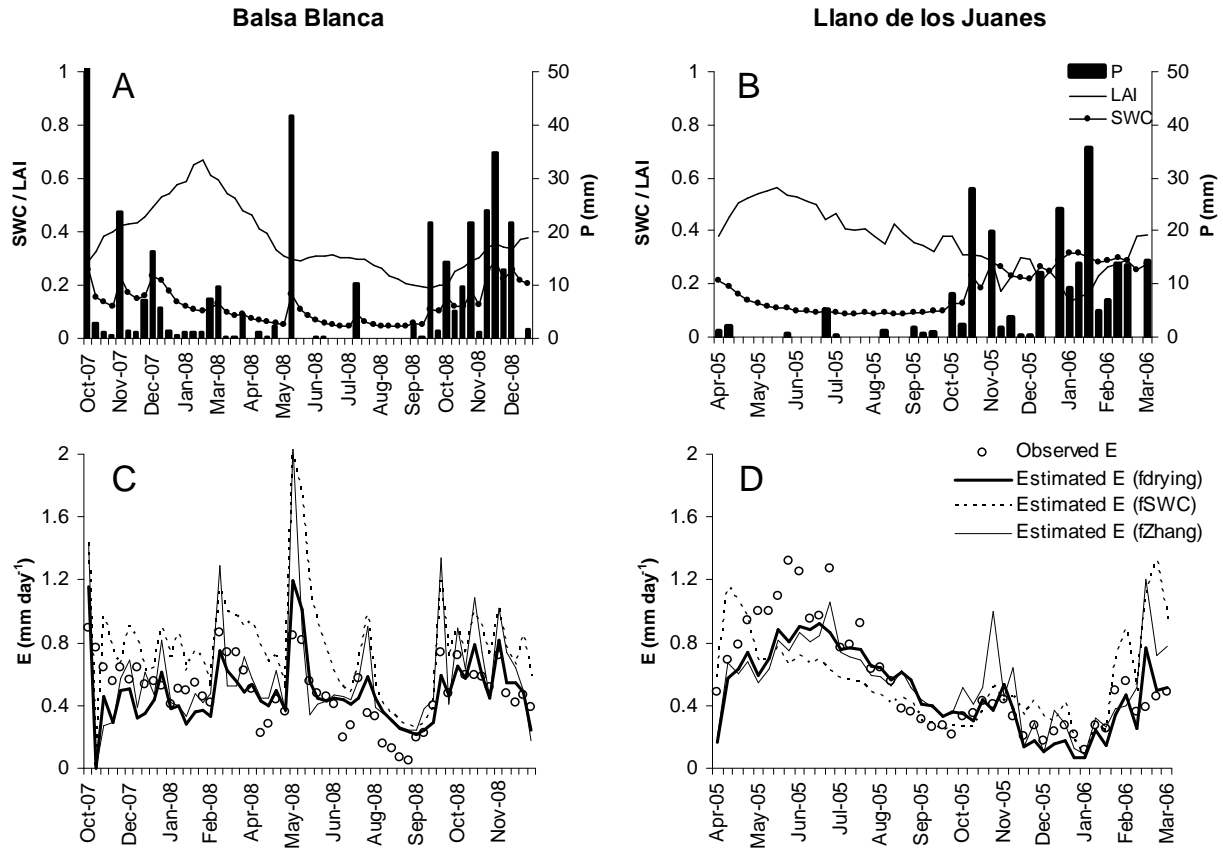


Figure 2. Time series of (top) 8-day accumulated precipitation (P) in mm, actual soil water content (SWC) in mm³ water in mm³ soil and 8-day averages of LAI and (bottom) and 8-day averages of observed E and estimated E in mm day⁻¹ using *f_{drying}*, *f_{SWC}* and *f_{Zhang}* respectively.

Estimated values of daily *E* from the PML model are compared to observations at both field sites in Figure 3. Using *f_{drying}* in the PML model resulted in the best slope ($a = 0.98$) and intercept ($b = 0.01$) for linear correlation versus observed *E*, though the coefficient of determination ($R^2 = 0.47$) using *f_{drying}* is slightly lower than with *f_{SWC}* ($R^2 = 0.54$) at Balsa Blanca field site. Despite the better correlation achieved using *f_{SWC}*, this method tends to overestimate *E* values, a problem not found using *f_{drying}*. The highest correlation at Llano de los Juanes was again obtained using *f_{drying}* ($R^2 = 0.59$), whereas using *f_{SWC}* and *f_{Zhang}* produced two clusters of high and low predictions and hence poor coefficients of determination ($R^2 = 0.24$ and $R^2 = 0.33$, respectively). The PML model with *f_{drying}* underestimates *E* at this site when $E > 1.10$ mm day⁻¹ (Fig. 3F), resulting in a linear regression slope of 0.79. Figure 2B shows that this site has highly seasonal wet and dry periods.

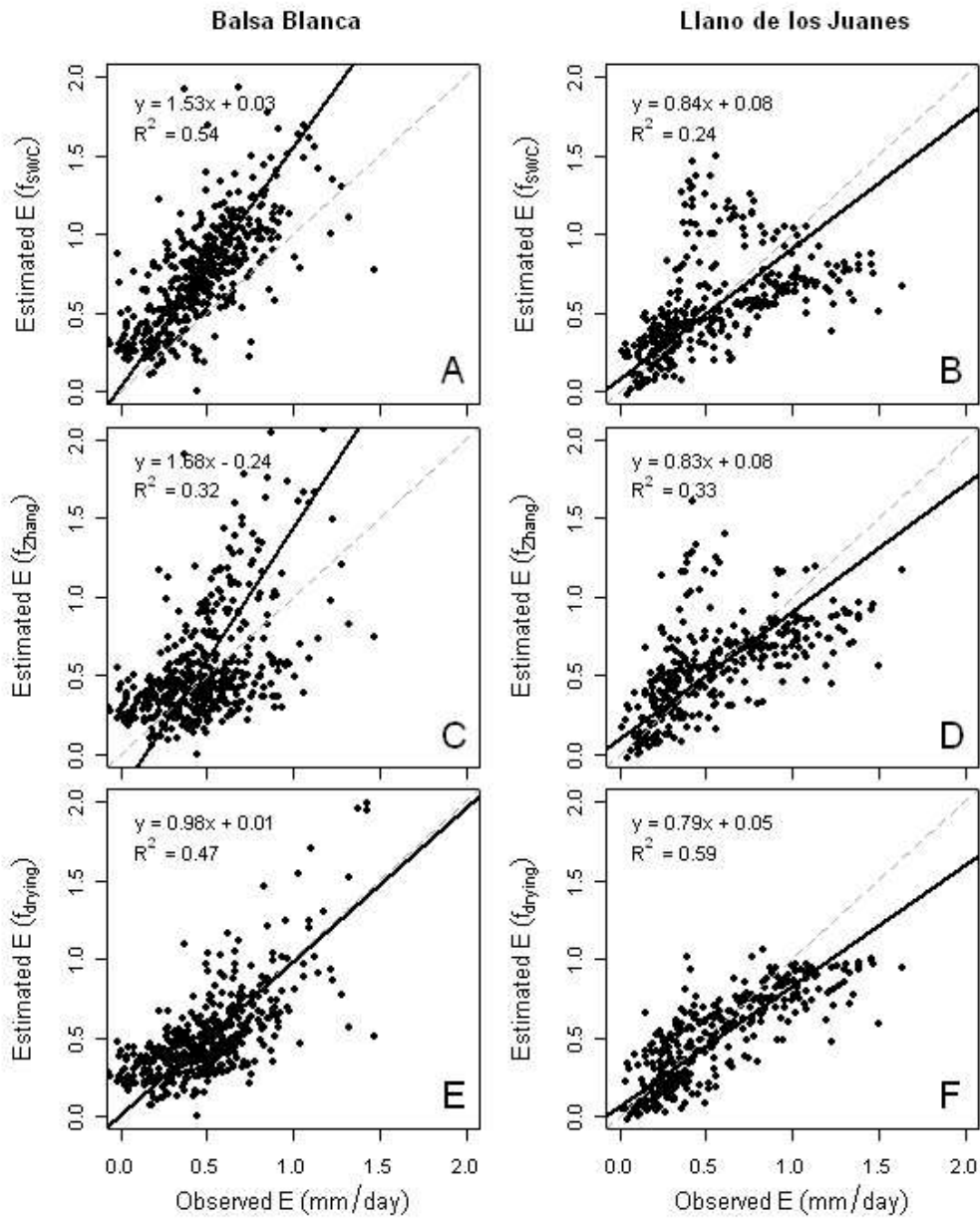


Figure 3. Scatterplots of estimated E using f_{SWC} , f_{Zhang} and f_{drying} , respectively versus observed E in mm day^{-1} . Grey dashed line is 1:1 line.

Table 3. Optimized model parameters and statistic of model performance for the whole validation period N= 440 days in Balsa Blanca and N = 355 days in Llano de los Juanes^a.

Balsa Blanca	f_{SWC}	f_{Zhang}	f_{drying}
g_{sx}	0.0097	0.0085	0.0080
ω	N/A	N/A	0.137
MAE	0.32	0.27	0.17
RMSE	0.41	0.40	0.22
% syst. error	52	5	18
% unsyst. error	49	95	82
E_{avg}	0.49 ± 0.28 mm day ⁻¹		
Llano de los Juanes	f_{SWC}	f_{Zhang}	f_{drying}
g_{sx}	0.0076	0.0098	0.0109
ω	N/A	N/A	0.478
MAE	0.25	0.22	0.17
RMSE	0.34	0.31	0.24
% syst. error	40	37	42
% unsyst. error	61	63	58
E_{avg}	0.56 ± 0.35 mm day ⁻¹		

^a Abbreviations as follows: g_{sx} , maximum conductance of leaves; ω , soil drying speed; MAE, mean absolute error (mm day⁻¹); RMSE, root mean square error both (mm day⁻¹); % syst. error, percentage of systematic error; % unsyst. error, percentage of unsystematic error, E_{avg} , mean observed value of daily evapotranspiration (mm day⁻¹) and N/A, not applicable parameter.

Optimized values of g_{sx} were similar for both field sites under the three proposed formulations for f (g_{sx} ranging from 0.0076 to 0.0109 m s⁻¹) (Table 3). On the other hand, $\omega = 0.137$ at Balsa Blanca is considerably lower than $\omega = 0.478$ at Llano de los Juanes, which indicates the model requires a faster drying rate for Llano de los Juanes than for Balsa Blanca.

Additional analysis were performed at Llano de los Juanes site to determine the reasons explaining the systematic underestimation of E found during the dry and growing season (April to June of 2005). Underestimates of E_c caused by a too low g_{sx} value could be a possible reason. To evaluate if underestimates of g_{sx} were being obtained by including in the optimization dataset periods showing a very different vegetation activity at this strongly seasonal site (the growing and the non-growing season) (Fig. 2), parameters optimizations were performed using specific periods (Table 4).

Table 4. Estimated model parameters by optimizing using the original optimization period, the growing season or the non-growing season ^a.

Parameter	Optimization period	Dates	<i>f</i> estimation method		
			<i>f</i> _{SWC}	<i>f</i> _{Zhang}	<i>f</i> _{driving}
<i>g</i> _{sx}	Original	27/March/2007	0.0076	0.0098	0.0109
ω		31/December/2007	N/A	N/A	0.4783
<i>g</i> _{sx}	Growing Season	18/April/2007	0.0088	0.0100	0.0105
ω		5/August/2007	N/A	N/A	0.5000
<i>g</i> _{sx}	Not Growing Season	10/August/2007	0.0015	0.0078	0.0099
ω		22/December/2007	N/A	N/A	0.4343

^a Abbreviations as follows: *g*_{sx}, maximum conductance of leaves; ω , soil drying speed; and N/A, not applicable parameter.

Estimates of model parameters (*g*_{sx} and ω) did not significantly differ using different optimization periods (Table 4). Only use of optimized parameters for the non-growing season using *f*_{SWC} provided a clearly lower *g*_{sx} (Table 4). This lower value of *g*_{sx} generated a better fit of model output using *f*_{SWC} during the non-growing season but very strong underestimates of *E* for the period when vegetation mostly controlled *E* (Fig. 4). Thus, no practical improvement of model performance during the dry and growing season of the validation period was found using specific optimization periods (Fig. 4) and similar *E* underestimates were still found even when using model parameters optimized specifically for growing season conditions. This test also showed a low sensitivity of optimization to the period used.

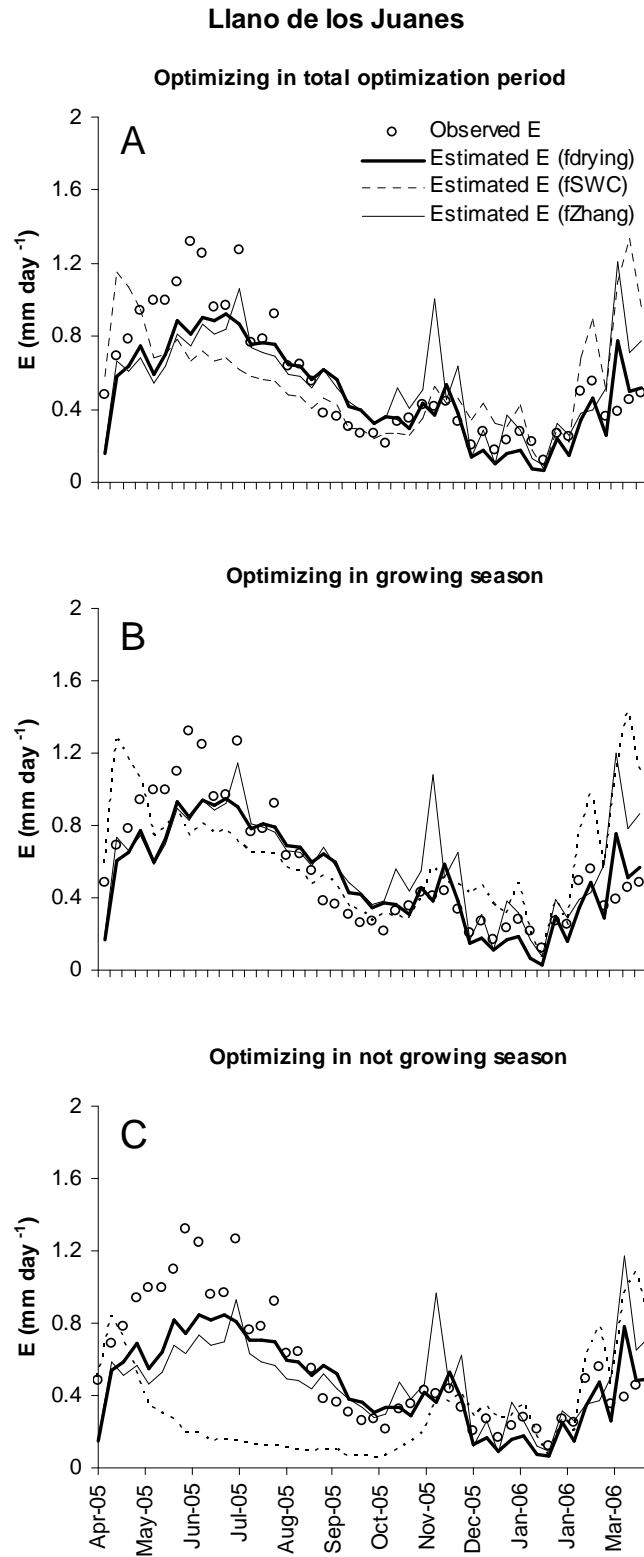


Figure 4. Time series of 8-day averages of observed E and estimated E in mm day^{-1} using f_{drying} , f_{SWC} and f_{Zhang} respectively using the total optimization period (A), the growing season of the optimization period (B) or the not growing season (C) for optimization of parameters g_{sx} and ω .

DISCUSSION

The development of E estimation methods under strongly water-limited conditions is a priority (Glenn et al. 2007) and an especially complex problem (Domingo et al. 2011). This study evaluated the potential of the PML model to estimate E in sparsely vegetated drylands where soil evaporation (E_s) is a major component of total E . In this model, energy consumed by E_s is modulated by the factor f (Eq. 2) which depends on the moisture content of soil near the surface (Leuning et al. 2008).

Despite the dependence of f on soil moisture content, using locally measured soil water content data for $f = f_{SWC}$ (Eq. 5) provided unsatisfactory estimates of E using the PML model (Table 3). This may be caused by uncertainties determining the experimental threshold values θ_{min} and θ_{max} used in Eq. 5. Moreover the differences in accuracy in estimating E using f_{SWC} at the two field sites (Fig. 3A and B) were related to functional differences between them. The daily pattern of E at our littoral site, Balsa Blanca, was strongly linked to the SWC pattern seen in Figures. 2A and C. SWC controls both soil evaporation and transpiration because the dominant species, *S. tenacissima*, is well-adapted to aridity showing opportunistic growth patterns with leaf conductance and photosynthetic rate largely dependant on water availability in the upper soil layer (Haase et al. 1999; Pugnaire and Haase 1996). This explains the good results obtained using f_{SWC} here. At the mountain site, Llano de los Juanes, the pattern in E was more closely linked with LAI than SWC (Fig. 2B and D). This was evident from a reduction of the influence of E_s to evaporation dynamics especially during the dry and growing seasons from April to August, where extraction of water by plants from deep cracks and fissures in the bedrock has been previously detailed (Cantón et al. 2010). In contrast, during the wet season (November to March 2006) using f_{SWC} led to an overestimate in E which may be explained by the effect of high stoniness and frequent rock outcrops (30-40% rock fragment content) which reduce the effective soil surface described by the SWC data. This limited the usefulness of the f_{SWC} method in stony soils. A further limitation to regional application was the lack of spatially distributed SWC data.

Use of f_{Zhang} in the PML model resulted in strong overestimation of E during periods following heavy or continuous rain events and a generally low correlation with observations (Fig. 2 and 3). This occurred because Eq. 6 results in f_{Zhang} oscillating between 0 and 1 during periods of heavy but intermittent rainfall, whereas in reality soil water content decreases progressively after rain events. Originally Zhang et al. (2010) used this approach to estimate f

over 32-day intervals during which this oscillation effect is less pronounced. They obtained an RMSE of 0.56 mm day^{-1} for a sparsely vegetated savannah site in Australia (Virginia Park) where mean annual E was 1.20 mm day^{-1} . Using f_{Zhang} resulted in an RMSE of $0.40 - 0.31 \text{ mm day}^{-1}$ at our sites, which is a relatively larger error than at Virginia Park, considering that mean annual E was 0.49 mm day^{-1} at Balsa Blanca and 0.56 mm day^{-1} at Llano de los Juanes. These results and Table 3 show that the f_{Zhang} method did not improve PML model performance for our ecosystems.

Adoption of the f_{drying} method (Eq. 7) notably improved PML model performance at both sites with relative errors (RMSE of $0.22 - 0.24 \text{ mm day}^{-1}$) which are similar to the relative errors obtained by Leuning et al. (2008) and Zhang et al. (2010) for Virginia Park. This method outperformed the other two approaches (f_{SWC} and f_{Zhang}) at both sites, showing a better capacity to describe the gradual drying of soil following rainfall. As a result, E estimated using f_{drying} did not show the strong overestimation obtained with the f_{SWC} and f_{Zhang} methods after rainfall (Figs. 2C and D). Like f_{Zhang} , f_{drying} shares the advantage of only requiring widely-available precipitation and equilibrium evaporation data, with the expense of a single additional parameter ω . With the use of f_{drying} the PML model was able to capture the varying controls on E_s at both field sites. The optimized value of $\omega = 0.137$ at Balsa Blanca, and thus the soil drying rate, was lower than $\omega = 0.478$ at Llano de los Juanes. The soil evaporative component at Balsa Blanca thus has a longer period of influence on total E than at Llano de los Juanes where the soil dried more quickly. Moreover, the importance of infiltration occurring in preferential flows through the abundant cracks, joints and fissures, typical of this karstic mountain area pointed out by Cantón et al. (2010) and Contreras et al. (2006) is characterised well by the high rate of modelled soil drying.

The stronger phenological control over E , the reduction of effective evaporative soil surface due to stoniness and rocky soil features and the importance of infiltration at Llano de los Juanes, contribute to E_s having a less important role in total E dynamics than at Balsa Blanca. This explains the systematically lower percentage errors found in this area because all three adapted model versions tested here better capture the system dynamics at Balsa Blanca, where soil evaporation plays a more important role than at Llano de los Juanes (Fig. 3).

The systematic underestimation of E by the PML model at the beginning of the dry season observed at Llano de los Juanes (Fig. 2D) using f_{Zhang} and f_{drying} could be caused by E_c or E_s underestimates. Underestimates of g_{sx} would be the main reason why PML could be underestimating E_c . The inclusion in the dataset used for optimization of both, the growing and the non-growing seasons, for which a clearly different vegetation activity is expected at this

strongly seasonal site (Fig. 2), could produce g_{sx} underestimates. However, tests optimizing model parameters using different optimization periods (Table 4) showed consistency for g_{sx} optimized values and weak sensitivity to the optimization period used. Therefore underestimates of E by the PML model at the beginning of the dry season can be explained by errors in E_s caused by too low values of f_{drying} , and f_{Zhang} . During this period, the effect of precipitation from the preceding wet season (finishing 20 days before our validation period) is not considered by f due to the time resolution of both methods for estimating f (16 and 8 days respectively). These methods are not able to capture high soil water availability levels resulting from the cumulative effect of a long prior wet season.

Constant model parameter values for g_{sx} and ω were used to test the performance of the PML model to estimate E for two dryland ecosystems where vegetation and soil are exposed to strong fluctuations of environmental conditions. While use of constant parameter values may provide sub-optimal model performance, such simplifications are necessary for regional application, with awareness of possible errors associated with the simplifications.

CONCLUSIONS

The capacity of Penman-Monteith-Leuning model (PML model) to estimate daily evapotranspiration in sparsely-vegetated drylands is demonstrated through the development of methods for temporal and spatial estimation of the soil evaporation parameter f . We advance Leuning et al. (2008) who found that estimating soil evaporation parameter f as a local time constant produced poor results in sparsely-vegetated areas ($LAI < 2.5$). Out of three proposed methods, f_{drying} showed the best results for PML model adaptation at two experimental sites. This method's results achieved reasonable agreement with EC-derived daily evapotranspiration rates bearing in mind the difficulties associated with E -modeling in drylands, where measured E rates are especially low, often not exceeding the error range of methods for estimating E from remote sensing (Domingo et al. 2011). In modeling the progressive soil drying process after precipitation events, the f_{drying} method avoided the strong overestimates of E obtained with two other f estimation approaches, f_{SWC} and f_{Zhang} . Nevertheless, the f_{drying} method showed some limitations in its ability to model the soil evaporation rate when this was influenced by high soil water availability levels during the growing season from the cumulative effect of a long prior wet season at Llano de los Juanes.

The use of time-invariant parameters for evapotranspiration modeling is a delicate issue in drylands and other extreme ecosystems where vegetation and soil are exposed to strong fluctuations in environmental conditions. Where a simplifying compromise is required in the design of operational and regionally applicable models, we show here that reasonable results can be obtained using temporally-constant estimates of g_{sx} and ω in the PML model.

REFERENCES

- Allen, R.G. (1986). A Penman for all seasons. *Journal of Irrigation & Drainage Engineering - ASCE*, 112, 348-368
- Berni, J.A.J., Zarco-Tejada, P.J., Sepulcre-Cantó, G., Fereres, E., & Villalobos, F. (2009). Mapping canopy conductance and CWSI in olive orchards using high resolution thermal remote sensing imagery. *Remote Sensing of Environment*, 113, 2380-2388
- Cantón, Y., Villagarcía, L., Moro, M.J., Serrano-Ortíz, P., Were, A., Alcalá, F.J., Kowalski, A.S., Solé-Benet, A., Lázaro, R., & Domingo, F. (2010). Temporal dynamics of soil water balance components in a karst range in southeastern Spain: Estimation of potential recharge. *Hydrological Sciences Journal*, 55, 737-753
- Ceccato, P., Flasse, S., & Grégoire, J.M. (2002). Designing a spectral index to estimate vegetation water content from remote sensing data: Part 1: Theoretical approach. *Remote Sensing of Environment*, 82, 188-197
- Cleugh, H.A., Leuning, R., Mu, Q., & Running, S.W. (2007). Regional evaporation estimates from flux tower and MODIS satellite data. *Remote Sensing of Environment*, 106, 285-304
- Contreras, S. (2006). Distribucion espacial del balance hídrico anual en regiones montañosas semiáridas. Aplicacion en Sierra de Gador (Almería). Tesis Doctoral. Almería: Universidad de Almeria, pp.135.
- Choler, P., Sea, W., Briggs, P., Raupach, M., & Leuning, R. (2010). A simple ecohydrological model captures essentials of seasonal leaf dynamics in semi-arid tropical grasslands. *Biogeosciences*, 7, 907-920
- Domingo, F., Serrano-Ortiz, P., Were, A., Villagarcía, L., García, M., Ramírez, D.A., Kowalski, A.S., Moro, M.J., Rey, A., & Oyonarte, C. (2011). Carbon and water exchange in semiarid ecosystems in SE Spain. *Journal of Arid Environments*, 75, 1271-1281
- Fuchs, M. (1986). Heat flux. In: A. Kute (Ed), *Methods of Soil Analysis Part I Physical and Meteorological Methods* (pp. 957-968). Madison, USA: American Society of Agronomy
- Glenn, E.P., Huete, A.R., Nagler, P.L., Hirschboeck, K.K., & Brown, P. (2007). Integrating remote sensing and ground methods to estimate evapotranspiration. *Critical Reviews in Plant Sciences*, 26, 139-168
- Guerschman, J.P., Van Dijk, A.I.J.M., Mattersdorf, G., Beringer, J., Hutley, L.B., Leuning, R., Pipunic, R.C., & Sherman, B.S. (2009). Scaling of potential evapotranspiration with MODIS data reproduces flux observations and catchment water balance observations across Australia. *Journal of Hydrology*, 369, 107-119
- Haase, P., Pugnaire, F.I., Clark, S.C., & Incoll, L.D. (1999). Environmental control of canopy dynamics and photosynthetic rate in the evergreen tussock grass *Stipa tenacissima*. *Plant Ecology*, 145, 327-339
- Hu, Z., Yu, G., Zhou, Y., Sun, X., Li, Y., Shi, P., Wang, Y., Song, X., Zheng, Z., Zhang, L., & Li, S. (2009). Partitioning of evapotranspiration and its controls in four grassland ecosystems: Application of a two-source model. *Agricultural and Forest Meteorology*, 149, 1410-1420
- Huxman, T.E., Smith, M.D., Fay, P.A., Knapp, A.K., Shaw, M.R., Lolk, M.E., Smith, S.D., Tissue, D.T., Zak, J.C., Weltzin, J.F., Pockman, W.T., Sala, O.E., Haddad, B.M., Harte, J., Koch, G.W., Schwinning, S., Small, E.E., & Williams, D.G. (2004). Convergence across biomes to a common rain-use efficiency. *Nature*, 429, 651-654

- Huxman, T.E., Wilcox, B.P., Breshears, D.D., Scott, R.L., Snyder, K.A., Small, E.E., Hultine, K., Pockman, W.T., & Jackson, R.B. (2005). Ecohydrological implications of woody plant encroachment. *Ecology*, 86, 308-319
- Isaac, P.R., Leuning, R., Hacker, J.M., Cleugh, H.A., Coppin, P.A., Denmead, O.T., & Raupach, M.R. (2004). Estimation of regional evapotranspiration by combining aircraft and ground-based measurements. *Boundary-Layer Meteorology*, 110, 69-98
- Kalma, J.D., McVicar, T.R., & McCabe, M.F. (2008). Estimating land surface evaporation: A review of methods using remotely sensed surface temperature data. *Surveys in Geophysics*, 29, 421-469
- Kowalski, A.S., Anthoni, P.M., Vong, R.J., Delany, A.C., & Maclean, G.D. (1997). Deployment and evaluation of a system for ground-based measurement of cloud liquid water turbulent fluxes. *Journal of Atmospheric and Oceanic Technology*, 14, 468-479
- Kustas, W.P., & Norman, J.M. (1996). Use of remote sensing for evapotranspiration monitoring over land surfaces. *Hydrological Sciences Journal*, 41, 495-516
- Kustas, W.P., & Norman, J.M. (1999). Evaluation of soil and vegetation heat flux predictions using a simple two-source model with radiometric temperatures for partial canopy cover. *Agricultural and Forest Meteorology*, 94, 13-29
- Leuning, R., Zhang, Y.Q., Rajaud, A., Cleugh, H., & Tu, K. (2008). A simple surface conductance model to estimate regional evaporation using MODIS leaf area index and the Penman-Monteith equation. *Water Resources Research*, 44, W10419
- Massman, W.J. (1992). Correcting errors associated with soil heat flux measurements and estimating soil thermal properties from soil temperature and heat flux plate data. *Agricultural and Forest Meteorology*, 59, 249-266
- McMillen, R.T. (1988). An eddy correlation technique with extended applicability to non-simple terrain. *Boundary-Layer Meteorology*, 43, 231-245
- Mebane, W.R., & Sekhon, J.S. (2009). R-GENetic Optimization Using Derivatives (RGENOUD). Available at: <http://sekhon.berkeley.edu/papers/rgenoudJSS.pdf>
- Moncrieff, J.B., Massheder, J.M., De Bruin, H., Elbers, J., Friborg, T., Heusinkveld, B., Kabat, P., Scott, S., Soegaard, H., & Verhoef, A. (1997). A system to measure surface fluxes of momentum, sensible heat, water vapour and carbon dioxide. *Journal of Hydrology*, 188-189, 589-611
- Monteith, J.L. (1964). Evaporation and environment. In: *The state and movement of water in living organisms. Symposium of society of experimental biology*, Vol 19 (pp. 205-234). Swansea, UK: Cambridge University Press.
- Monteith, J.L., & Unsworth, M.H. (1990). *Principles of Environmental Physics*. London, UK: Edward Arnold, pp.291.
- Mu, Q., Heinsch, F.A., Zhao, M., & Running, S.W. (2007). Development of a global evapotranspiration algorithm based on MODIS and global meteorology data. *Remote Sensing of Environment*, 111, 519-536
- Mu, Q., Zhao, M., & Running, S.W. (2011). Improvements to a MODIS global terrestrial evapotranspiration algorithm. *Remote Sensing of Environment*, 115, 1781-1800
- Noy-Meir, I. (1973). Desert ecosystems: environment and producers. *Annual Reviews*, 4, 25-51

- Priestley, C.H.B., & Taylor, R.J. (1972). On the assessment of surface heat flux and evaporation using large-scale parameters. *Monthly Weather Review*, *100*, 81-92
- Pugnaire, F.I., & Haase, P. (1996). Comparative physiology and growth of two perennial tussock grass species in a semi-arid environment. *Annals of Botany*, *77*, 81-86
- Ritchie, J.T. (1972). Model for predicting evaporation from a row crop with incomplete cover. *Water Resources Research*, *8*, 1204-1213
- Serrano-Ortiz, P. (2008). Intercambios de CO₂ entre atmósfera y ecosistemas kársticos: aplicabilidad de las técnicas comúnmente empleadas. Tesis Doctoral. Granada: Universidad de Granada, pp.296.
- Serrano-Ortiz, P., Domingo, F., Cazorla, A., Were, A., Cuezva, S., Villagarcía, L., Alados-Arboledas, L., & Kowalski, A.S. (2009). Interannual CO₂ exchange of a sparse Mediterranean shrubland on a carbonaceous substrate. *Journal of Geophysical Research*, *114*, G04015
- Serrano-Ortiz, P., Kowalski, A.S., Domingo, F., Rey, A., Pegoraro, E., Villagarcía, L., & Alados-Arboledas, L. (2007). Variations in daytime net carbon and water exchange in a montane shrubland ecosystem in southeast Spain. *Photosynthetica*, *45*, 30-35
- Stewart, J.B., Kustas, W.P., Humes, K.S., Nichols, W.D., Moran, M.S., & de Bruin, H.A.R. (1994). Sensible Heat Flux-Radiometric Surface Temperature Relationship for Eight Semiarid Areas. *Journal of Applied Meteorology*, *33*, 1110-1117
- Villagarcía, L., Were, A., Domingo, F., Garcia, M., & Alados-Arboledas, L. (2007). Estimation of soil boundary-layer resistance in sparse semiarid stands for evapotranspiration modelling. *Journal of Hydrology*, *342*, 173-183
- Wang, K., & Dickinson, R.E. (2012). A review of global terrestrial evapotranspiration: Observation, modeling, climatology, and climatic variability. *Reviews of Geophysics*, *50*, RG2005
- Warton, D.I., Wright, I.J., Falster, D.S., & Westoby, M. (2006). Bivariate line-fitting methods for allometry. *Biological Reviews of the Cambridge Philosophical Society*, *81*, 259-291
- Webb, E.K., Pearman, G.I., & Leuning, R. (1980). Correction of flux measurements for density effects due to heat and water vapour transfer. *Quarterly Journal Royal Meteorological Society*, *106*, 85-100
- Wilson, K., Goldstein, A., Falge, E., Aubinet, M., Baldocchi, D., Berbigier, P., Bernhofer, C., Ceulemans, R., Dolman, H., Field, C., Grelle, A., Ibrom, A., Law, B.E., Kowalski, A., Meyers, T., Moncrieff, J., Monson, R., Oechel, W., Tenhunen, J., Valentini, R., & Verma, S. (2002). Energy balance closure at FLUXNET sites. *Agricultural and Forest Meteorology*, *113*, 223-243
- Willmott, C.J. (1982). Some comments on the evaluation of model performance. *Bulletin - American Meteorological Society*, *63*, 1309-1313
- Willmott, C.J., & Matsuura, K. (2005). Advantages of the mean absolute error (MAE) over the root mean square error (RMSE) in assessing average model performance. *Climate Research*, *30*, 79-82
- Zhang, Y.Q., Chiew, F.H.S., Zhang, L., Leuning, R., & Cleugh, H.A. (2008). Estimating catchment evaporation and runoff using MODIS leaf area index and the Penman-Monteith equation. *Water Resources Research*, *44*, W10420

Zhang, Y.Q., Leuning, R., Hutley, L.B., Beringer, J., McHugh, I., & Walker, J.P. (2010). Using long-term water balances to parameterize surface conductances and calculate evaporation at 0.05° spatial resolution. *Water Resources Research*, 46, W05512

CAPITULO 4

Actual Evapotranspiration in Drylands derived from in-situ and Satellite Data: Assessing biophysical constraints

*Publicado en *Remote Sensing of Environment* como:

García, M., Sandholt, I., Ceccato, P., Ridler, M., Mougin, E., Kergoat, L., Morillas, L., Timouk, F., Fensholt, R., & Domingo, F. (2013). Actual evapotranspiration in drylands derived from in-situ and satellite data: Assessing biophysical constraints. *Remote Sensing of Environment*, 131, 103-118

ABSTRACT

Improving regional estimates of actual evapotranspiration (LE) in water-limited regions located at climatic transition zones is critical. This study assesses an LE model (PT-JPL model) based on downscaling potential evapotranspiration according to multiple stresses at daily time-scale in two of these regions using MSG-SEVIRI (surface temperature and albedo) and MODIS products (NDVI, LAI and f_{PAR}). An open woody savanna in the Sahel (Mali) and a Mediterranean grassland (Spain) were selected as test sites with Eddy Covariance data used for evaluation. The PT-JPL model was modified to run at a daily time step and the outputs from eight algorithms differing in the input variables and also in the formulation of the biophysical constraints (stresses) were compared with the LE from Eddy Covariance. Model outputs were also compared with other modeling studies at similar global dryland ecosystems.

The novelty of this paper is the computation of a key model parameter, the soil moisture constraint, relying on the concept of Apparent Thermal Inertia (f_{SM-ATI}) computed with surface temperature and albedo observations. Our results showed that f_{SM-ATI} from both in-situ and satellite data produced satisfactory results for LE at the Sahelian savanna, comparable to parameterizations using field-measured Soil Water Content (SWC) with R^2 greater than 0.80. In the Mediterranean grasslands however, with much lower daily LE values, model results were not as good as in the Sahel ($R^2=0.57-0.31$) but still better than reported values from more complex models applied at the site such as the Two Source Model (TSM) or the Penman-Monteith Leuning model (PML).

PT-JPL-daily model with a soil moisture constraint based on apparent thermal inertia, f_{SM-ATI} offers great potential for regionalization as no field-calibrations are required and water vapor deficit estimates, required in the original version, are not necessary, being air temperature and the available energy (Rn-G) the only input variables required, apart from routinely available satellite products.

Keywords: evapotranspiration, surface temperature, Priestley-Taylor, thermal inertia, MSG-SEVIRI, water-limited ecosystems, MODIS

INTRODUCCION

Evapotranspiration (or latent heat flux expressed in energy terms, LE) represents 90% of the annual precipitation in water-limited regions which cover 40% of the Earth's surface (Glenn et al. 2007). In these regions there is a close link between carbon and water cycles (Baldocchi 2008) where water availability is the main control for biological activity (Brogaard et al. 2005). LE rates also determine groundwater recharge (Huxman et al. 2005) and feedbacks to continental precipitation patterns (Huntington 2006). The Sahel and the Mediterranean basin are both located in transitional climate regions and are thus expected to be extremely sensitive to climate change (Giorgi and Lionello 2008). The land surface is a strong amplifier on the inter-annual variability of the West African Monsoon leading to the observed persistency patterns (Nicholson 2000; Taylor et al. 2011; Timouk et al. 2009). Therefore, improving estimates of temporal and spatial variations of LE is crucial for understanding land surface-atmosphere interactions and to improve hydrological and agricultural management (Yuan et al. 2010).

LE can be estimated at regional scales using remote sensing data. One way is to use models based on the bulk resistance equation for heat transfer (Brutsaert 1982), relying on the difference between surface temperature (T_R) and air temperature (T_a) and the aerodynamic resistance to turbulent heat transport. In this case, LE is estimated indirectly as a residual of the surface energy balance equation (Anderson et al. 2007; Chehbouni et al. 1997). This approach circumvents the problem of estimating soil and canopy surface resistances to water vapor, needed to compute LE , that tend to be more critical in LE modeling than aerodynamic resistances in dryland regions (Verhoef 1998; Were et al. 2007). In those regions, two-source models treating the land surface as a composite of soil and vegetation elements with different temperatures, fluxes, and atmospheric coupling provide better results than single-source models (Anderson et al. 2007). However, despite the strong physical basis of two-source models (Kustas and Norman 1999; Norman et al. 1995) their spatialization is difficult because the task of estimating aerodynamic resistances at instantaneous time scales is not trivial, requiring knowledge about atmospheric stability, several vegetation and soil parameters as well as meteorological data (Fisher et al. 2008). Further complications arise from the partition of T_R between soil and vegetation (Kustas and Norman 1999) because the radiative surface temperature differs from the aerodynamic surface temperature especially over sparsely vegetated surfaces (Chehbouni et al. 1997).

A second group of models using remote sensing data directly solve the LE term using the Penman-Monteith (PM) combination equation. In this case, LE can be partitioned into soil and

vegetation components (Leuning et al. 2008). With this approach, the challenge is to characterize the spatial and temporal variation in surface conductances to water vapor without using field calibration (Zhang et al. 2010). A simple way to estimate surface conductances is to use prescribed sets of parameters based on biome-type maps (Zhang et al. 2010). Other approaches perform optimization with field data but can lead to a lack of estimates over vast regions of the globe, such as the Sahel, due to the scarcity of field measurements (Yuan et al. 2010). One of the first attempts to characterize surface conductance without optimization proposed an empirical relationship with *LAI* derived from MODIS (Moderate Resolution Imaging Spectroradiometer) (Cleugh et al. 2007). Mu et al. (2007; 2011) refined this approach using the empirical multiplicative model proposed by Jarvis (1976) estimating moisture and temperature constraints on stomatal conductance and upscaling leaf stomatal conductance to canopy. Alternatively, Leuning et al. (2008) used a biophysical model for surface conductance based on Kelliher et al. (1995) method. However, this method required optimization with field data for g_{sx} , the maximum stomatal conductance of leaves, and for the soil water content. As both parameters were held constant along the year *LE* was overestimated at drier sites. To address this shortcoming, Zhang et al. (2008) introduced a variable-soil moisture fraction dependent on rainfall, and optimized g_{sx} using outputs from an annual water balance model or a Budyko-type model (Zhang et al. 2008; 2010). Although this represented a step-forward for operational applications, results at dry sites were still poorer than at more humid sites (Zhang et al. 2008; 2010).

A solution to overcome those parameterization problems using the Penman-Monteith equation, was the simplification proposed by Priestley and Taylor (1972) (PT) for equilibrium evapotranspiration over large regions by replacing the surface and aerodynamic resistance terms with an empirical multiplier α_{PT} (Zhang et al. 2009). The PT equation is theoretically less accurate than PM although uncertainties in parameter estimation using PM can result in higher errors (Fisher et al. 2008). Fisher et al. (2008) proposed a model based on PT to estimate monthly actual *LE*. The authors used biophysical constraints to reduce *LE* from a maximum potential value, LE_p , in response to multiple stresses. One advantage of this approach is that it does not require information regarding biome-type or calibration with field data. The modeling framework can be seen as conceptually similar to the so-called Production Efficiency Models (PEM) for estimating *GPP* (Gross Primary Productivity) (Houborg et al. 2009; Monteith 1972; Potter et al. 1993; Verstraeten et al. 2006a;) where maximum light use efficiency of conversion of absorbed energy f_{APAR} into carbon is reduced below its maximum potential due to environmental stresses. In fact, part of the formulation from the PT-JPL model has been

introduced into some PEM models (Yuan et al. 2010). The main model assumption is that plants optimize their capacity for energy acquisition in a way that changes in parallel with the physiological capacity for transpiration (Fisher et al. 2008; Nemani and Running 1989). This idea is to some extent related to the hydrological equilibrium hypothesis stating that in water-limited natural systems, plants adjust canopy development to minimize water losses and maximize carbon gains (Eagleson 1986) but applied over shorter time-scales. The modeling approach described above neglects the behavior of individual leaves and considers the canopy response to its environment in bulk for which it can be refer to as a top-down approach (Houborg et al. 2009). Top-down approaches use simpler scaling rules compared to bottom-up models that require detailed mechanistic descriptions of leaf-level processes up-scaled to the canopy (Schymanski et al. 2009). Although top-down approaches require less parameters than bottom-up approaches, they are subjected to a higher degree of empiricism with high uncertainty on the functional responses of ecosystem processes to environmental stresses (Yuan et al. 2010).

The use of global satellite vegetation products and meteorological gridded databases as input to top-down approaches based on the PM or the PT equations has made possible to obtain regional estimates of evapotranspiration (Mu et al. 2007). However, there are still limitations regarding the use of such databases. One hand, existing global climatic data sets interpolated from observations such as the Climatic Research Unit data set (CRU, University of East Anglia) are available on a monthly but not a daily basis (New et al. 2000). Moreover, data from reanalyses such as ECMWF (European Centre for Medium-Range Weather forecasts) or NCEP/NCAR present coarse spatial resolutions ($\approx 1.25^\circ$) (Mu et al. 2007) being desirable to minimize the use of climatic data when possible.

On the other hand, PM and PT satellite-based approaches have taken advantage of optical remote sensing data to estimate vegetation properties but thermal remotely sensed data has been used only marginally and with coarse spatial resolution data such as the microwave AMSR-E at 0.25° (Miralles et al. 2011). Incorporation of long-wave infrared thermal data at spatial resolutions of 1-3 km available from the MODIS (Moderate Resolution Imaging Spectroradiometer) or the SEVIRI (Spinning Enhanced Visible and Infrared Imager) sensors could help to track changes in surface conductance (Berni et al. 2009; Boegh et al. 2002), soil evaporation (Qiu et al. 2006), surface water deficit (Boulet et al. 2007; Moran et al. 1994) or soil water content (Gillies and Carlson 1995; Nishida et al. 2003; Sandholt et al. 2002). In relation to soil moisture a promising approach is the mapping of soil moisture based on soil thermal inertia

(Cai et al. 2007; Sobrino et al. 1998; Verstraeten et al. 2006b), following the early work of Price (1977) and Cracknell and Xue (1996).

The objective of this work was to adapt and evaluate a daily version of the PT-JPL model and introduce a new formulation for soil moisture based on the thermal inertia concept. The aim is to minimize the need for climatic reanalyses data by incorporating thermal remote sensing information in order to facilitate future model regionalization. The PT-JPL model in its original formulation has proven to be successful over 36 FLUXNET sites at monthly time scales, ranging from boreal to temperate and tropical ecosystems. However, none of those included semiarid vegetation with annual rainfall below 400 mm (Fisher et al. 2008; 2009). Model performance using in-situ and satellite data was compared with field data from Eddy Covariance systems at two semiarid sites: an open woody savannah in the Sahel (Mali) and Mediterranean tussock grassland (Spain). Finally, to place the results in the context of global drylands, model results were compared to published results from similar models using remote sensing at dryland savanna and grasslands sites across the globe.

FIELD SITES AND DATA

Two field sites (Fig. 1) have been used to test the model in semiarid conditions: an open woody savannah in Mali and tussock grassland in Spain. A general description of the sites is included in Table 1.

Table 1. General characteristics of the two instrumented field sites in the Sahel region and in the Mediterranean basin.

Site name (location)	Vegetation type	Mean annual rainfall	Soil type	Dominant herbaceous species	Dominant woody species
Agoufou (Mali) (15.34°N, 1.48°W)	Open woody savannah	375 mm	Fixed dunes- Arenosol	<i>Cenchrus biflorus</i> , <i>Aristida mutabilis</i> , <i>Zornia glochidiata</i> , <i>Tragus berteronianus</i>	<i>Acacia raddiana</i> , <i>Acacia senegal</i> , <i>Combretum glutinosum</i> , <i>Balanites aegyptiaca</i> , <i>Leptadenia pyrotechnica</i>
Balsa Blanca (Spain) (36.94°N, 2.03°W)	Tussock grassland	370 mm	Calcium crusts- Mollic leptosol	<i>Stipa tenacissima</i>	<i>Thymus hyemalis</i> , <i>Chamaerops humilis</i> L., <i>Brachypodium retusum</i> (Pers.) P. Beauv, <i>Ulex parviflorus</i>

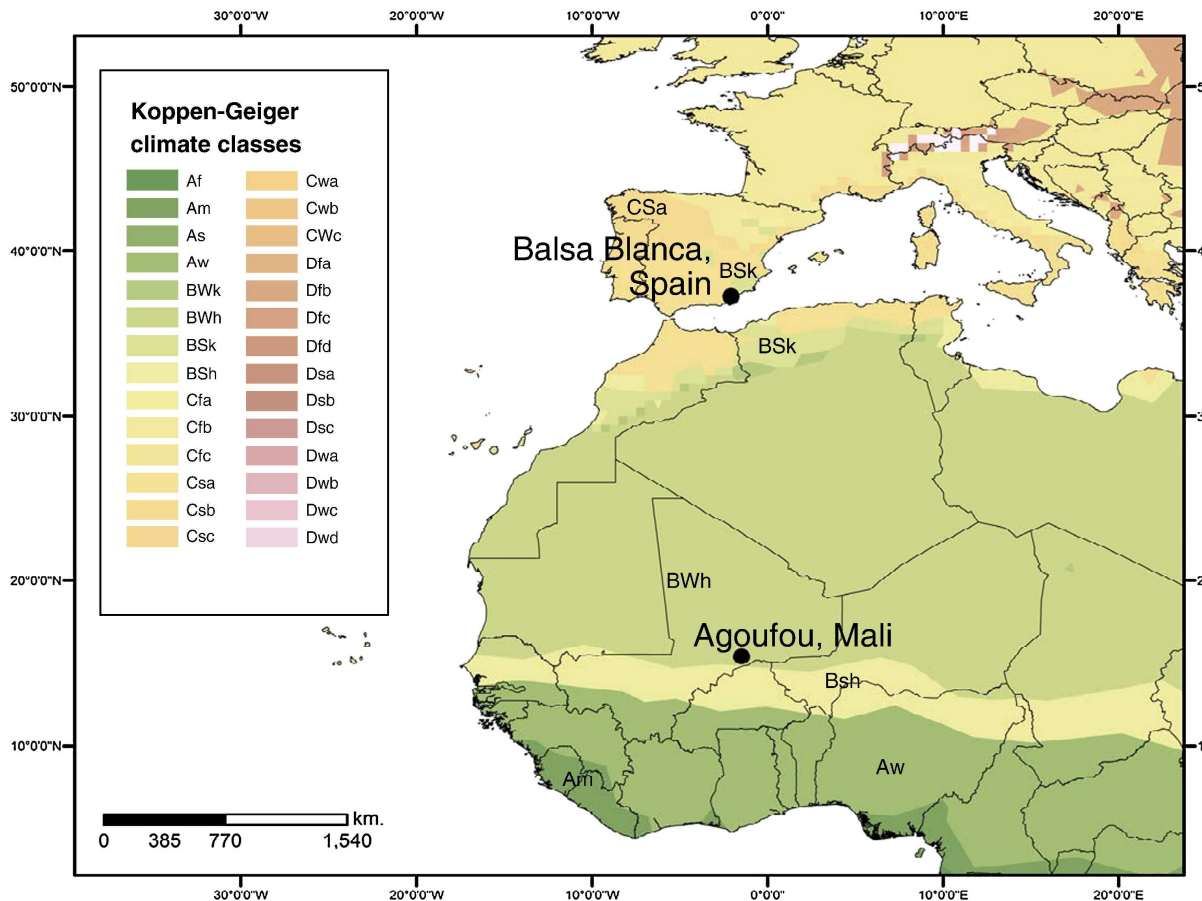


Figure 1: Location of the two study sites: an open woody savanna (15.34°N, 1.48°W) in the Sahel (Mali) and Mediterranean tussock grassland (36.94°N, 2.03°W) in Spain. The map with Köppen-Geiger climate classes (Kottek et al. 2006) overlaps country boundaries. The Mediterranean site presents Cold semiarid climate (BSk) and the Sahelian site Arid/desert/hot climate (BWh).

Sahelian Open Woody Savannah site

The Agoufou site is an open woody savannah, homogeneous over several kilometers, with trees representing less than 5% of vegetation cover. A comprehensive description of the site is provided by Mougin et al. (2009). The top 0–0.06 m of the soil is 91% sand, 3.3% silt and 4.6% clay (de Rosnay et al. 2009). The region experiences a single rainy season with most precipitation falling between late June and mid September followed by a long dry season of around 8 months.

In-situ data for the 2007 growing season were provided by the African Monsoon Multidisciplinary Analyses (AMMA) project. Sensible heat flux was measured with sonic anemometers (CSAT) measuring the three vector components of the wind at 20 Hz. Latent heat fluxes were measured with the Eddy Covariance system (logger CR3000, anemometer CSAT3 and IRGA LiCor7500, Campbell Scientific Inc. and Li–Cor Inc., USA). The four components of the net radiation were measured with a CNR1 (Kipp and Zonen CNR1, Delft, Holland).

Measurement height for the flux sensors are 2.2 m. Soil heat fluxes were computed from soil temperature measurements. See Timouk et al. (2009) for more details. Wind speed and direction (Vector A100R), land surface temperature (Everest 4000.4zl), air temperature and humidity (HMP 45C, Vaisala) and precipitation (Delta T, RG1) were also measured. Time domain reflectometry sensors (CS616, Campbell Scientific Inc., USA) measured volumetric Soil Water Content at several depths with the shallower probe, the one used in this work, located at 0.05 m.

Leaf area index (*LAI*) and fractional cover were monitored approximately every 10 days during the 2007 growing season (DOY 184 to 269) along a 1 km long vegetation transect using hemispherical photographs. *LAI* was validated using destructive measurements (Mougin et al. 2009). Comparisons with MODIS *LAI* during three years produced $R^2=0.82$ and RMSE 0.26 (Mougin et al. 2009). The fraction of vegetation cover is 50%, with a maximum average height of 0.4 m for the herbaceous cover. A period starting prior and finishing after the rains was evaluated (DOY 170 to 315). No gap filling has been performed. Gaps in flux data are present notably in late July to early August (Fig. 2).

Mediterranean grassland site

Balsa Blanca site is a tussock grassland steppe dominated by *Stipa tenacissima* L. (91% cover) located within the “Cabo de Gata-Níjar Natural Park” (Spain) the only subdesertic protected region in Europe, with a semiarid Mediterranean climate. Annual rainfall is highly variable from year to year with mean values of 375 mm and mean annual temperature of 18.1 °C. In the closer long-term station the average was 200 mm (records from the closest meteorological station, Níjar, distant 30 km) (Rey et al. 2012) with rainfall falling mostly in fall and winter and a prolonged summer drought. The fraction of vegetation cover is 60%, with mean average height of 0.7 m. The soil is classified as Mollic Leptosol (WRB) (*World Reference Base for Soil Resources, FAO 1998*) with depth ranging from 0.15 to 0.25 m.

In-situ data were acquired during the 2011 growing season between January and June. This period should capture most of the annual variability in *LE* although it is only part of a complete growing season that starts in fall until early summer (Fig. 2). Latent and sensible heat fluxes were measured with respective Eddy Covariance (EC) systems (logger CR3000, anemometer CSAT3 and IRGA LiCor7500, Campbell Scientific Inc. and Li-Cor Inc., USA). The measurement heights were 3.5 m. Sensors measured at 10 Hz and fluxes were estimated and

stored half-hourly applying the corrections for axis-rotation (Kowalski et al. 1997; Mcmillen 1988) and density fluctuations (Webb et al. 1980).

Net radiation was obtained using NR-Lite (Kipp&Zonen). Four soil heat flux plates (HFP01SC; Campbell Sci. Inc.) were placed at 0.08 m depth, two under plant and two under bare soil, and connected via multiplexer to a datalogger. The soil heat flux at the surface was determined by adding the measured heat flux at 0.08 m (G) to the energy stored in the layer above the heat plate estimated from soil temperature and soil moisture measurements. Soil temperature was measured using soil thermocouples (TCAV) at 0.02 and 0.06 m depth adjacent to the heat flux plates. Land surface temperature was measured with three Apogee sensors over bare soil, vegetation, and a composite of bare soil and vegetation, (IRTS-P). Air temperature and relative humidity were measured with thermohygrometers (HMP45C, Campbell Scientific Ltd.). Rainfall was measured using a tipping bucket rain gauge of 0.25 mm of resolution (ARG100 Campbell Scientific INC., USA). Time domain reflectometry sensors (CS616, Campbell Scientific Ltd) measured Volumetric ($\text{m}^3 \text{m}^{-3}$) soil water content (SWC) under bare soil and under plants with 0.04 m being the top most measured soil moisture.

Figure 2 shows the seasonal dynamics for volumetric soil water content, expressed in % (SWC), rainfall (mm), evapotranspiration (LE) in W m^{-2} , and $NDVI$ for the two study sites.

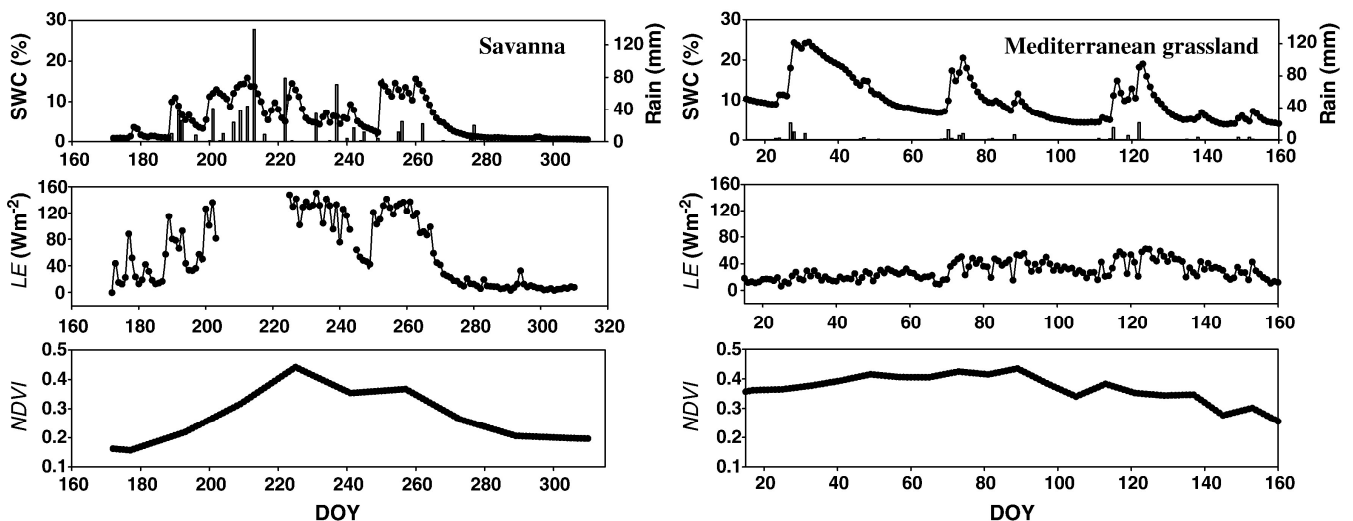


Figure 2: Volumetric soil water content % (SWC), rainfall (mm), evapotranspiration (LE) in W m^{-2} , and $NDVI$ dynamics during the periods of analyses in the Sahelian savanna (Agoufou) in 2007 and in the Mediterranean grasslands (Balsa Blanca) in 2011. SWC probes were located at 0.05 m and 0.04 m depth respectively.

Satellite Data

NDVI data were acquired from the Moderate Resolution Imaging Spectroradiometer (MODIS) Terra and Acqua sensors products MOD13Q1 and MY13Q1 (collection 5) over the two study sites. This product consists of 16-day composites of 250 m pixel (Huete et al. 2002). *LAI* and f_{PAR} products from Terra and Acqua (MOD15A2, MY15A2) consisting of 8-day composites of 1 km pixel (collection 5) (Myneni et al. 2002) were acquired as well. To get daily estimates a linear interpolation using both Terra and Acqua values was performed within the 8-day or 16 day interval in each case.

Land Surface Temperature (*LST*) and broadband surface albedo (α) products used in this work were developed by the Satellite Application Facility for Land Surface Analysis (LSA SAF) with data from the Spinning Enhanced Visible and Infrared Imager (SEVIRI) radiometer, onboard of the MSG (Meteosat Second Generation). The MSG-SEVIRI sensor includes 12 separate channels and 15 min temporal resolution making it attractive for applications requiring intra-daily information. As for any geostationary satellite the trade-off is the low spatial resolution of 4.8 km at nadir (spatial sampling is 3 km) and large view angles (Schmetz et al. 2002). The *LST* algorithm is based on a generalized split window, following (Wan and Dozier 1996) formulation adapted to SEVIRI data (Trigo et al. 2008). It requires information on clear-sky conditions and TOA brightness temperatures for the split-window channels 10.8 μm and 12.0 μm . Channel and broadband emissivity is estimated as a weighted average of that of bare ground and vegetation elements within each pixel using the fraction of vegetation cover derived from *NDVI* (Trigo et al. 2008). The albedo product is based on short-wave channels at 0.6, 0.8 and 1.6 μm . It has an effective temporal scale of 5 days and updated on a daily basis using cloud-free reflectance observations that are corrected for atmospheric effects using the simplified radiative transfer code SMAC (Geiger et al. 2008). Dynamic information on the atmospheric pressure and total column water vapor comes from the European Centre for Medium-range Weather Forecasts (ECMWF) NWP model. Cloud identification and cloud type classification are used in the processing of all LSA SAF products.

METHODS

PT-JPL-daily Model Description

The daily model proposed here (hereafter PT-JPL-daily) is a modified version of the algorithm described in Fisher et al. (2008) where LE is partitioned into canopy transpiration (LE_c) and soil evaporation (LE_s) (Eq. 1). In this paper, we did not consider interception evaporation (LE_i), or evaporation from a wet canopy surface, as in low LAI ecosystems it accounts for a limited amount of the total water flux (Mu et al. 2011) and in turn using it requires observations of relative humidity at the sites. However, preliminary model evaluations showed that including it did not improve or worsen the results.

Actual LE is calculated based on potential evapotranspiration of soil (LEp_s) and canopy (LEp_c) which are reduced from their potential level using different constraints (multipliers) based on plant physiological status and soil moisture availability (Fisher et al. 2008). LE_p was calculated using (Priestley and Taylor 1972) equation.

$$LE = LE_c + LE_s \quad (1)$$

Three plant physiological constraints were considered to regulate evapotranspiration: green canopy fraction, a plant temperature constraint (f_T) and a plant moisture constraint (f_M) (Eq. 2).

$$LE_c = f_g f_T f_M LEp_c \quad (2)$$

All the equations and variables are described in Table 2. Considering that the physiological capacity for energy acquisition should be adjusted with the capacity for transpiration, the green canopy fraction, that represents the canopy fraction actively transpiring, should reflect an upper limit for transpiration. f_g was estimated as the ratio between intercepted and absorbed photosynthetic active radiation f_{APAR}/f_{IPAR} (Table 2). The original model formulation for estimating LAI and f_{APAR} using $NDVI$ and the extinction of radiation equation (Table 2) was used as well as new estimates of LAI and f_{APAR} derived from MODIS standard products.

The plant temperature constraint (f_T) accounts for reductions in photosynthetic efficiency when plants grow at temperatures departing from their optimum temperature range (Potter et al. 1993). f_T depends on the optimum air temperature for plant growth T_{opt} (°C) and T_{a_m} (°C) the average daily temperature. In the original model, T_{opt} was assumed to coincide with maximum canopy activity and was estimated as the air temperature of the month with the highest $NDVI$ and radiation and minimum vapor pressure deficit (VPD) (June et al. 2004). However, this approach in Mediterranean semiarid environments is prone to unrealistic T_{opt} values due to the decoupling

between warm and rainy seasons, with the maximum peak for vegetation activity occurring in late winter (García et al. in review). In a preliminary evaluation we observed that the f_T from the Carnegie-Ames-Stanford Approach model (CASA) performed better. In the CASA model f_T has an asymmetric bell shape reflecting a higher sensitivity to high than to low temperatures (see Table 2 for equations) (Potter et al. 1993). To avoid calibrations of T_{opt} depending on the site, we fixed T_{opt} in 25°C, a value that has been applied in global modeling studies across different type of biomes (Yuan et al. 2010). We checked in preliminary analyses that variations of ± 5 °C around this value of T_{opt} did not affect model outputs.

The third constraint for LE_c was a plant moisture constraint, f_M , defined as the relative change in light absorptance with respect to the maximum ($f_{APAR}/f_{APARMax}$). This approach assumes that plant absorptance decreases mostly due to moisture stress (Fisher et al. 2008).

The soil evaporation component was constrained by a soil moisture limitation, f_{SM} (Eq. 3).

$$LE_s = f_{SM} LEp_s \quad (3)$$

In this work, we evaluated an f_{SM} estimate based on the thermal inertia (TI) concept using T_R and albedo. Thermal inertia is a physical property of soil at the land surface measuring the thermal response of a material to the changes in its temperature (Nearing et al. 2012). The higher the TI the lower its diurnal temperature fluctuation. Estimating thermal inertia requires knowing thermal conductivity of the material (K), its density (ρ) and specific heat (C) (Price 1977).

Increasing soil moisture content modifies soil thermal conductivity and reduces the diurnal surface temperature fluctuation (Verstraeten et al. 2006b). In early studies, this diurnal T_R variation was linked theoretically to thermal inertia resulting in the apparent thermal inertia (ATI) index (Price 1977). Estimating thermal inertia using remote sensing was first introduced by Price (1977) and expanded by Cracknell and Xue (1996), Sobrino et al. (1998) and Lu et al. (2009). In this study we estimated ATI following Verstraeten et al. (2006b) which was based on Mitra and Majumdar (2004) (see Eq. 4). ATI relies on broadband albedo (α), and the difference between maximum daytime (T_{RDMax}) and minimum nighttime (T_{RDmin}) surface temperature, and a solar correction factor C (equation 5) that normalizes for changes in solar irradiance with latitude, ϑ and the solar declination angle φ , the angle between sun rays and the plane of the Earth's equator. It is assumed that ATI reflects both soil and canopy water content if the T_R includes both soil and vegetation components (Tramutoli 2000; Verstraeten et al. 2006b). In fact, a composite T_R might track better changes in root-zone SWC as the canopy temperature responds rapidly to changes in root zone SWC , which can be decoupled from the bare soil surface SWC . From the 15

minute T_R data the minimum (T_{R-Dmin}) and maximum (T_{R-DMax}) values from each day were extracted. Observations flagged as cloudy in the METEOSAT LST data and days when the midday observation was missing were excluded from the analyses. A smoothing procedure averaging with the prior and following day was applied to the ATI assuming that the soil moisture conditions could be interpolated between subsequent days and to remove noise.

$$ATI = C \frac{1 - \alpha}{T_{R-DMax} - T_{R-Dmin}} \quad (4)$$

$$C = \sin \vartheta \sin \varphi \cdot (1 - \tan^2 \vartheta \cdot \tan^2 \varphi) + \cos \vartheta \cdot \cos \varphi \cdot \arccos(-\tan \vartheta \cdot \tan \varphi) \quad (5)$$

Where ϑ is latitude, and φ solar declination estimated using the method of (Iqbal 1983).

However, the coupling between ATI and soil moisture is not straightforward. Thermal inertia could be converted directly to soil moisture provided soil properties are known (Lu et al. 2009; Minacapilli et al. 2009; Van doninck et al. 2011). Since those properties only change over geologic time scales, short-term changes in ATI can be linked to changes in soil moisture using time-series (Van Doninck et al. 2011). Verstraeten et al. (2006b) related soil moisture to remotely sensed ATI derived from METEOSAT imagery by assuming that the minimum and maximum seasonal ATI (ATI_{min} and ATI_{Max}) correspond to residual and saturated soil moisture contents obtaining f_{SM-ATI} (see equation in Table 2).

To evaluate f_{SM} derived from ATI two additional formulations of f_{SM} used in the original model formulation have been also tested (see Table 2). The first is based on field measurements of volumetric soil water content (SWC) (f_{SM-SWC}), where SWC was rescaled between a minimum (SWC_{min}) and a maximum value (SWC_{Max}) (Fisher et al. 2008). In our case, SWC_{min} was estimated as the minimum value of the dry season. SWC_{Max} was estimated as the value of SWC in the 24 hours after a strong rainfall event, which can be considered as an estimate of the field capacity. If $SWC > SWC_{Max}$ then $f_{SM-SWC} = 1$. In the Mediterranean site, the 2006-2011 period was used to extract SWC_{min} and SWC_{Max} as the period used to apply PT-JPL-daily was not a complete season.

The second approach to estimate f_{SM} was the original PT-JPL model formulation based on the link between atmospheric water deficit and soil moisture ($f_{SM-Fisher}$) (Bouchet 1963; Morton 1983). This link is compromised if the vertical adjacent atmosphere is not in equilibrium with the

underlying soil (Fisher et al. 2008). The β parameter indicates the relative sensitivity of soil moisture to VPD (see Table 2).

Table 2: Equations and variables involved in estimating PT-JPL-daily model biophysical constraints, plant variables and energy variables. f_{APAR} is the fraction of Absorbed Photosynthetically Active Radiation, f_{IPAR} the fraction of intercepted photosynthetically active radiation, T_{opt} is optimum temperature for plant growth (25 °C), Ta_m (daily mean air temperature, °C), $f_{APARMAX}$ is maximum f_{APAR} , SWC , Soil Water Content (m^3m^{-3}), RH is relative humidity (%), VPD is the vapor pressure deficit (kPa), ATI is the observed apparent thermal inertia index ($^{\circ}C^{-1}$), ATI_{min} is the seasonal minimum ATI , ATI_{MAX} is the seasonal maximum ATI . Rn is daily net radiation (Wm^{-2}). Values for parameters: $k_{Rn}=0.6$ (Impens and Lemeur 1969); $k_{PAR}=0.5$ (Brownsey et al. 1976); $m_1=1.16$; $b_1=-0.14$; (Myneni and Williams 1994); $m_2=1.0$; $b_2=-0.05$ (Fisher et al. 2008), γ (psychrometric constant)= $0.066 kPaC^{-1}$; $\beta=1kPa$, $\alpha_{PT}=1.26$ Priestley -Taylor coefficient; Δ is the slope of the saturation-to-vapor pressure curve (PaK^{-1}). In the reference column it has been added original model for the cases when the formulation was used in Fisher et al. (2008) or this study if the formulation has been implemented in this study.

	Variable	Description	Equation	Reference
Biophysical constraints	f_g	Green canopy fraction	$f_g = \frac{f_{APAR}}{f_{IPAR}}$	Fisher et al. (2008) original model
	f_T	Plant temperature constraint	$f_T = 1.1814 \cdot \left[1 + e^{\frac{0.2(T_{opt}-10-Ta_m)}{\Delta}} \right]^{-1}$ $\left[1 + e^{\frac{0.3(-T_{opt}-10-Ta_m)}{\Delta}} \right]^{-1}$	Potter et al. (1993) this study
	f_M	Plant moisture constraint	$f_M = \frac{f_{APAR}}{f_{APARMAX}}$	Fisher et al. (2008) original model
	f_{SM}	Soil moisture constraint	$f_{SM-SWC} = 1 - \left(\frac{SWC - SWC_{min}}{SWC_{Max} - SWC_{min}} \right)$ $f_{SM-Fisher} = RH^{VPD / \beta}$ $f_{SM-ATI} = \left(\frac{ATI - ATI_{min}}{ATI_{Max} - ATI_{min}} \right)$	Fisher et al. (2008) original model Fisher et al. (2008) original model Verstraeten et al (2006b) this study
Plant variables	f_{APAR}	PAR fraction absorbed by green vegetation	$f_{APAR-NDVI} = m_1 \cdot NDVI + b_1$ $f_{APAR-MODIS}$	Myneni and Williams (1994) original model Myneni et al. (2002) this study
	f_{IPAR}	PAR fraction intercepted by total vegetation	$f_{IPAR} = m_2 \cdot NDVI + b_2$	Fisher et al. (2008) original model
	f_c	fractional vegetation cover	$f_c = f_{IPAR}$	Campbell and Norman (1998) original model
	LAI	Leaf Area Index	$LAI_{NDVI} = -Ln(1 - f_c) / k_{PAR}$ LAI_{MODIS}	Norman et al. (1995); Ross (1976) original model Myneni et al. (2002) this study
Energy variables	Rn_s	Net radiation to the soil	$Rn_s = Rn \cdot e^{(-k_{Rn}LAI)}$	Norman et al. (1995); Ross (1976) original model
	LEp_c	Priestley-Taylor potential evapotranspiration for canopy	$LEp_c = \alpha_{PT} \frac{\Delta}{\Delta + \gamma} (Rn - Rn_s)$	Norman et al. (1995) original model
	LEp_s	Priestley-Taylor potential evapotranspiration for soil	$LEp_s = \alpha_{PT} \frac{\Delta}{\Delta + \gamma} (Rn_s - G)$	Norman et al. (1995) original model

Global sensitivity analyses (EFAST) approach

Sensitivity analysis can be used to evaluate the effects of uncertainty on input or parameters on model output or to evaluate which variables or parameters have the largest effect on model output (Matsushita et al. 2004). In this study Global Sensitivity Analysis (GSA) of PT-JPL-daily model was performed using Extended Fourier Amplitude Sensitivity Test (EFAST) (Saltelli et al. 1999). EFAST was originally developed by Cukier et al. (1978) and improved by Saltelli et al. (1999). The advantage of EFAST compared to traditional sensitivity analyses such as one-at-a-time (OAT) or experimental design (ED) is that it allows several input variables to vary simultaneously considering interactions among them. It can be used for non-linear and non-monotonic models providing similar results to more complex methods based as well on analyses of variance but being computationally more efficient (Saltelli et al. 1999). A Fourier decomposition is used to obtain the fractional contribution of the individual input factors to the variance of the model prediction (Campolongo et al. 2000).

To identify the relative importance of each model input in terms of its contribution to the output variance of daily evapotranspiration, perturbations for each variable were applied around the mean value of the growing season and also around mean monthly values. R_n , G , $NDVI$ and T_a were varied by $\pm 10\%$ around their monthly means and annual mean based on reported uncertainty of field measurements for those variables (Garcia et al. 2008). For the constant model parameters: m_1 , b_1 , m_2 , b_2 , k_{Rn} , and k_{PAR} , the range of uncertainty was based on values used in the literature (Table 3). A perturbation of $\pm 25\%$ around the mean was considered for the soil moisture constraint (f_{SM}) and the plant temperature constraint (f_T).

Table 3: Ranges of variation for input parameters and variables in PT-JPL-daily model. For R_n , G , $NDVI$ and T_a ranges of $\pm 10\%$ around monthly means and annual mean was considered. For the constant model parameters: m_1 , b_1 , m_2 , b_2 , k_{Rn} , and k_{PAR} , the range of uncertainty was based on values used in the literature. For the soil moisture constraint (f_{SM}) and the plant temperature constraint (f_T) a range of $\pm 25\%$ around the mean was considered. Description of variables and parameters can be found in Table 2.

Input var	Range	Reference
T_a	$\pm 10\%$ of mean value	This study
R_n	$\pm 10\%$ of mean value	This study
G	$\pm 10\%$ of mean value	This study
f_T	$\pm 25\%$ of mean value	This study
f_{SM}	$\pm 25\%$ of mean value	This study
$NDVI$	$\pm 10\%$ of mean value	This study
m_1	[1.16, 1.42]	This study
b_1	[-0.039, -0.025]	This study
m_2	[0.9, 1.2]	Fisher et al. (2008)
b_2	[-0.06, -0.04]	Fisher et al. (2008)
k_{Rn}	[0.3, 0.6]	Ross (1976)
k_{PAR}	[0.3, 0.6]	Ross (1976)

Evaluation of the PT-JPL-daily evapotranspiration model

PT-JPL-daily was run using a combination of field and remotely-sensed data as inputs to parameterize the biophysical constraints and partition the energy between soil and canopy (Table 4). Two versions (the original version and one version using MODIS products) of LAI and f_{APAR} were tested which modify two of the plant constraints f_g and f_M as well as the energy partition between soil and vegetation (Table 2). In addition, three versions of f_{SM} were used as explained in the model description Section (Table 2). Model results were compared with LE from Eddy Covariance fluxes and the coefficient of determination (R^2), Mean Average Error (MAE), the bias, the RMSE (Root Mean Square Error) and MAPE (Mean Absolute Percentage Error) were used as indicators of model performance. To compare modeled LE with LE measurements from Eddy Covariance the energy balance from the Eddy Covariance data should be forced to zero (Twine et al. 2000). We used the criteria of preserving the Bowen ratio that assumes that the Bowen ratio (H/LE) is well measured by the EC system and the closure error is proportionally distributed into LE and H (Twine et al. 2000).

The evaluation results (R^2 , errors and biases) are presented in four steps. First, model performance using measured soil moisture constraint (f_{SM-SWC}) was analyzed. Here, the accuracy of the two different versions for LAI and f_{APAR} was compared as, in principle, this model version using f_{SM-SWC} should be the most precise from the point of view of soil moisture constraint and can be used as a benchmark. In the second step, the feasibility of using $f_{SM-Fisher}$, from atmospheric variables at daily time-scale in semiarid conditions was evaluated. In the third step, the performance of the model run with the apparent thermal inertia index f_{SM-ATI} from in-situ and also satellite data was evaluated. In these three steps the two versions for estimating LAI and f_{APAR} were evaluated as well resulting in a total of eight algorithm versions evaluated (see Table 4). Finally, to place model results in the context of global drylands, our accuracy results were compared to published accuracy results from other models that used remote sensing information at the same and at other dryland savanna and grasslands sites across the globe. In those cases when model outputs were provided by the authors at 30 minutes time step, they were aggregated at daily time scale and compared with the eddy covariance data to have comparable statistics.

Table 4: Eight versions of PT-JPL-daily (FD) were run based on different combinations of equations and data used for the variables: f_{SM} , f_{IPAR} and LAI . Rn is Net radiation (Wm^{-2}), G is soil heat flux (Wm^{-2}), T_a , air temperature ($^{\circ}C$), SWC , Soil Water Content (%), VPD , Vapor pressure deficit (kPa), RH , Relative humidity (%), T_s , Surface temperature ($^{\circ}C$), LAI (Leaf Area Index), f_{PAR} (fraction of Photosynthetic Active Radiation) and α broadband surface albedo. The soil moisture constraints used were: f_{SM-SWC} (from measured volumetric soil water content), $f_{SM-Fisher}$ (from atmospheric water deficit), and f_{SM-ATI} (from apparent thermal inertia). Two different f_{APAR} and LAI were used (a) $f_{APAR-NDVI}$ and LAI_{NDVI} (FDa model versions) and (b) used $f_{APAR-MODIS}$ and LAI_{MODIS} (in FDb model versions). All equations are described in Table 2.

Algorithm version	Algorithm name	f_{SM}		f_{APAR} and LAI		Common variables Data/source
		estimate	data/source	estimate	Data/source	
1	FDa _{SWC}	f_{SM-SWC}	SWC/in-situ	$f_{APAR-NDVI}$	NDVI/MODIS	Rn, G, T_a /in-situ
2	FDb _{SWC}			$f_{APAR-MODIS}$	f_{PAR} , LAI/MODIS	
3	FDa _{Fisher}	$f_{SM-Fisher}$	VPD, RH/in- situ	$f_{APAR-NDVI}$	NDVI/MODIS	
4	FDb _{Fisher}			$f_{APAR-MODIS}$	f_{PAR} , LAI/MODIS	
5	FDa _{ATI-in situ}	f_{SM-ATI}	T_s, α /in-situ	$f_{APAR-NDVI}$	NDVI/MODIS	
6	FDb _{ATI-in-situ}			$f_{APAR-MODIS}$	f_{PAR} , LAI/MODIS	
7	FDa _{ATI-MSG}			$f_{APAR-NDVI}$	NDVI/MODIS	
8	FDb _{ATI-MSG}			$f_{APAR-MODIS}$	f_{PAR} , LAI/MODIS	

RESULTS AND DISCUSSION

Global Sensitivity Analyses (EFAST) approach

Considering the variability around mean annual conditions, the contribution to uncertainty was less than 20% for most parameters and variables in the Sahelian savanna. The greatest uncertainty was due to two of the biophysical constraints: f_{SM} and f_T with 22.19% and 17.68 % respectively (total effect). Five other variables involved in LAI estimation and energy partition between soil and canopy contributed around 12% to model uncertainty (Fig. 3). However, the relative importance of each variable depends on the time of the year. At the beginning of the season, LE was most sensitive to accuracy in f_{SM} reaching the maximum value of explained variance among all variables and months (40%). During the maximum peak of $NDVI$, in the middle of the season, the greatest sensitivity was due to f_T , and m_l (involved in f_M and f_g estimates via f_{APAR}). During the senescent phase, the model was more sensitive to accuracy in k_{PAR} and k_{Rn} , involved in energy partition into soil and vegetation.

Under annual Mediterranean conditions, most of the uncertainty was related to the partition of energy between soil and vegetation, shown by the highest sensitivity to the two coefficients of extinction of radiation: k_{PAR} (50%) involved in LAI estimates, and k_{Rn} (20%) both contributing to estimate the net radiation reaching the soil component. This is similar to the situation during the senescent phase in the Sahel. Seasonally, the relative importance of each variable was similar to the annual pattern, except in January when modeled LE was more sensitive to accuracy in Rn .

Figure 3 shows how in both ecosystem types, mean effect and total effect (that considers interactions) on evapotranspiration were very similar with differences around 1-2%, indicating low effect of variable interactions.

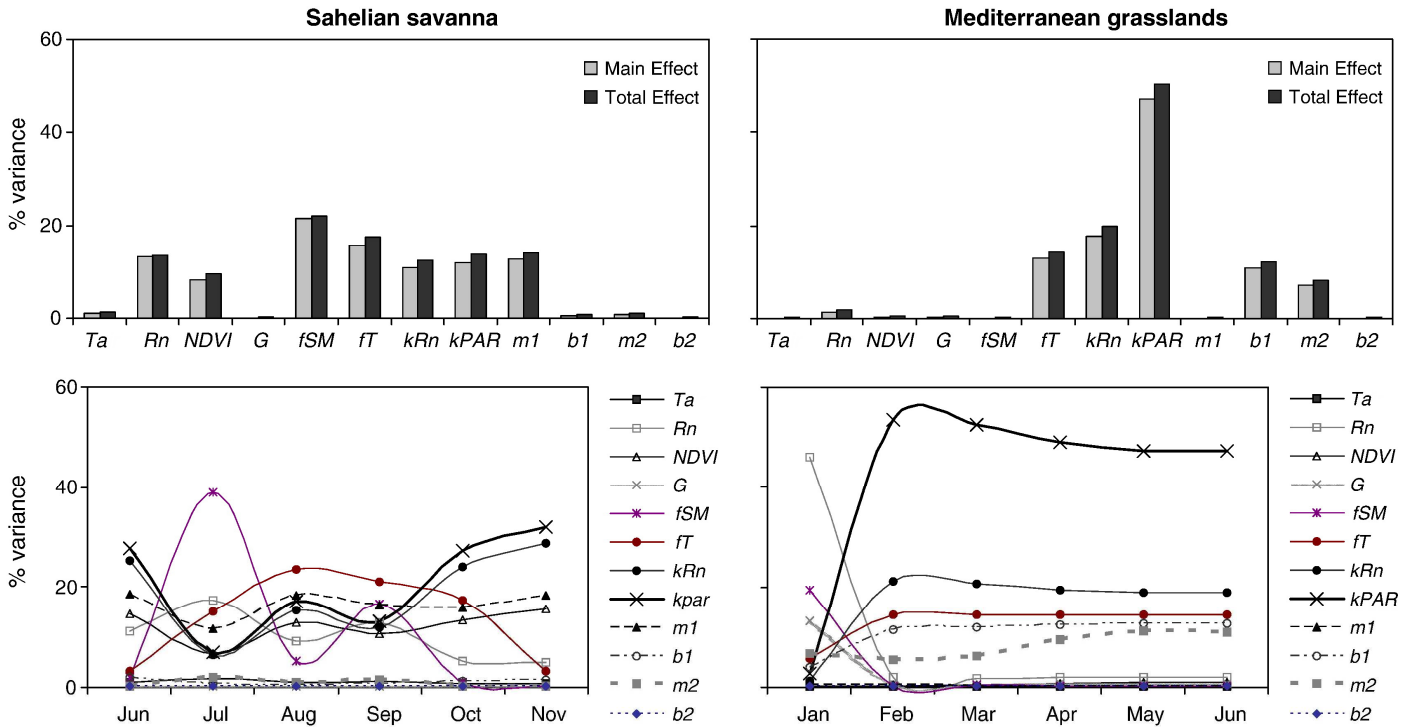


Figure 3. Upper panels: sensitivity of modeled evapotranspiration according to mean annual conditions (% percentage of explained variance). Main effect is the variance explained without considering interactions among variables and total effect considering interactions. Lower panels: sensitivity of modeled evapotranspiration considering monthly conditions in the Sahelian savanna and Mediterranean grasslands (total effect). Uncertainty levels were set as $\pm 10\%$ of the mean for input variables $NDVI$, T_a , R_n , and G and of $\pm 25\%$ of the mean for the soil moisture (f_{SM}) and plant temperature (f_T) constraints. For constant model parameters: $m1$, $b1$, $m2$, $b2$, kRn , and $kPAR$, the range of uncertainty was based on values used in the literature.

Evaluation of the PT-JPL-daily evapotranspiration model with Eddy Covariance data

Soil Moisture Constraint from Measured Soil Moisture (f_{SM-SWC})

In the Sahelian savanna the performance of PT-JPL-daily LE model using measured SWC (f_{SM-SWC}) was similar regardless of the f_{APAR} and LAI estimate used (FD_{aSWC} or FD_{bSWC}) ($R^2=0.85-0.86$ and $MAE=14.14-13.54$) (Table 5 and Fig. 4a and 4b). In the Mediterranean grasslands, both the coefficient of determination and errors were also similar regardless of the f_{APAR} and LAI used ($R^2=0.75-0.74$; $MAE=10.66-11.44$) (Table 5 and Fig. 5a and 5b). Therefore, PT-JPL-daily formulation is capable to reproduce the dynamics of LE in the Mediterranean grasslands, as it explained 75% of the LE variance. Considering that the uncertainty of the energy balance closure from Eddy Covariance data in this Mediterranean site, calculated at daily time scale, represents 21.7% of the available energy (R_n-G), the accuracy obtained with PT-JPL-daily using f_{SM-SWC} is closest to the one from Eddy Covariance. In the Sahel, the model explains up to 86% of the variance, which considering that the closure error is 5.78% of the available energy at daily scale is also close to the instrumental accuracy. However, in this site during the growing season there

was a systematic underestimate of LE during the period of maximum growth followed by an overestimate, independently of the f_{APAR} and LAI used (Fig. 4a and 4b).

Table 5: Evaluation of PT-JPL-daily LE with Eddy Covariance data. In the savanna the results have been evaluated between June and December 2007 and in the Mediterranean grasslands between January and June 2011. Model versions starting with “FDa” were run with $f_{APAR-NDVI}$ and LAI_{NDVI} and with “FDb” with $f_{APAR-MODIS}$ and LAI_{MODIS} . f_{SM-SWC} is the soil moisture constraint derived from measured volumetric Soil Water Content, and f_{SM-ATI} from Apparent Thermal Inertia. Surface temperature and albedo could be acquired from in-situ sensors or from satellite (MSG) sensors.

Site	f_{SM}	Model version	R^2	MAE ^a	bias ^b	RMSE ^c	MAPD (%) ^d
Sahelian savanna (all dates)	in -situ	FDa _{SWC}	0.85	14.14	7.59	21.45	22.69
		FDb _{SWC}	0.86	13.54	4.02	20.39	21.72
		FDa _{ATI-in-situ}	0.82	20.69	-1.48	23.88	33.20
		FDb _{ATI-in-situ}	0.83	19.72	-7.14	23.10	31.65
	satellite	FDa _{ATI-MSG}	0.79	23.11	16.52	30.55	37.09
		FDb _{ATI-MSG}	0.80	20.21	11.78	26.53	32.43
Mediterranean grasslands (growing season)	in -situ	FDa _{SWC}	0.75	10.66	10.10	12.43	30.89
		FDb _{SWC}	0.74	11.44	10.96	13.2	33.16
		FDa _{ATI-in-situ}	0.58	9.66	5.70	11.10	28.01
		FDb _{ATI-in-situ}	0.57	9.85	6.21	11.58	28.57
	satellite	FDa _{ATI-MSG}	0.32	10.16	-3.01	14.48	29.46
		FDb _{ATI-MSG}	0.31	10.78	-3.80	15.03	31.26

^a Mean absolute difference $MAE = (\sum_{i=1}^n |O_i - P_i|) / n$

^b bias $bias = (\sum_{i=1}^n (O_i - P_i)) / n$

^c Root mean square error $RMSE = [(\sum_{i=1}^n (O_i - P_i)^2 / n)]^{1/2}$

^d Mean absolute percentage difference $MAPE = \frac{100}{\langle O \rangle} (\sum_{i=1}^n |O_i - P_i| / n)$, where P_i is the model-predicted value, O_i

is the observed value, $\langle O \rangle$ is the mean observed value, n is the number of observations.

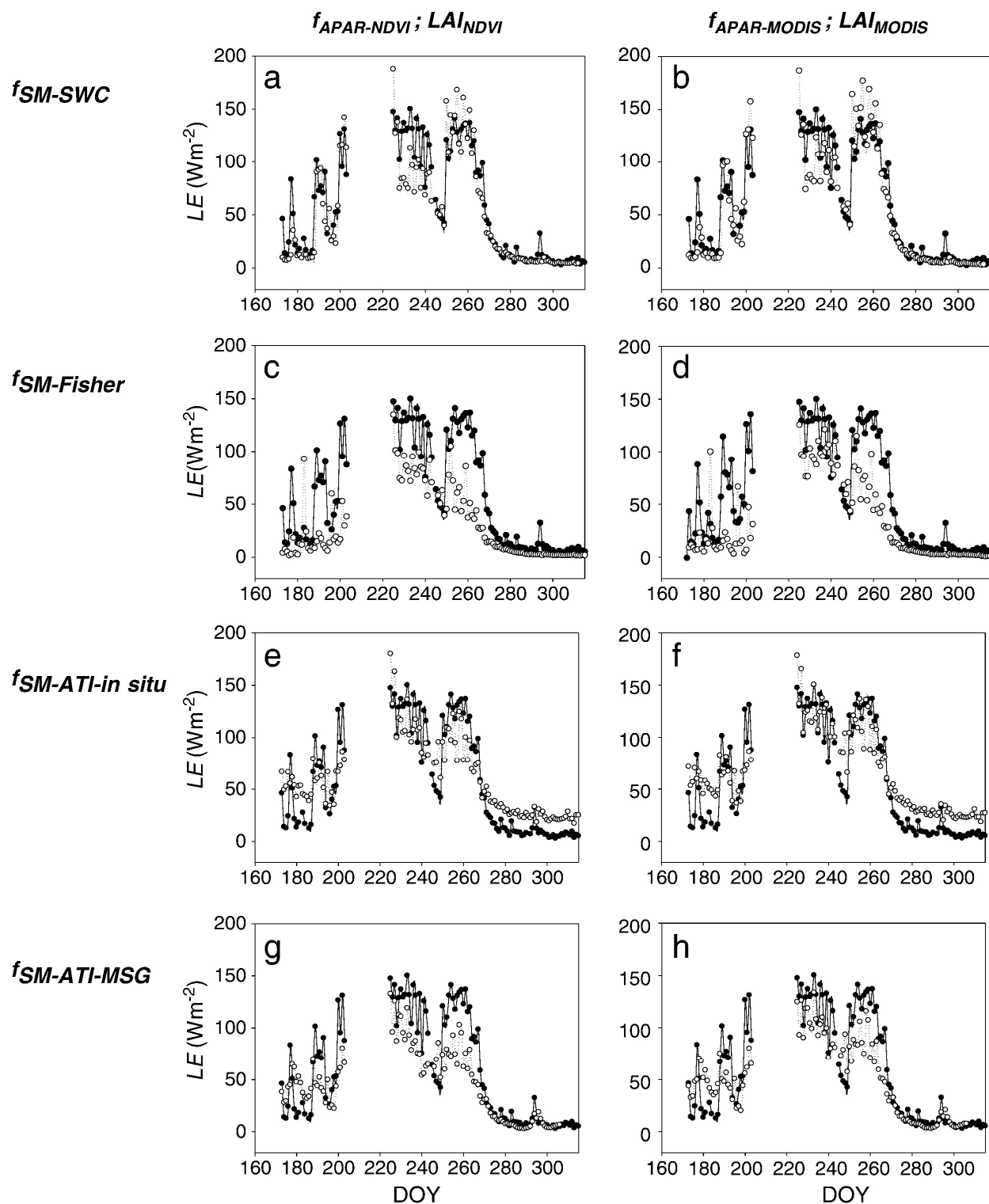


Figure 4. Daily LE (Wm^{-2}) in the Sahelian savanna (Agoufou, Mali) from Eddy Covariance data (black dots) and modeled (white dots) during 2007. In the first column (figures a, c, e, g) the model was run using $f_{APAR-NDVI}$ and LAI_{NDVI} and in the second column (figures b, d, f, h) using $f_{APAR-MODIS}$ and LAI_{MODIS} . In each of the six rows, the model was run a different soil moisture constraint: f_{SM-SWC} from measured volumetric soil water content (figures a, b), $f_{SM-Fisher}$ from atmospheric water deficit (figures c, d), $f_{SM-ATI-in-situ}$ from apparent thermal inertia from in-situ measurements (figures e, f), $f_{SM-ATI-MSG}$ from apparent thermal inertia from MSG-SEVIRI measurements (figures g, h).

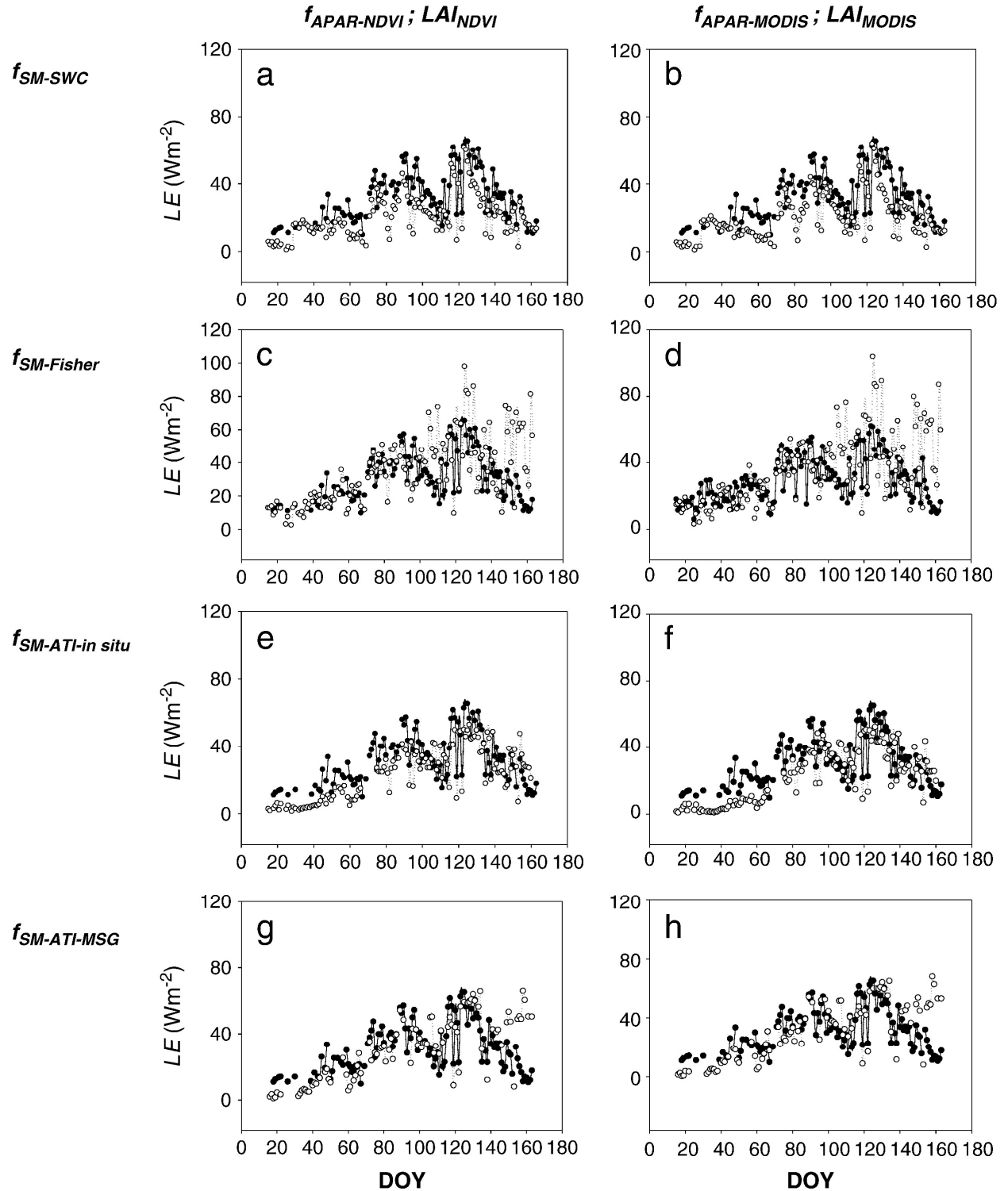


Figure 5. Daily LE (Wm^{-2}) in the Mediterranean grassland (Balsa Blanca, Spain) from Eddy Covariance data (black dots) and modeled (white dots) during 2007. In the first column (figures a, c, e, g) the model was run using $f_{APAR-NDVI}$ and LAI_{NDVI} and in the second column (figures b, d, f, h) using $f_{APAR-MODIS}$ and LAI_{MODIS} . In each of the six rows, the model was run a different soil moisture constraint: f_{SM-SWC} from measured volumetric soil water content (figures a, b), $f_{SM-Fisher}$ from atmospheric water deficit (figures c, d), $f_{SM-ATI-in-situ}$ from apparent thermal inertia from in-situ measurements (figures e, f), $f_{SM-ATI-MSG}$ from apparent thermal inertia from MSG-SEVIRI measurements (figures g, h).

To assess whether this mismatch in the Sahelian site could be related to the LAI and f_{PAR} estimates, we compared satellite LAI estimates with field estimates and also evaluated the evapotranspiration model ran with field estimates for LAI and f_{PAR} . Comparison of LAI satellite products with field estimates (Fig. 6a) showed better correlations with MODIS LAI ($R^2=0.93$) than for LAI estimated from NDVI ($R^2=0.71$). Although MODIS LAI underestimated the maximum peak and overestimated LAI during growing and senescence stages its phenology pattern matched better with the field data than the LAI derived from NDVI (Fig. 6a). In this case, the maximum LAI happened earlier in the season than the field maximum LAI , showing also greater overestimates during growing and senescent phases. This could explain a slightly better performance of the LE model using MODIS products during the growing season (Table 6).

However, model outputs ran using field measured LAI , fc and f_{APAR} (estimated as described in Mougouin et al. 2009) did not improve model performance (see Table 6). Therefore, using satellite products for vegetation (LAI and f_{PAR}) to run the model produce similar results than using field vegetation estimates.

Table 6: Comparison of model performance during the period of field sampling (DOY: 184-269) in the Sahelian savanna (Agoufou). Note that the period used is slightly shorter than for Table 4, and explains why the model statistics for FDa_{SWC} and FDb_{SWC} differ slightly from Model 4 statistics.

f_{APAR} LAI	Model version	R^2	MAE ^a	bias ^b	RMSE ^c
$f_{APAR-NDVI}$, LAI_{NDVI}	FDa_{SWC}	0.67	20.53	9.50	26.29
$f_{APAR-MODIS}$, LAI_{MODIS}	FDb_{SWC}	0.69	19.66	3.13	24.97
$f_{APAR-field}$, LAI_{field}	$FD_{field-SWC}$ ($k_{Rn}=0.60$)	0.68	21.39	11.26	26.10
$f_{APAR-field}$, LAI_{field}	$FD_{field-SWC}$ ($k_{Rn}=0.75$)	0.76	19.23	9.31	20.96

^a Mean absolute difference $MAE = (\sum_{i=1}^n |O_i - P_i|) / n$

^b bias $bias = (\sum_{i=1}^n (O_i - P_i)) / n$

^c Root mean square error $RMSE = [(\sum_{i=1}^n (O_i - P_i)^2) / n]^{1/2}$

where P_i is the model-predicted value, O_i is the observed value, $\langle O \rangle$ is the mean observed value, n is the number of observations.

It seems that when vegetation is changing very rapidly around the seasonal peak in the Sahel, the model can account for the general pattern of LE but not for minor ups and downs observed in the Eddy Covariance LE . Increasing the energy partition allocated to vegetation by using k_{Rn} of 0.75, a value obtained by optimization at the site (Ridler et al. 2012), improved significantly the results ($R^2=0.76$ vs. $R^2=0.68$) (Table 6). Using this coefficient reduced the LE offset after the LAI peak, but not before (Fig. 6b). It should be noted that field LAI estimates (Fig. 7) present uncertainty as well, as they were interpolated between the field samplings, acquired every ≈ 10 days. Thus, before the maximum LAI peak (DOY=235) the previous field sampling was 10 days earlier, making it possible to miss a higher and earlier maximum peak. In

that case, LAI underestimates would produce LE underestimates between the period DOY225 and DOY235 (Fig. 6).

These results suggest that the model could benefit from an improved energy partitioning between soil and canopy considering variable extinction coefficients and separate long-wave and short-wave components (Kustas and Norman 1999), as well as from shorter-time scale estimates of LAI and f_{PAR} .

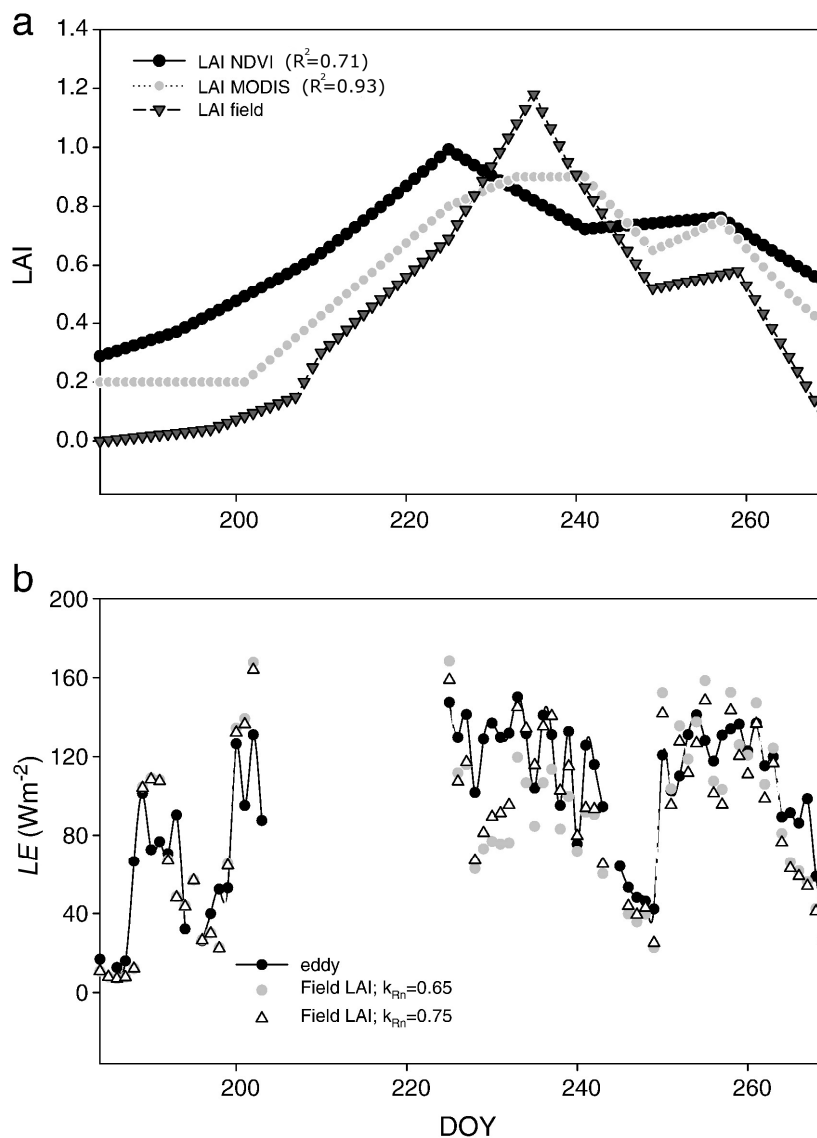


Figure 6. a) Comparison of LAI estimated from $NDVI$ (LAI_{NDVI}), LAI from MODIS, and LAI from field estimates during the growing season of 2007 in the Sahelian savanna. b) Daily LE (Wm^{-2}) from Eddy Covariance data (black dots) and modeled using LAI from field estimates and $k_{Rn}=0.65$ (grey dots) and $k_{Rn}=0.75$ (Triangles). R^2 refers to the coefficient of determination comparing with LAI from field estimates.

Soil Moisture Constraint from Atmospheric Variables ($f_{SM-Fisher}$)

Estimating LE using $f_{SM-Fisher}$ with the same parameterization as in Fisher et al. (2008) ($\beta=1$; midday conditions) did not provide meaningful results in the Mediterranean grasslands ($R^2\sim 0.16$) (Table 7). In the savanna, correlations were better but well below those found for f_{SM-SWC} ($R^2=0.61-0.62$) and with high biases around $25-29 \text{ W m}^{-2}$ (Table 4, Fig. 5 and 6). This constraint diagnosed the major water stress during the growing season around DOYs 240-250. We evaluated the sensitivity of $f_{SM-Fisher}$ to β values between 0.05 to 2, and to the use of daily average or midday conditions for RH and VPD . Table 7 shows the results when the model was run with two different values of β . They are shown in the table as they provided the best results in each site: $\beta=0.1 \text{ kPa}$, that was applied at a global scale in Mu et al. (2007), and $\beta=1 \text{ kPa}$ applied in Fisher et al. (2008)

In the savanna, the best results corresponded to $\beta=1 \text{ kPa}$ and daily average conditions ($R^2=0.80$; $MAE=18.08 \text{ W m}^{-2}$). In the Mediterranean grasslands PT-JPL-daily performed better using $\beta=0.1$ (Table 7), especially for midday conditions ($R^2=0.64-0.53$) although LE was systematically underestimated (biases $\approx 15-17 \text{ W m}^{-2}$). These results suggest a stronger control of atmospheric conditions on soil moisture changes in the Mediterranean conditions than in the Sahel. Therefore, parameterization using $f_{SM-Fisher}$ should be tuned according to the conditions in each site for successful results.

Table 7: Evaluation of PT-JPL-daily LE with Eddy Covariance data for different parameterizations of the soil moisture constraint derived from atmospheric water deficit: $f_{SM-Fisher} = RH^{VPD/\beta}$. Results are shown for midday and daily average conditions for RH (relative humidity) and VPD (Vapor Pressure Deficit) and for $\beta=0.1$ kPa and $\beta=1$ kPa. Results from the best performing combination of parameters in each site are shown in bold font. In the savanna results were evaluated between June and December 2007 and in the Mediterranean grasslands from January to June 2011. Model versions starting with “FDa” were run with $f_{APAR-NDVI}$ and LAI_{NDVI} and with “FDb” with $f_{APAR-MODIS}$ and LAI_{MODIS} .

Site	period	conditions	β (kPa)	Model version	R^2	MAE	bias	RMSE	MAPE (%)
Savanna (Agoufou)	All dates	daily	1	FDa _{Fisher}	0.69	26.09	14.87	32.81	41.87
				FDb _{Fisher}	0.80	18.08	8.47	24.35	29.01
			0.1	FDa _{Fisher}	0.71	20.49	41.13	53.18	32.88
				FDb _{Fisher}	0.66	23.60	37.92	49.94	37.87
		midday	1	FDa _{Fisher}	0.62	32.19	29.27	43.05	51.65
				FDb _{Fisher}	0.61	35.72	25.62	40.61	57.32
			0.1	FDa _{Fisher}	0.68	18.65	43.04	56.21	29.93
				FDb _{Fisher}	0.65	21.86	39.71	52.45	35.09
Mediterranean grasslands (Balsa Blanca)	growing season	daily	1	FDa _{Fisher}	0.16	15.08	-6.68	19.40	43.73
				FDb _{Fisher}	0.17	28.25	-	34.44	81.89
			0.1	FDa _{Fisher}	0.36	21.22	8.49	14.74	66.67
				FDb _{Fisher}	0.27	20.40	9.49	16.24	64.10
		midday	1	FDa _{Fisher}	0.16	35.03	-7.02	20.48	110.05
				FDb _{Fisher}	0.13	36.24	-8.23	21.92	113.87
			0.1	FDa _{Fisher}	0.64	14.42	15.61	18.23	45.30
				FDb _{Fisher}	0.53	12.24	17.92	20.66	38.44

Soil Moisture Constraint from Apparent Thermal Inertia (f_{SM-ATI})

Using in-situ data, model performance in the savanna for the thermal inertia index f_{SM-ATI} was practically equivalent to that using SWC (f_{SM-SWC}), with $R^2 \approx 0.82$ and slightly higher errors but similar or lower biases (Table 5). Non significant differences were found when using f_{APAR} and LAI from MODIS or a linear function of $NDVI$ except from a slightly lower bias with the latter. At the end of the rainy season (DOY 270), f_{SM-ATI} overestimated LE as even at an entirely dry soil the ATI index will never become zero, since that would require an infinite temperature amplitude (Van doninck et al. 2011).

In the Mediterranean grasslands, statistics from model performance using f_{SM-ATI} from in-situ data were again not as good as than in the savanna. Although the R^2 using f_{SM-ATI} was lower than those obtained with f_{SM-SWC} , the errors decreased and the biases were half of those obtained with f_{SM-SWC} . Similar to the savanna site, results were quite similar independently of the LAI and f_{PAR} estimate used to run the model.

When running the model using satellite MSG instead of in-situ data for f_{SM-ATI} , good results were obtained in the savanna site in terms of $R^2 \sim 0.80$ and $MAE=23.1-20.1 \text{ W m}^{-2}$ (Table 5) but

higher biases were detected due to LE underestimates during the growing season (Fig. 4g, 4h). This was due to the fact that the diurnal T_R difference ($T_{R-DMax}-T_{R-Dmin}$) was always higher for MSG than for in-situ data (Fig. 7), producing lower soil moisture (f_{SM}) values.

In the Mediterranean grasslands, using MSG data instead of in-situ to estimate f_{SM-ATI} produced a greater loss of accuracy in R^2 than in the savanna although errors were similar and biases even lower than with in-situ data (Table 5). On one hand, results using in-situ data were worse to start with than in the savanna with correlations around $R^2=0.58$. As in the Mediterranean site LE is lower (Fig. 2) the model is less tolerant to different error sources. Besides the noise apparent in the MSG time-series, the comparability of the diurnal temperature difference ($T_{R-DMax}-T_{R-Dmin}$) between in-situ and MSG data was more problematic than in the savanna, with systematically higher MSG values (Fig. 7). Additional inspection of T_R (15 minute) observations between field and satellite (Fig. 8) showed that differences between in-situ and satellite were larger in the grasslands (MAE=2.43 °C) than in the savanna (MAE=1.56 °C). In the Mediterranean site the sensor viewing angle is 42.68° while in the Sahel it is only 18.01°. This results in a larger scale mismatch at the Mediterranean site between the satellite pixel and the footprint of the in-situ sensors as well as greater atmospheric effects due to a larger atmospheric path radiance.

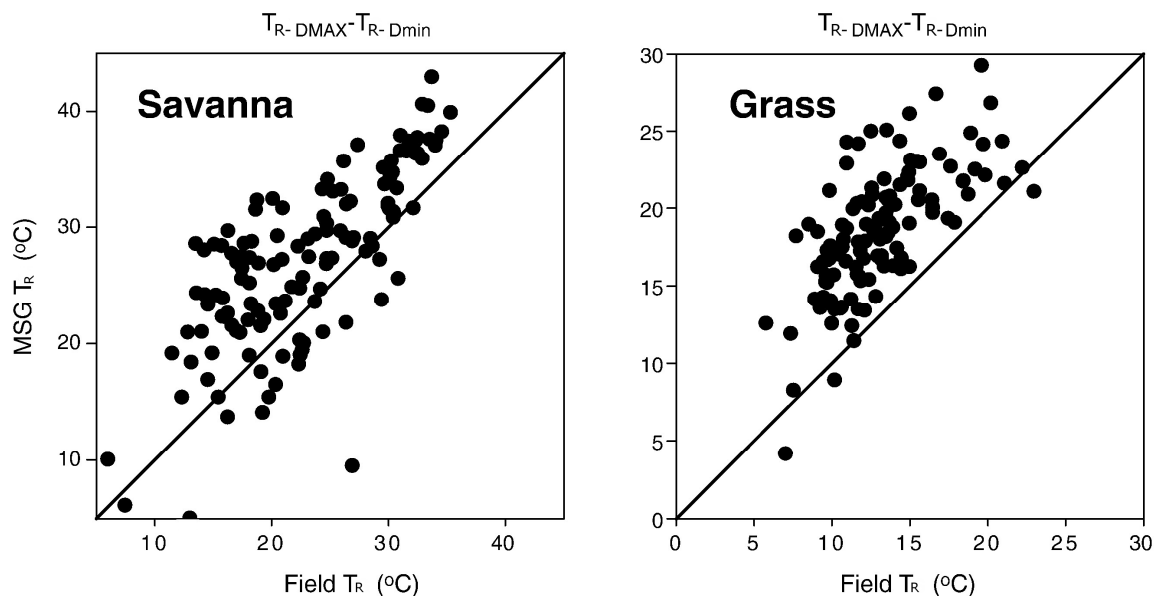


Figure 7: Comparison of the diurnal surface temperature difference ($T_{R-DMAX}-T_{R-Dmin}$) from field (Apogee) and satellite (MSG-SEVIRI) sensors in the savanna and in the Mediterranean grassland.

The f_{SM-ATI} approach is very sensitive to uncertainty in thermal data since day and night T_R are used in the denominator (Cai et al. 2007; Sobrino et al. 1998; Verstraeten et al. 2006b). Sensitivity to errors is greater when Rn is higher which occurs at the end of the study period in the Mediterranean site and the middle of the season in the Sahelian site (Guichard et al. 2009) (see Fig. 4g 4h and 5g 5h). In fact, in the Mediterranean grasslands, the lack of fit for f_{SM-ATI} MSG ($R^2 = 0.32-0.31$) was caused by the last 10 days of the study period (see Fig. 5g and 5h). Another important limitation of the ATI methodology is the vulnerability to noise introduced by meteorological conditions (Van doninck et al. 2011). Although we have compared only dates without clouds according to LSA SAF Quality Flags, inspection of SEVIRI images revealed a large cumulus cloud affecting the adjacent pixel of the Mediterranean grasslands location unreported in the Quality Flags during the last 10 days of the period. When excluding those days R^2 increased to 0.64-0.66.

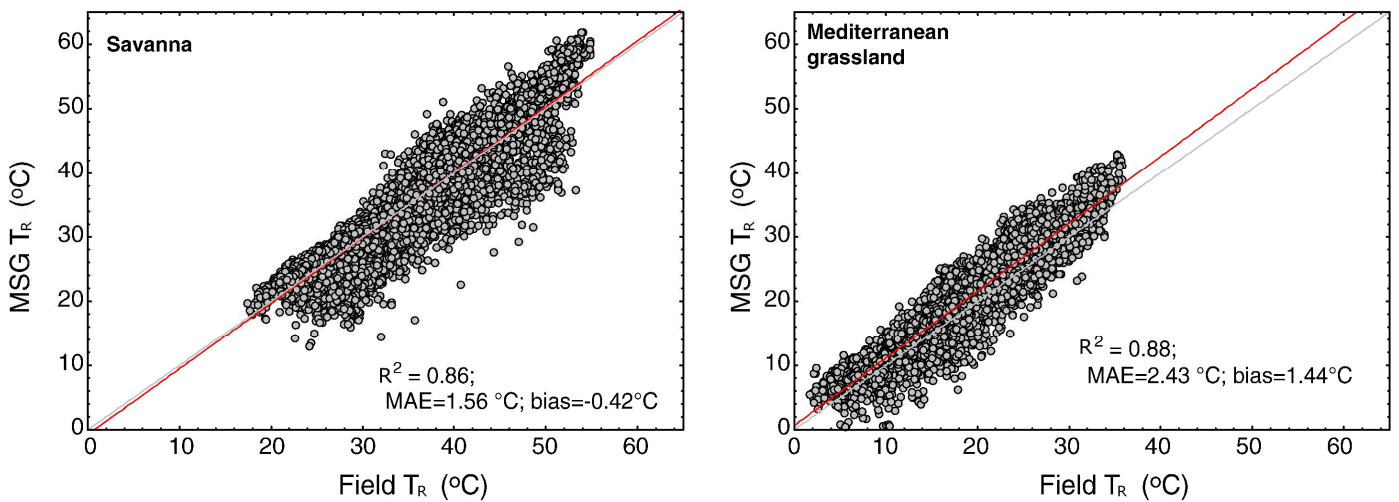


Figure 8: Comparison of 15 minute observations of radiometric surface temperature from field (Apogee) and satellite (MSG-SEVIRI) sensors in the savanna and in the Mediterranean grassland during the study period.

Comparison with other Evapotranspiration Models in Global Dryland Ecosystems

In the Sahelian savanna site, a Soil-Vegetation-Atmosphere Transfer (SVAT) model forced with some of the same in-situ climatic inputs and vegetation parameters was calibrated using multi-objective functions during the 2007 growing season (Ridler et al. 2012).

Calibration of the SVAT model with in-situ T_R and SWC showed better results ($R^2=0.81$) (Table 8) than PT-JPL-daily during the growing season calibrated with field data when correlations were around $R^2=0.67-0.65$ (see Table 6). Nonetheless, daily errors were similar in magnitude and in fact underestimates were higher (bias= 12.26 W m^{-2} , not shown) than with PT-JPL-daily (Table 6). These results are reasonable as the SVAT model, based on the two-source (Shuttleworth and Wallace 1985) model coupled to a hydrological model, has a stronger physical basis (Overgaard 2005). It requires several plant and soil parameters such as root depth, minimum stomatal conductance, soil hydraulic conductivity, as well as atmospheric variables including rainfall, wind speed, and relative humidity at 15-minute time scale. However, calibration of the SVAT model with both MSG and AMSR-E (Advanced Microwave Scanning Radiometer) satellite data for operational purposes decreased correlations to $R^2=0.63$ equivalent to PT-JPL-daily results during the growing season (Table 8 and Table 6). Results from a simpler modeling approach based on the triangle relationship (Stisen et al. 2008), estimated LE in the Sahel in a site with higher rainfall (487 mm in 2005) with similar error levels to our Agoufou site and also underestimates: RMSE= 31.00 W m^{-2} . Correlations were higher ($R^2=0.75$) than in our model. Sun et al. (2011) model results based on a water-deficit index in an open savanna in Sudan using a combination of MODIS and SEVIRI products, produced similar results than PT-JPL-daily run with satellite products ($R^2=0.73$ and MAE= 26 W m^{-2}) considering the fact that they acquired T_a from ECMWF weather forecasts product and we used in-situ T_a . In this case, the peak LE was also underestimated. Although the model captures LE changes at the beginning of the season, it seems that the transpiration processes in conditions of the Sahel are difficult to reproduce during the period of plant growth as different studies underestimate LE during the growing season independently of model complexity (Ridler et al. 2012). For instance, in the semiarid savanna in Niger, the SVAT model *SEt_HyS-savanna* that presents an additional tree-layer, systematically underestimated peak LE despite of added model complexity and a high degree of parameterization (Saux-Picart et al. 2009) ($R^2=0.66-0.64$, their results have not included in Table 7 as they represent 30 minute and not daily estimates).

Compared to other models using remote sensing information in the same Mediterranean grasslands site, PT-JPL-daily performed better. For instance, LE estimates using f_{SM-SWC} were

more accurate ($R^2=0.75$; MAE $\sim 10 \text{ W m}^{-2}$) than those from a Penman-Monteith model adapted by Leuning et al. (2008) (hereinafter PML). In the PML the soil evaporation fraction was estimated with measured *SWC*, similarly to f_{SM-SWC} (Capítulo 3) (Table 8). In addition, the PML required optimization with field-measured *LE* and meteorological variables such as *VPD*, or estimation of aerodynamic and surface conductances. Two more operational parameterizations of PML for the soil evaporation fraction based on measured rainfall produced also poorer results for PML at the same site (Table 8) (Capítulo 3), with similar results to PT-JPL-daily run with satellite MSG data for f_{SM-ATI} , and poorer than PT-JPL-daily run with f_{SM-ATI} in-situ ($R^2 \approx 0.58$, MAE $\approx 10 \text{ W m}^{-2}$).

PT-JPL-daily *LE* estimates using MSG data for f_{SM} provided also better correlations than a triangle approach run with MODIS T_R and *NDVI* ($R^2=0.24$) despite of lower errors (MAE= 3.56 W m^{-2}) (Garcia et al. in review). *LE* estimates from the more physically based two source model (TSM) (Norman et al. 1995) run with in-situ T_R from exactly the same dataset and aggregated at daily-time scale (applying the Bowen ratio to ensure the energy closure for EC measurements) were also less accurate ($R^2 = 0.34-0.31$) than PT-JPL-daily run with in-situ or MSG T_R results (Capítulo 1) (Table 8). TSM results using separate measurements of soil and vegetation T_R instead of an aggregated measure did not improved the results (Capítulo 1).

Finally, to place the results from PT-JPL-daily ran with *ATI* in the context of global drylands, we compared them with studies using Penman-Monteith remote sensing (PM) or Priestley-Taylor (PT) models over savannas and grasslands at dryland sites from different regions of the globe (Table 8). These comparisons should always be considered with caution as each model uses different input data sources and both the environmental conditions and the vegetation change. However, we have focused on the less accurate PT-JPL-daily algorithm, amenable for regionalization (FDa_{ATI-MSG}) ran with satellite MSG and MODIS data both for vegetation and soil moisture constraints, leaving T_a and available energy as the only field input variables used.

Table 8: Statistics from actual evapotranspiration models using remote sensing data over dryland savanna and grassland sites. Climate classification is based on Köppen-Geiger (Kottek et al. 2006) where BWh: Arid/desert/hot air; BSk: cold/semiarid, Aw: Equatorial/desert; Csb: warm temperate/summer dry/warm summer; Cfb: Warm temperate/fully humid/warm summer; Csa: Warm temperate/summer dry/hot summer. A brief description of model type is included. When errors were reported in mm day⁻¹ they have been converted into W m⁻². Statistics in parenthesis refer to the model type explanations in parenthesis

Ecosystem type	Site	Country	Lat ° Lon°	Climate type	Model type	R ²	MAE	RMSE	Reference
Open woody savanna	Sahel (Agoufou)	Mali	15.34, -1.48	BWh	PT-JPL-daily f_{SM-ATI} satellite (in-situ)	0.80 (0.83)	20.21 (19.72)	26.53 (23.10)	This study
Open woody savanna	Sahel (Agoufou)	Mali	15.34, -1.48	BWh	SVAT in-situ calibration	0.81	16.57	9.90	Ridler et al. (2012)*
Open woody savanna	Sahel (Agoufou)	Mali	15.34, -1.48	BWh	SVAT satellite calibration	0.63	39.24	46.66	Ridler et al. (2012)*
Open woody savanna	Sahel (Dahra)	Senegal	15.41 -15.47	BWh	Triangle using SEVIRI/MODIS	0.75	-	31.00	Stisen et al. (2008)
Open woody savanna	Sahel (SD-DEM)	Sudan	13.28 -0.48	BWh	Sim-ReSET using SEVIRI/MODIS	0.73	26.00	-	Sun et al. (2011)
Open woody savanna	Virginia Park	Australia	146.55	Aw	PM- in- situ meteorological	0.23	-	112.1	Cleugh et al. (2007)
Open woody savanna	Virginia Park	Australia	-19.88 146.55	Aw	PML-optimized with hydrol. model	0.49	-	15.94	Zhang et al. (2010)
Savanna	Howard Springs	Australia	-12.50° 131.15	Aw	PML-optimized with hydro. model	0.53	-	32.18	(Zhang et al. 2010)
Woody savanna	AZ - Flagstaff - Wildfire	USA	35.40 -111.80	Csb	MOD16. PM new version (old version)	0.06 (0.42)	-	23.92 (18.51)	Mu et al. (2011)
Woody savanna	TX -Freeman Ranch Mesquite	USA	29.9 -98.0	Cfa	MOD16. PM new version (old version)	0.48 (0.52)	-	25.91 (30.76)	Mu et al. (2011)
Mediterranean savanna	CA - Tonzi Ranch	USA	38.4 -121.0	Csa	MOD16. PM new version (old version)	0.61 (0.53)	-	19.08 (21.36)	Mu et al. (2011)
Mediterranean savanna	CA - Tonzi Ranch	USA	38.4 -121.0	Csa	PM (field eddy calibration)	0.57	-	30.19	Yuan et al. (2010)
Mediterranean savanna	CA - Tonzi Ranch	USA	38.4	Csa	PT-JPL-daily	0.74 (Kendall)	-	19.39	Vinukollu et al. (2011)
Mediterranean grasslands	Balsa Blanca	Spain	36.94 -2.03	BSk	PT-JPL-daily f_{SM-ATI} satellite (in-situ)	0.31 (0.57)	10.78 (11.44)	15.03 (10.96)	This study
Mediterranean grasslands	Balsa Blanca	Spain	36.94 -2.03	BSk	PML-input SWC	0.54	13.03	-	Capítulo 3
Mediterranean grasslands	Balsa Blanca	Spain	36.94 -2.03	BSk	PML -input rainfall (two methods)	0.32-0.47	13.88-9.92	-	Capítulo 3
Mediterranean grasslands	Balsa Blanca	Spain	36.94 -2.03	BSk	Triangle using MODIS	0.24	3.56	-	Garcia et al. (in rev.)
Mediterranean grasslands	Balsa Blanca	Spain	36.94 -2.03	BSk	TSM with T_s composite in parallel (series)	0.34 (0.31)	39.05 (53.82)	43.89 (58.52)	Capítulo 1*
Mediterranean grasslands	Balsa Blanca	Spain	36.94 -2.03	BSk	TSM with T_s soil, T_s canopy in parallel (series)	0.14 (0.25)	44.86 (57.67)	51.00 (62.50)	Capítulo 1*
Arid steppe grasslands	AZ - Audubon Research Ranch	USA	31.6 -110.5	BSk	MOD16. PM new version (old version)	0.22 (0.48)	-	23.07 (23.07)	Mu et al. (2011)
Arid steppe grasslands	AZ - Audubon Research Ranch	USA	31.6 -110.5	BSk	PT-JPL-daily	0.37 (Kendal)	-	18.75	Vinukollu et al. (2011)
Arid steppe grasslands	AZ - Walnut Gulch Kendall Grasslands	USA	31.7 -109.9	BSk	MOD16. PM new version (old version)	0.07 (0.25)	-	19.36 (18.51)	Mu et al. (2011)
Mediterranean grassland	CA- Vairaranch	USA	38.40 -120.9	Csa	PM (field eddy calibration)	0.51	-	-4.56	Yuan et al. (2010)

*30 minute model outputs provided by the authors have been aggregated to daily time scale, applying the Bowen ratio method for ensure the energy closure of EC derived fluxes, in this work to compare with the rest of the models.

It can be seen in Table 8 that PT-JPL-daily $FD_{a_{ATI-MSG}}$ in the Sahelian savanna ($R^2=0.80$; $RMSE=26.53 \text{ W m}^{-2}$) performed better in general than PM models at other savanna sites although it has to be considered that not all these models were forced with local meteorological inputs (Table 8). Thus, the PML improved algorithm from Zhang et al. (2010) where maximum stomatal conductance is optimized with a hydro-meteorological model, showed lower R^2 at two Australian savannas ($R^2= 0.53$ and 0.49) less arid than our site (with 1764 mm and 526 mm of annual rainfall respectively) with the PT-JPL-daily error within the range of those two sites (Table 8). Results from a PM model in one of the Australian savannas forced with in-situ meteorological inputs were also poorer than our results ($R^2=0.23$) (Cleugh et al. 2007). Our algorithm performed also better than the MODIS product for evapotranspiration (MOD16) of Mu et al. (2011), in three woody savannas in arid regions of the USA (with R^2 ranging from 0.06-0.61). Again, PT-JPL-daily errors were within Mu et al. (2011) ranges of error at those savanna sites ($RMSE = 18.51\text{-}30.6 \text{ W m}^{-2}$). In another global study (Yuan et al. 2010) used a PM approach optimized with Eddy Covariance LE from 21 sites. Their model in the Mediterranean savanna of Tonzi performed worse (Table 8) than PT-JPL-daily using $f_{SM-ATI-MSG}$ in the Sahelian savannah although it should be noted that they used air temperature from reanalysis. In the same savanna of Tonzi ranch, Vinukollu et al. (2011) applied a daily version of the PT-JPL model with the soil moisture constraint based on the water vapor deficit although the error was low ($RMSE=18.75 \text{ W m}^{-2}$) the non-parametric Kendall's Tau (equivalent to Pearson-correlation coefficient) was 0.74 using only satellite input data.

Regarding the Mediterranean grassland site, our model LE results using satellite data for soil moisture and vegetation ($FD_{a_{ATI-MSG}}$) ($R^2=0.32$; $RMSE=15.03 \text{ W m}^{-2}$) were in the range of the MOD16 algorithm of Mu et al. (2011) for two arid steppe grasslands in the USA with $R^2=0.48$ (Audubon) and 0.25 (Walnut Gulch) respectively with the old algorithm version and $R^2=0.05$ and 0.49 with the new version. Our PT-JPL-daily model errors were lower than Mu et al. (2011); $RMSE=22.95$ and 18.42 W m^{-2} with the old algorithm and $RMSE=22.95$ and 19.26 W m^{-2} with the new algorithm. In Audubon steppe the PT-JPL-daily model of Vinukollu et al. (2011) was not very successful in capturing the temporal dynamics (Kendall's Tau = 0.37) but showed still a better performance than Mu et al. (2011) algorithm ran during the same time (not shown in Table 8). Results from Yuan et al. (2010) PM model calibrated with field data at another Mediterranean grassland (Vairaranch) were better than our model results $R^2=0.51$ and $bias=0.16 \text{ W m}^{-2}$.

CONCLUSIONS

The Priestley Taylor-Jet Propulsion Laboratory (PT-JPL) evapotranspiration LE model, developed by Fisher et al. (2008) is based on the Priestley-Taylor equation downscaled according to multiple stresses. The PT-JPL is attractive for its simplicity and potential for regionalization using satellite data. In this study, a daily version of the model was evaluated in some of the most extreme conditions from the point of water availability: an open woody savanna in the Sahel and a Mediterranean grassland, both with annual rainfall below 400 mm. A new approach was tested with in-situ and satellite data using a soil moisture constraint based on the Apparent Thermal Inertia concept (f_{SM-ATI}) relying on remotely sensed observations of surface temperature and albedo.

When using field measured soil water content (SWC) to estimate the soil moisture constraint, the daily PT-JPL model reproduced the LE dynamics measured from Eddy Covariance systems within the uncertainty levels of the closure error system. When using the Apparent Thermal Inertia index f_{SM-ATI} at the Sahelian savanna, results with in-situ data were equivalent to those obtained using field measured SWC . When up-scaling the f_{SM-ATI} to MSG-SEVIRI satellite data, a satisfactory agreement with field data was also found ($R^2=0.80$; $MAE=20.21 \text{ W m}^{-2}$). At the Mediterranean grassland, results using f_{SM-ATI} were less accurate both for in-situ and satellite data ($R^2=0.57-0.31$; $MAE=9.85-10.78 \text{ W m}^{-2}$ respectively) but still outperformed reported results of two more complex models ran at the site: the Two Source Model (TSM) and the Penman-Monteith-Leuning (PML) model.

In the context of global drylands, the PT-JPL LE model using f_{SM-ATI} provide results comparable in accuracy to more complex models at similar savanna and grassland biomes. Nonetheless, efforts should be made when using f_{SM-ATI} to reduce evapotranspiration overestimates when the soil is completely dry and to improve the cloud-mask algorithm as the f_{SM-ATI} is very sensitive to changes in solar irradiance.

This study also showed that the original model formulation for soil moisture constraint, f_{SM} , relying on the atmospheric water deficit should be calibrated differently in each site to obtain meaningful LE results. Therefore, the use of soil moisture constraints like ATI based on routinely available products like surface temperature or albedo or from soil moisture missions like the SMOS (Soil Moisture & Ocean Salinity mission) or the future NASA mission SMAP (Soil Moisture Active Passive) would eliminate the need of water vapor data and field site calibrations at dryland regions. The described modeling framework is also suitable for introducing

information from spectral regions currently under-used in evapotranspiration models. For example, canopy water status could be tracked by short-wave infrared indices (Ceccato et al. 2002; Zarco-Tejada et al. 2003) and photosynthetic activity by narrow-band indices like the Photochemical Reflectance Index, PRI (Gamon et al. 1997). Due to the strong coupling between evapotranspiration and carbon assimilation fluxes in dryland regions, some of the biophysical constraints used in this model could be used to regionalize Gross Primary Productivity (GPP) estimates based on Light Use Efficiency models.

REFERENCES

- Anderson, M.C., Norman, J.M., Mecikalski, J.R., Otkin, J.A., & Kustas, W.P. (2007). A climatological study of evapotranspiration and moisture stress across the continental United States based on thermal remote sensing: 2. Surface moisture climatology. *Journal of Geophysical Research-Atmospheres*, 112, D11112
- Baldocchi, D. D. (2008). Breathing of the terrestrial biosphere: lessons learned from a global network of carbon dioxide flux measurement systems. *Australian Journal of Botany*, 56, 1-26
- Berni, J.A.J., Zarco-Tejada, P.J., Sepulcre-Canto, G., Fereres, E., & Villalobos, F. (2009). Mapping canopy conductance and CWSI in olive orchards using high resolution thermal remote sensing imagery. *Remote Sensing of Environment*, 113, 2380-2388
- Boegh, E., Soegaard, H., & Thomsen, A. (2002). Evaluating evapotranspiration rates and surface conditions using Landsat TM to estimate atmospheric resistance and surface resistance. *Remote Sensing of Environment*, 79, 329-343
- Bouchet, R.J. (1963). Evapotranspiration réelle et potentielle, signification climatique. *International Association of Hydrological Sciences (IAHS), Pub.*, 62, 134-142
- Boulet, G., Chehbouni, A., Gentine, P., Duchemin, B., Ezzahar, J., & Hadria, R. (2007). Monitoring water stress using time series of observed to unstressed surface temperature difference. *Agricultural and Forest Meteorology*, 146, 159-172
- Brogaard, S., Runnstrom, M., & Seaquist, J. (2005). Primary production of Inner Mongolia, China, between 1982 and 1999 estimated by a satellite data-driven light use efficiency model. *Global and Planetary Change*, 45, 313-332
- Brownsey, G.J., Eldridge, J.W., Jarvis, D.A., Ross, G., & Sanders, I. (1976). New Light-Scattering Photogoniometer for Accurate Measurements. *Journal of Physics E-Scientific Instruments*, 9, 654-658
- Brutsaert, W. (1982). Evaporation into the atmosphere-Theory, history, and applications. Dordrecht, Holland: D. Reidel Publishing Company, pp.299.
- Cai, G., Xue, Y., Hu, Y., Wang, Y., Guo, J., Luo, Y., Wu, C., Zhong, S., & Qi, S. (2007). Soil moisture retrieval from MODIS data in Northern China Plain using thermal inertia model. *International Journal of Remote Sensing*, 28, 3567-3581
- Campbell, G. S., & Norman, J. M. (1998). An introduction to environmental biophysics. New York: Springer, pp 286.
- Campolongo F., S.A., Sørensen, T., Tarantola S. (2000). Hitchhiker's guide to sensitivity analysis. *Sensitivity analysis*, New York: Wiley, pp. 15-47
- Ceccato, P., Gobron, N., Flasse, S., Pinty, B., & Tarantola, S. (2002). Designing a spectral index to estimate vegetation water content from remote sensing data: Part 1 - Theoretical approach. *Remote Sensing of Environment*, 82, 188-197
- Cleugh, H.A., Leuning, R., Mu, Q.Z., & Running, S.W. (2007). Regional evaporation estimates from flux tower and MODIS satellite data. *Remote Sensing of Environment*, 106, 285-304
- Cracknell, A.P., & Xue, Y. (1996). Thermal inertia determination from space - A tutorial review. *International Journal of Remote Sensing*, 17, 431-461
- Cukier, R.I., Levine, H.B., & Shuler, K.E. (1978). Nonlinear sensitivity analysis of multiparameter model systems. *Journal of Computational Physics*, 26, 1-42

- Chehbouni, A., LoSeen, D., Njoku, E.G., Lhomme, J.P., Monteny, B., & Kerr, Y.H. (1997). Estimation of sensible heat flux over sparsely vegetated surfaces. *Journal of Hydrology*, 189, 855-868
- de Rosnay, P., Gruhier, C., Timouk, F., Baup, F., Mougin, E., Hiernaux, P., Kergoat, L., & LeDantec, V. (2009). Multi-scale soil moisture measurements at the Gourma meso-scale site in Mali. *Journal of Hydrology*, 375, 241-252
- Eagleson, P.S. (1986). The Emergence of Global-Scale Hydrology. *Water Resources Research*, 22, S6-S14
- Fisher, J.B., Malhi, Y., Bonal, D., Da Rocha, H.R., De Araújo, A.C., Gamo, M., Goulden, M.L., Rano, T.H., Huete, A.R., Kondo, H., Kumagai, T., Loescher, H.W., Miller, S., Nobre, A.D., Nouvellon, Y., Oberbauer, S.F., Panuthai, S., Roupsard, O., Saleska, S., Tanaka, K., Tanaka, N., Tu, K.P., & Von Randow, C. (2009). The land-atmosphere water flux in the tropics. *Global Change Biology*, 15, 2694-2714
- Fisher, J.B., Tu, K.P., & Baldocchi, D.D. (2008). Global estimates of the land-atmosphere water flux based on monthly AVHRR and ISLSCP-II data, validated at 16 FLUXNET sites. *Remote Sensing of Environment*, 112, 901-919
- Gamon, J.A., Serrano, L., & Surfus, J.S. (1997). The photochemical reflectance index: an optical indicator of photosynthetic radiation use efficiency across species, functional types, and nutrient levels. *Oecologia*, 112, 492-501
- Garcia, M., Oyonarte, C., Villagarcía, L., Contreras, S., Domingo, F., & Puigdefabregas, J. (2008). Monitoring land degradation risk using ASTER data: The non-evaporative fraction as an indicator of ecosystem function. *Remote Sensing of Environment*, 112, 3720-3736
- Garcia, M., Were, A., Villagarcía, L., Fernandez, N. Domingo, F., Puigdefabregas, J., Sandholt, I. (in review). Accuracy of a water deficit index derived from the NDVI-surface temperature relationship under water-limited or energy -limited conditions. *Remote Sensing of Environment*
- Geiger, B., Carrer, D., Franchisteguy, L., Roujean, J.L., & Meurey, C. (2008). Land Surface Albedo Derived on a Daily Basis From Meteosat Second Generation Observations. *Ieee Transactions on Geoscience and Remote Sensing*, 46, 3841-3856
- Gillies, R.R., & Carlson, T.N. (1995). Thermal remote sensing of surface soil water content with partial vegetation cover for incorporation into climate models. *Journal of Applied Meteorology*, 34, 745-756
- Giorgi, F., & Lionello, P. (2008). Climate change projections for the Mediterranean region. *Global and Planetary Change*, 63, 90-104
- Glenn, E.P., Huete, A.R., Nagler, P.L., Hirschboeck, K.K., & Brown, P. (2007). Integrating Remote Sensing and Ground Methods to Estimate Evapotranspiration. *Critical Reviews in Plant Sciences*, 26, 139-168
- Guichard, F., Kergoat, L., Mougin, E., Timouk, F., Baup, F., Hiernaux, P., & Lavenu, F. (2009). Surface thermodynamics and radiative budget in the Sahelian Gourma: Seasonal and diurnal cycles. *Journal of Hydrology*, 375, 161-177
- Houbourg, R., Anderson, M. C., Norman, J. M., Wilson, T., & Meyers, T. (2009). Intercomparison of a “botton-up” and “top-down” Modeling paradigm for estimating carbon and energy fluxes over a variety of vegetative regimes across the U.S. *Agricultural and Forest Meteorology*, 149(11), 1875-1895

- Huete, A., Didan, K., Miura, T., Rodriguez, E.P., Gao, X., & Ferreira, L.G. (2002). Overview of the radiometric and biophysical performance of the MODIS vegetation indices. *Remote Sensing of Environment*, 83, 195-213
- Huntington, T.G. (2006). Evidence for intensification of the global water cycle: Review and synthesis. *Journal of Hydrology*, 319, 83-95
- Huxman, T.E., Wilcox, B.P., Breshears, D.D., Scott, R.L., Snyder, K.A., Small, E.E., Hultine, K., Pockman, W.T., & Jackson, R.B. (2005). Ecohydrological implications of woody plant encroachment. *Ecology*, 86, 308-319
- Impens, I., & Lemeur, R. (1969). Extinction of net radiation in different crop canopies. *Archiv für Meteorologie, Geophysik und Bioklimatologie Serie B*, 17, 403-412
- Iqbal, M. (1983). Introduction to Solar Radiation. Toronto: Academic Press
- Jarvis, P.G. (1976). Interpretation of Variations in Leaf Water Potential and Stomatal Conductance Found in Canopies in Field. *Philosophical Transactions of the Royal Society of London Series B-Biological Sciences*, 273, 593-610
- June, T., Evans, J.R., & Farquhar, G.D. (2004). A simple new equation for the reversible temperature dependence of photosynthetic electron transport: a study on soybean leaf. *Functional Plant Biology*, 31, 275-283
- Kelliher, F.M., Leuning, R., Raupach, M.R., & Schulze, E.D. (1995). Maximum Conductances for Evaporation from Global Vegetation Types. *Agricultural and Forest Meteorology*, 73, 1-16
- Kottek, M., Grieser, J., Beck, C., Rudolf, B., & Rubel, F. (2006). World map of the Köppen-Geiger climate classification updated. *Meteorologische Zeitschrift*, 15, 259-263
- Kowalski, A.S., Anthoni, P.M., Vong, R.J., Delany, A.C., & Maclean, G.D. (1997). Deployment and evaluation of a system for ground-based measurement of cloud liquid water turbulent fluxes. *Journal of Atmospheric and Oceanic Technology*, 14, 468-479
- Kustas, W.P., & Norman, J.M. (1999). Evaluation of soil and vegetation heat flux predictions using a simple two-source model with radiometric temperatures for partial canopy cover. *Agricultural and Forest Meteorology*, 94, 13-29
- Leuning, R., Zhang, Y.Q., Rajaud, A., Cleugh, H., & Tu, K. (2008). A simple surface conductance model to estimate regional evaporation using MODIS leaf area index and the Penman-Monteith equation. *Water Resources Research*, 44, W10419
- Lu, S., Ju, Z., Ren, T., & Horton, R. (2009). A general approach to estimate soil water content from thermal inertia. *Agricultural and Forest Meteorology*, 149, 1693-1698
- Matsushita, B., Xu, M., Chen, J., Kameyama, S., & Tamura, M. (2004). Estimation of regional net primary productivity (NPP) using a process-based ecosystem model: How important is the accuracy of climate data? *Ecological Modelling*, 178, 371-388
- McMillen, R.T. (1988). An Eddy-Correlation Technique with Extended Applicability to Non-Simple Terrain. *Boundary-Layer Meteorology*, 43, 231-245
- Minacapilli, M., Iovino, M., & Blanda, F. (2009). High resolution remote estimation of soil surface water content by a thermal inertia approach. *Journal of Hydrology*, 379, 229-238
- Miralles, D.G., Holmes, T.R.H., De Jeu, R.A.M., Gash, J.H., Meesters, A.G.C.A., & Dolman, A.J. (2011). Global land-surface evaporation estimated from satellite-based observations. *Hydrology and Earth System Sciences*, 15, 453-469

- Mitra, D.S., & Majumdar, T.J. (2004). Thermal inertia mapping over the Brahmaputra basin, India using NOAA-AVHRR data and its possible geological applications. *International Journal of Remote Sensing*, 25, 3245-3260
- Monteith, J. L. (1972). Solar radiation and productivity in tropical ecosystems. *Journal of Applied Ecology*, 9, 747-766
- Moran, M.S., Clarke, T.R., Inoue, Y., & Vidal, A. (1994). Estimating crop water deficit using the relation between surface-air temperature and spectral vegetation index. *Remote Sensing of Environment*, 49, 246-263
- Morton, F.I. (1983). Operational estimates of areal evapotranspiration and their significance to the science and practice of hydrology. *Journal of Hydrology*, 66, 1-76
- Mougin, E., Hiernaux, P., Kergoat, L., Grippa, M., de Rosnay, P., Timouk, F., Le Dantec, V., Demarez, V., Lavenu, F., Arjounin, M., Lebel, T., Soumaguel, N., Ceschia, E., Mougénot, B., Baup, F., Frappart, F., Frison, P.L., Gardelle, J., Gruhier, C., Jarlan, L., Mangiarotti, S., Sanou, B., Tracol, Y., Guichard, F., Trichon, V., Diarra, L., Soumaré, A., Koité, M., Dembélé, F., Lloyd, C., Hanan, N.P., Damesin, C., Delon, C., Serça, D., Galy-Lacaux, C., Seghier, J., Becerra, S., Dia, H., Gangneron, F., & Mazzega, P. (2009). The AMMA-CATCH Gourma observatory site in Mali: Relating climatic variations to changes in vegetation, surface hydrology, fluxes and natural resources. *Journal of Hydrology*, 375, 14-33
- Mu, Q.Z., Zhao, M.S., & Running, S.W. (2011). Improvements to a MODIS global terrestrial evapotranspiration algorithm. *Remote Sensing of Environment*, 115, 1781-1800
- Mu, Q.Z., Heinsch, F.A., Zhao, M., & Running, S.W. (2007). Development of a global evapotranspiration algorithm based on MODIS and global meteorology data. *Remote Sensing of Environment*, 111, 519-536
- Myneni, R.B., Hoffman, S., Knyazikhin, Y., Privette, J.L., Glassy, J., Tian, Y., Wang, Y., Song, X., Zhang, Y., Smith, G.R., Lotsch, A., Friedl, M., Morisette, J.T., Votava, P., Nemani, R.R., & Running, S.W. (2002). Global products of vegetation leaf area and fraction absorbed PAR from year one of MODIS data. *Remote Sensing of Environment*, 83, 214-231
- Myneni, R.B., & Williams, D.L. (1994). On the Relationship between Fapar and Ndvi. *Remote Sensing of Environment*, 49, 200-211
- Nearing, G.S., Moran, M.S., Scott, R.L., & Ponce-Campos, G. (2012). Coupling diffusion and maximum entropy models to estimate thermal inertia. *Remote Sensing of Environment*, 119, 222-231
- Nemani, R.R., & Running, S.W. (1989). Estimation of Regional Surface-Resistance to Evapotranspiration from Ndvi and Thermal-Ir Avhrr Data. *Journal of Applied Meteorology*, 28, 276-284
- New, M., Hulme, M., & Jones, P. (2000). Representing twentieth-century space-time climate variability. Part II: Development of 1901-96 monthly grids of terrestrial surface climate. *Journal of Climate*, 13, 2217-2238
- Nicholson, S. (2000). Land surface processes and Sahel climate. *Reviews of Geophysics*, 38, 117-139
- Norman, J.M., Kustas, W.P., & Humes, K.S. (1995). Source Approach for Estimating Soil and Vegetation Energy Fluxes in Observations of Directional Radiometric Surface-Temperature. *Agricultural and Forest Meteorology*, 77, 263-293

- Overgaard, J., 2005. Energy- based land-surface modelling: new opportunities in integrated hydrological modelling. PhD thesis. Lyngby: Institute of Environment and Resources, Technical University of Denmark.
- Potter, C.S., Randerson, J.T., Field, C.B., Matson, P.A., Vitousek, P.M., Mooney, H.A., & Klooster, S.A. (1993). Terrestrial Ecosystem Production - a Process Model-Based on Global Satellite and Surface Data. *Global Biogeochemical Cycles*, 7, 811-841
- Price, J.C. (1977). Thermal inertia mapping: A new view of the earth. *Journal of Geophysical Research*, 82, 2582-2590
- Priestley, C.H.B., & Taylor, R.J. (1972). On the Assessment of Surface Heat Flux and Evaporation Using Large-Scale Parameters. *Monthly Weather Review*, 100, 81-92
- Qiu, G.Y., Shi, P.J., & Wang, L.M. (2006). Theoretical analysis of a remotely measurable soil evaporation transfer coefficient. *Remote Sensing of Environment*, 101, 390-398
- Rey, A., Belelli-Marchesini, L., Were, A., Serrano-Ortiz, P., Etiope, G., Papale, D., Domingo, F., & Pegoraro, E. (2012). Wind as a main driver of the net ecosystem carbon balance of a semiarid Mediterranean steppe in the South East of Spain. *Global Change Biology*, 18, 539-554
- Ridler, M.E. (2012). Calibrating a soil-vegetation-atmosphere transfer model with remote sensing estimates of surface temperature and soil surface moisture in a semi arid environment. *Journal of hydrology (Amsterdam)*, 436-437, 1-12
- Ross, J. (1976). Radiative transfer in plant communities. In: J.L. Monteith (Ed.), *Vegetation and the atmosphere* (pp. 13-56). London: Academic Press
- Saltelli, A., Tarantola, S., & Chan, K.P.S. (1999). A quantitative model-independent method for global sensitivity analysis of model output. *Technometrics*, 41, 39-56
- Sandholt, I., Rasmussen, K., & Andersen, J. (2002). A simple interpretation of the surface temperature/vegetation index space for assessment of surface moisture status. *Remote Sensing of Environment*, 79, 213-224
- Saux-Picart, S., Otle, C., Perrier, A., Decharme, B., Coudert, B., Zribi, M., Boulain, N., Cappelaere, B., & Ramier, D. (2009). SEtHyS_Savannah: A multiple source land surface model applied to Sahelian landscapes. *Agricultural and Forest Meteorology*, 149, 1421-1432
- Schmetz, J., Pili, P., Tjemkes, S., Just, D., Kerkmann, J., Rota, S., & Ratier, A. (2002). An introduction to Meteosat Second Generation (MSG). *Bulletin of the American Meteorological Society*, 83, 977
- Schymanski, S.J., Sivapalan, M., Roderick, M.L., Hutley, L.B., & Beringer, J. (2009). An optimality-based model of the dynamic feedbacks between natural vegetation and the water balance. *Water Resources Research*, 45, W01412
- Shuttleworth, W.J., & Wallace, J.S. (1985). Evaporation from Sparse Crops - an Energy Combination Theory. *Quarterly Journal of the Royal Meteorological Society*, 111, 839-855
- Sobrino, J.A., El Kharraz, M.H., Cuenca, J., & Raissouni, N. (1998). Thermal inertia mapping from NOAA-AVHRR data. *Synergistic Use of Multisensor Data for Land Processes*, 22, 655-667
- Stisen, S., Jensen, K., Sandholt, I., & Grimes, D. (2008). A remote sensing driven distributed hydrological model of the Senegal River basin. *Journal of Hydrology*, 354, 131-148

- Sun, Z., Gebremichael, M., Ardö, J., & de Bruin, H.A.R. (2011). Mapping daily evapotranspiration and dryness index in the East African highlands using MODIS and SEVIRI data. *Hydrology and Earth System Sciences*, *15*, 163-170
- Taylor, C.M., Gounou, A., Guichard, F., Harris, P.P., Ellis, R.J., Couvreur, F., & De Kauwe, M. (2011). Frequency of sahelian storm initiation enhanced over mesoscale soil-moisture patterns. *Nature Geoscience*, *4*, 430-433
- Timouk, F., Kergoat, L., Mougin, E., Lloyd, C.R., Ceschia, E., Cohard, J.M., Rosnay, P.d., Hiernaux, P., Demarez, V., & Taylor, C.M. (2009). Response of surface energy balance to water regime and vegetation development in a Sahelian landscape. *Journal of Hydrology*, *375*, 178-189
- Tramutoli, V., P. Claps, M. Marella, N. Pergola, C. Sileo (2000). Feasibility of hydrological application of thermal inertia from remote sensing. *2nd Plinius Conference on Mediterranean Storms, 16–18* Siena, Italy.
- Trigo, I.F., Peres, L.F., DaCarnara, C.C., & Freitas, S.C. (2008). Thermal land surface emissivity retrieved from SEVIRI/meteosat. *Ieee Transactions on Geoscience and Remote Sensing*, *46*, 307-315
- Twine, T.E., Kustas, W.P., Norman, J.M., Cook, D.R., Houser, P.R., Meyers, T.P., Prueger, J.H., Starks, P.J., & Wesely, M.L. (2000). Correcting eddy-covariance flux underestimates over a grassland. *Agricultural and Forest Meteorology*, *103*, 279-300
- Van Doninck, J., Peters, J., De Baets, B., De Clercq, E.M., Ducheyne, E., & Verhoest, N.E.C. (2011). The potential of multitemporal Aqua and Terra MODIS apparent thermal inertia as a soil moisture indicator. *International Journal of Applied Earth Observation and Geoinformation*, *13*, 934-941
- Verhoef, A. (1998). The relative importance of surface and aerodynamic resistances in a multi-source energy-CO₂ model. *Physics and Chemistry of the Earth*, *23*, 459
- Verstraeten, W.W., Veroustraete, F., & Feyen, J. (2006a). On temperature and water limitation of net ecosystem productivity: Implementation in the C-Fix model. *Ecological Modelling*, *199*, 4-22
- Verstraeten, W.W., Veroustraete, F., van der Sande, C.J., Grootaers, I., & Feyen, J. (2006b). Soil moisture retrieval using thermal inertia, determined with visible and thermal spaceborne data, validated for European forests. *Remote Sensing of Environment*, *101*, 299-314
- Vinukollu, R.K., Wood, E.F., Ferguson, C.R., & Fisher, J.B. (2011). Global estimates of evapotranspiration for climate studies using multi-sensor remote sensing data: Evaluation of three process-based approaches. *Remote Sensing of Environment*, *115*, 801-823
- Wan, Z.M., & Dozier, J. (1996). A generalized split-window algorithm for retrieving land-surface temperature from space. *Ieee Transactions on Geoscience and Remote Sensing*, *34*, 892-905
- Webb, E.K., Pearman, G.I., & Leuning, R. (1980). Correction of Flux Measurements for Density Effects Due to Heat and Water-Vapor Transfer. *Quarterly Journal of the Royal Meteorological Society*, *106*, 85-100
- Were, A., Villagarcía, L., Domingo, F., Alados-Arboledas, L., & Puigdefabregas, J. (2007). Analysis of effective resistance calculation methods and their effect on modelling evapotranspiration in two different patches of vegetation in semi-arid SE Spain. *Hydrology and Earth System Sciences*, *11*, 1529-1542

- Yuan, W.P., Liu, S.G., Yu, G.R., Bonnefond, J.M., Chen, J.Q., Davis, K., Desai, A.R., Goldstein, A.H., Gianelle, D., Rossi, F., Suyker, A.E., & Verma, S.B. (2010). Global estimates of evapotranspiration and gross primary production based on MODIS and global meteorology data. *Remote Sensing of Environment*, 114, 1416-1431
- Zarco-Tejada, P.J., Rueda, C.A., & Ustin, S.L. (2003). Water content estimation in vegetation with MODIS reflectance data and model inversion methods. *Remote Sensing of Environment*, 85, 109-124
- Zhang, K., Kimball, J.S., Mu, Q., Jones, L.A., Goetz, S.J., & Running, S.W. (2009). Satellite based analysis of northern ET trends and associated changes in the regional water balance from 1983 to 2005. *Journal of Hydrology*, 379, 92-110
- Zhang, Y.Q., Chiew, F.H.S., Zhang, L., Leuning, R., & Cleugh, H.A. (2008). Estimating catchment evaporation and runoff using MODIS leaf area index and the Penman-Monteith equation. *Water Resources Research*, 44, W10420
- Zhang, Y.Q., Leuning, R., Hutley, L.B., Beringer, J., McHugh, I., & Walker, J.P. (2010). Using long-term water balances to parameterize surface conductances and calculate evaporation at 0.05° spatial resolution. *Water Resources Research*, 46, W05512

CONCLUSIONES GENERALES

1. El modelo residual *Two-source model*, TSM, basado en medidas de temperatura superficial, no fue capaz de ofrecer estimas con errores aceptables de la evapotranspiración a escala instantánea de 15 minutos. Sin embargo, sí fue capaz de estimar el calor sensible y la radiación neta con un grado de exactitud aceptable demostrando así la efectividad del proceso iterativo incluido en su formulación para desagregar la temperatura superficial (T_R) en sus componentes, suelo (T_s) y vegetación (T_c). Estos resultados evidencian las limitaciones de la estimación residual de LE en áreas semiáridas mediterráneas, en donde errores aceptables en H y Rn (del 30% y el 10% respectivamente), tuvieron un fuerte impacto sobre los valores de LE obtenidos de forma residual dada la reducida magnitud de LE en este tipo de ecosistemas.
2. La exactitud del TSM presentó una variación diurna, viéndose afectada tanto por la elevación solar como por la hora del día. Nuestros resultados demuestran que al menos en áreas semiáridas naturales, la aplicación del TSM ofrece mejores resultados en condiciones de elevación solar mayor a 25° y durante las horas del día comprendidas entre las 10:00 y las 15:00 (ambos factores incluidos) ya que, en condiciones distintas a estas, el TSM generó mayores errores en sus estimas.
3. Las condiciones meteorológicas que mas afectaron a la exactitud del modelo en zonas semiáridas naturales fueron el gradiente de temperatura entre la superficie y el aire ($T_R - T_a$) y la velocidad del viento (WS), siendo mejores los resultados del TSM cuando ambos fueron altos. En áreas semiáridas el TSM no se vio afectado por la presencia de nubes o por condiciones de vegetación senescente, ambas condiciones bajo las que el TSM ha demostrado una reducción de su exactitud según trabajos previos efectuados en áreas no limitadas hídricamente. Esto demuestra una diferente sensibilidad del TSM en áreas semiáridas naturales.
4. En condiciones semiáridas naturales el TSM fue capaz de ofrecer buenas estimas diurnas del calor sensible, H_D , aplicando métodos de extrapolación temporal, pero no del calor latente cuyo valor fue fuertemente sobreestimado en todos los casos con errores mayores del 100% aunque un alto porcentaje de su variación fue recogido por el modelo ($R^2 > 0.8$). Para obtener valores diurnos de H y LE mediante el TSM con los menores errores es necesario promediar las estimas instantáneas obtenidas a lo largo de todo el periodo diurno (*Averaging method*). Este método es

más eficaz que asumir que el valor estimado de la fracción evaporativa al medio día se mantiene constante a lo largo del periodo diurno (*NEF* o *EF method*).

5. Las dos formulaciones posibles del TSM, con las resistencias *en serie* (TSM_S) o *en paralelo* (TSM_P), ofrecieron resultados instantáneos similares aunque el TSM_P redujo los porcentajes de error promedio de H y LE , mientras que el TSM_S permitió una mejor partición de los flujos entre suelo y vegetación y mostró un comportamiento más robusto ante la variación de las condiciones meteorológicas. Sin embargo, para obtener valores diurnos de H y LE , el empleo de TSM_P presentó claras ventajas sobre TSM_S , ofreciendo mejores resultados.

6. El modelo directo *Penman-Monteith-Leuning*, PML, logró obtener estimas de la evapotranspiración diaria con un grado de exactitud razonable (30-35%) en condiciones semiáridas, gracias a la adaptación de su formulación original mediante la incorporación de la variación temporal de la evaporación del suelo. La modificación introducida logró reproducir el comportamiento pulsátil típico de la evaporación del suelo en zonas semiáridas de vegetación dispersa, mejorando la eficacia del modelo PML en dichas condiciones en las que la evaporación del suelo no puede considerarse constante tal como plantea su formulación original.

7. De los tres métodos evaluados para estimar la evaporación del suelo, el mejor es el método *f_{drying}* que emplea la relación entre la precipitación y la evaporación potencial del suelo acumuladas durante los 16 días previos a un evento de lluvia e incluye un factor para la simulación del secado del suelo posterior a la lluvia. Empleando *f_{drying}* la aplicación del PML precisa de la calibración local de dos parámetros: la conductancia máxima de las hojas (g_{sx}) y la velocidad de secado del suelo (ω).

8. La adaptación del modelo directo *Priestley-Taylor-Jet Propulsion Laboratory*, PT-JPL, para la estimación diaria de E mediante la modelización de la evaporación del suelo en función de los cambios en la humedad del suelo representados mediante la inercia térmica (f_{SM-ATI}) empleando datos de temperatura superficial y albedo, presentó mejores resultados en un área de sabana en el Sahel que en un espantal mediterráneo. Aún así, en dicho espantal mediterráneo el modelo PT-JPL ofreció mejores estimas diarias de E que los modelos PML y TSM.

9. En el área de sabana del Sahel, el empleo de datos de temperatura y albedo ofrecidos por el sensor remoto MSG-SEVIRI ofreció resultados similares al empleo de mediciones in-situ de

dichas variables, mientras que en el espartal mediterráneo los resultados empeoraron al emplear datos remotos. La adaptación propuesta del modelo PT-JPL, permite obtener resultados similares a los obtenidos en áreas semiáridas naturales mediante otros modelos más complejos que requieren un mayor número de datos de medición local o parámetros calibrados experimentalmente.

10. Nuestros resultados evidencian la mayor idoneidad de los modelos directos para la estimación regional de E en áreas semiáridas de vegetación dispersa frente a los modelos residuales. Dentro de los modelos directos, la adaptación propuesta del modelo PT-JPL se presenta como la mejor opción, tanto por su sencillez, como por su aplicabilidad regional, gracias al empleo de la inercia térmica (f_{SM-ATI}), mediante datos remotos de albedo y temperatura superficial.

“Esto es un desafío, es decir: voy a poder con este reto, voy a poder con el vértigo, con el frío, con el agotamiento.... es igual. Es meterse algo en la cabeza y conseguirlo.
Nunca tires la toalla, nunca, siempre hay una oportunidad.
Cima! reunión! fuera!”

Jesus Calleja,
Ascensión cara oeste del Naranjo de Bulnes